Light trapping in Si thin film solar cell

Ahmadpanahi, Hamed

DOI
10.4233/uuid:b4288708-cc36-40de-966a-534b7090a7fc

Publication date
2019

Document Version
Final published version

Citation (APA)
Ahmadpanahi, H. (2019). *Light trapping in Si thin film solar cell*. [Dissertation (TU Delft), Delft University of Technology]. https://doi.org/10.4233/uuid:b4288708-cc36-40de-966a-534b7090a7fc

Light trapping

In Si thin film solar cells

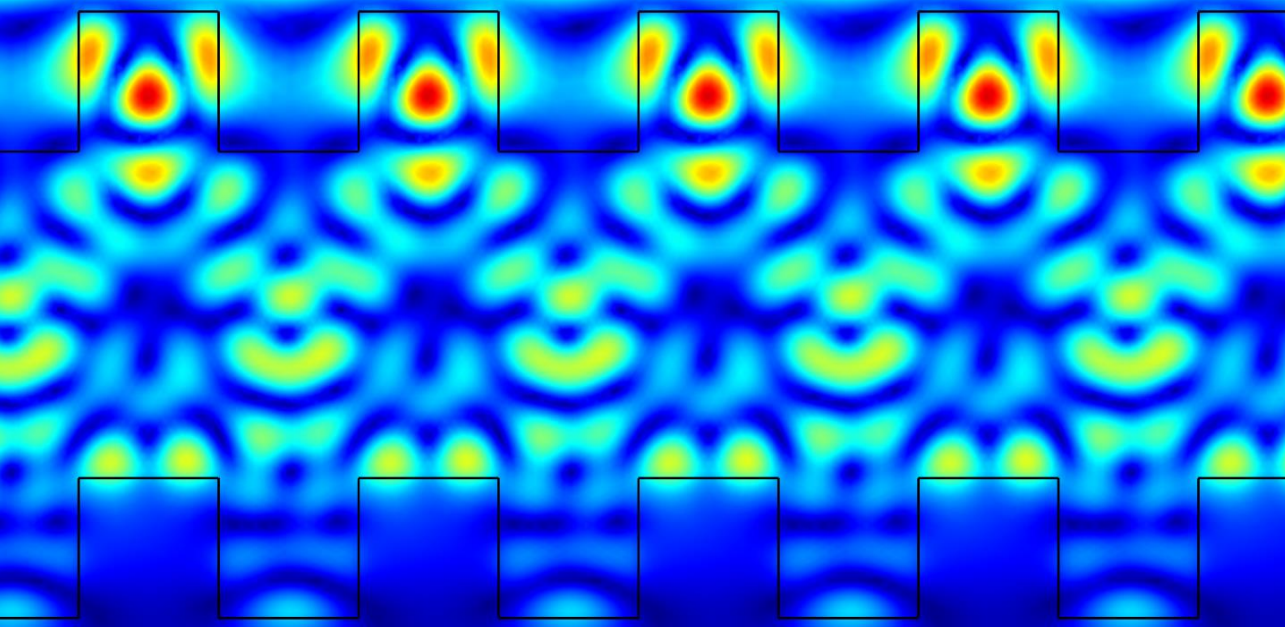

Hamed Ahmadpanahi

LIGHT TRAPPING

IN SILICON THIN FILM SOLAR CELLS

Proefschrift

Dissertation
for the purpose of obtaining the degree of doctor
at Delft University of Technology
by the authority of the Rector Magnificus, Prof.dr.ir. T.H.J.J. van der Hagen,
chair of the Board for Doctorates
to be defended publicly on:
Monday 16 September 2019 at 12:30 o' clock

by

Hamed AHMADPANAHI

Master of Science in Photonics, Kungliga Tekniska högskolan, Sweden
born in Semnan, Iran

This dissertation has been approved by the promotors.

promotor: prof. dr. M. Zeman
copromotor: dr. O. Isabella

Composition of the doctoral committee::

Prof. dr. ir. P.G. Luscuere,	Chairperson
Prof. dr. M. Zeman,	Technische Universiteit Delft
Dr. O. Isabella,	Technische Universiteit Delft

Independent members:

Prof. dr. J. Krĉ	University of Ljubljana
Prof. dr. A. Neto,	Technische Universiteit Delft
Prof. dr. J. Poortmans	IMEC & Catholic University of Leuven
Dr. O. El Gawhary	Dutch Metrology Institute (VSL) & Technische Universiteit Delft
Dr. C. Seassal,	École centrale de Lyon

Reserved memebers:

Prof. dr. ir. A.H.M. Smets	Technische Universiteit Delft

Keywords: Light trapping, Thin-film solar cell, Grating structure.

Front & Back: The amplitude of TE polarized electric field with wavelength 905 nm outside and inside a periodically textured Silicon thin film (Associated with the absorption peak at 905 nm in Figure 4-4 (A)).

Printed by ADC-Dereumaux

An electronic version of this dissertation is available at
https://doi.org/10.4233/uuid:b4288708-cc36-40de-966a-534b7090a7fc

CONTENTS

1

INTRODUCTION

1.1. ENERGY AND SOCIETY

The human evolution and the development of our society is directly linked with the energy resources. Industrial revolution, intercontinental transport, mass production and automation could not have been possible without providing a reliable and low-cost source of energy. Since the last century, fossil fuels are the main source of energy for our modern society. Food and agriculture industry, road transport system, electricity, internet and communications are all somehow linked to fossil fuels. However, future generations cannot rely on them, because we are exploiting this resource much faster than nature can provide. In addition, our environment cannot withstand the amount of pollution due to consumption of fossil fuels. The era of fossil fuel will soon be over [1–3] and, then, a clean, sustainable and affordable energy source is needed to fulfil the ever increasing demand for energy. Sunlight, which is the main source of energy in our planet, is the best substitute of fossil fuels. The history of producing energy from sunlight is as old as the life on our planet, but producing electricity from sunlight goes back to 1839 [4]. However, only in 1954 the first practical photovoltaic cell was publicly demonstrated[5]. Photovoltaics (PV) is one of the promising technologies to produce clean and sustainable electricity from the Sun [6]. Nowadays, electricity generated by PV is, in many countries of the world, competitive to the electricity generated via fossil fuels. To render PV appealing in all markets, increasing the overall efficiency-to-cost is one of the main challenges in solar cell research [6, 7]. To improve this factor, the production cost needs to be reduced while the efficiency being increased. One of the methods to decrease the solar electricity cost is to decrease the amount of used materials. The cost of solar cell material counts for almost 40% of the total production cost [6]. Therefore, reducing the utilized material can reduce the production cost dramatically [8] and thus, it is very desirable [9]. Thin-film solar cell technology aims at reducing the intake material by deploying thinner absorbers and thus lowering the production cost. However, this does not necessarily improve the efficiency-to-cost ratio. This is because a thin absorber is less likely to optimally absorb photons with low energy, indicating that the efficiency of a thin-film solar cell would be much lower than conventional cell. Therefore, more

1

thin-film solar cells are needed to produce the desire amount of energy. This lower absorption efficiency for low energy photons is a common problem for any semiconductor, but much more pronouced for indirect band-gap semiconduction such as silicon.

1.2. NEAR INFRA-RED PROBLEM FOR SILICON BASED SOLAR CELLS

The absorption coefficient of semiconductors drops significantly for photons with energy smaller than its band gap energy. Generally speaking, semiconductors are divided into two category, direct band-gap or indirect band-gap semiconductors. The light absorption in indirect band gap semiconductor is much weaker for photons with eanrgy smaller than the bang gap. Silicon is one of the indirect band gap semiconductors. Its band gap falls in the near infra-red (NIR) part of the spectrum and, therefore, Si-based solar cells have much lower absorption for red and NIR photons. Even though this is a common issue for all Si-based solar cells, including the wafer-based devices [10], it is more pronounced for thin-film solar cells. For example, to absorb a photon with a wave-

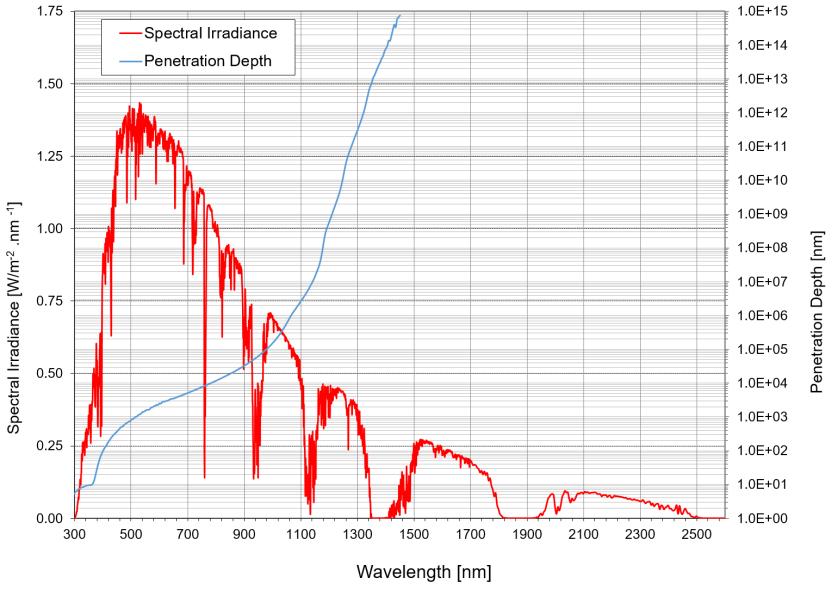

Figure 1.1: Si penetration depth vs the sun light wavelength and its spectral irradiance. A flat Si slab with thickness about 200 μm can absorb in one pass up to 1000 nm. To enhance the absorption of 1300 nm photons, the slab needs to be 1-km thick.

length of 1200 nm using Si, the absorber would need to be 1-m thick (see Figure 1.1), while the thickness of the absorber layer in thin-film solar cells is typically few hundreds of nanometres. This means that the penetration depth [1] for wavelength larger than the

[1] The absorption depth is the distance into the material at which the light drops to about 36% of its original intensity, or alternately has dropped by a factor of $1/e$.

semiconductor band gap, is much larger than the thickness of the absorber (The situation hols for photons with energy slightly smaller or equal to the semiconductor band gap). Therefore, the device is unable to effectively absorb the low energy photons. To overcome this problem, one needs to increase the optical thickness of the absorber while keeping its physical thickness the same. In temporal domain, this translates into increasing the time that incidence energy interacts with the absorber (i.e. *stays* or *travels* inside the absorber). Increasing light–matter interaction can be done using light management techniques.

1.3. LIGHT MANAGEMENT

In general, any technique that enhances the optical efficiency of solar cell is part of light management. In bulk crystalline silicon (c-Si) solar cells, light management is accomplished by multiple techniques such as

1. The deployment of anti-reflection (AR) layer (coating and textured) to enhance light in-coupling at the front side.
2. The implementation of a back reflector to prevent escaping of light from the back side.
3. The texturing of interfaces to promote scattering and thus enhance the light path in the absorber.

Anti-reflection (AR) coating decreases the Fresnel reflection at the interface between air and solar cell and allows more photons to get into the absorber. Photons with absorption depth larger than the thickness of the absorber, can escape from the back side or the absorber (Figure 1.2 (A). Adding a reflector at the back side of the absorber prevents the low energy photons from escaping the solar cells. Back reflector simply duplicates the optical thickness of the absorber and creates larger chance for low energy photons to be absorbed. If the absorption depth of a photon is larger than the two times the optical thickness of the absorber, since AR coating prevents any reflection at I-II interface, then those photons can escape the structure (Figure 1.2 (B)). In this situation, surface texturing needs to be implemented to increase light absorption (Figure 1.2 (C)). The surface texturing scatters the incidence light into many different angels, allowing the incident energy to travel inside the absorber in distances much longer than absorber thickness.
In c-Si wafer-based PV technology, the absorber thickness is much larger than the incidence wavelengths. Thus, the thick absorber (about 200 μm) can be seen as bulk for a large wavelength range in solar spectrum and, therefore, the interaction between incident light and the solar cell can be explained using ray optics. This is one of the main differences between c-Si and thin-film (Si) solar cells, where the thickness of the absorber is comparable or equal to the light wavelength and thus some of the basic assumptions in conventional optics is not applicable anymore. In this situation, the wave effect of the light becomes prominent and thus wave optics needs to be employed to explain the light behaviour inside the thin film absorber. Another difference between a c-Si solar cell and a thin-film solar cell lies in their angular response. The angular response of a c-Si cell is isotropic, meaning that all rays that are propagating along different directions inside

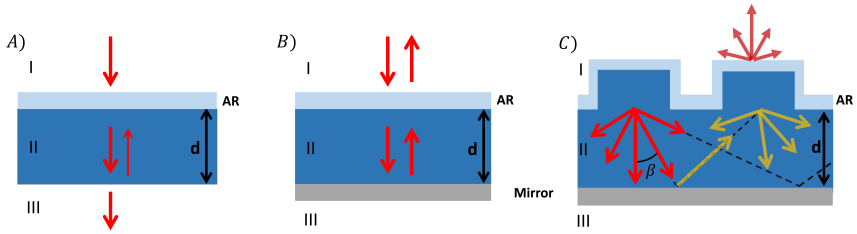

Figure 1.2: A) shows light entering a thin film with AR coating. B) Light entering a slab with AR coating on top and a perfect mirror at second interface. C) Shows the light scattering in a textured slab.

the absorber experience the same material properties. On the contrary, in thin-film solar cell the angular response of the absorber is not isotropic anymore and can be exploited to our benefit.

1.4. LIGHT TRAPPING

Based on this principle, thin-film absorber can be seen as a resonator which supports many modes. Each of those modes keep the electromagnetic energy inside the absorber for a particular amount of time. The longer the confinement time is, the larger the absorption is. This is the main concept for light trapping: to couple the light into absorber (increase the probability of light absorption inside the absorber), and to keep the low energy photons inside the absorber as long as possible. This can usually be done by using surface texturing [11–13], or nano-particles (metal and dielectric)[14–16]. They both promote light scattering and facilitate light coupling into the absorber layer [17]. In thin-film silicon solar cells however, the texturing size is in the range of tens of nanometres. The texturing type (periodic or random), geometry and arrangement play a significant role in absorption enhancement in thin-film silicon solar cells [18–21]. In today's thin-film Si solar cells, using randomly textured interfaces is the standard approach to achieve light scattering [22–25]. Alternative method to achieve light scattering is to implement periodic surface texturing such as periodic gratings. Although random and periodic texturing are used to achieve the same goal, they have different properties.

Random texturing distributes the incidence energy into a continuous range of directions, with an energy distribution inversely proportional to the scattering angle . Periodic texturing instead diffracts the incident energy in to a discrete set of angles with a predictable energy distribution. This implies that a randomly textured structure is less sensitive to angular and spectral variation than a periodically textured thin film. On the other hand, the light coupling efficiency can be much larger in a periodically textured structured than in a structure with random texturing. From the design point of view, a periodic structure can be tuned such that it has a larger efficiency in excitation of the guided modes of the structure.

1.5. GUIDED AND NON-GUIDED MODES

Generally speaking, in a dielectric waveguide with flat interfaces, two types of mode can be recognized, guided and non-guided modes. All the modes with $k_{||} > k_0$ (where $k_{||}$ is the projection of light propagation vector in the dielectric on the interface and k_0 is the wave number in vacuo) are guided mode. In a flat dielectric waveguide, it is relatively straightforward to distinguish between guided and non-guided resonances using the dispersion diagram of the waveguide. On the other hand, in grating waveguide structure the presence of grating on top of the waveguide alters the optical properties of the waveguide and changes dramatically the dispersion diagram. Therefore, it is more complicated to distinguish between guided and non-guided resonance in grating waveguide structure. Chapter 3 and 4 in this thesis focus on this topic. In these chapters, we provide a semi analytical approach based on Fourier expansion to calculate the contribution of different type of resonance in total absorption. Using this method one can distinguish between guided and non-guided resonance in a periodically-textured thin-film structure.

1.6. MAXIMUM ABSORPTION ENHANCEMENT

One of the main goals of light trapping is to enhance the light absorption in thin films. Random or periodic texturing allow to excite more resonance in the structure and thus enhance the light absorption. But what is the maximum absorption we can achieve using light management techniques? For a two-dimensional (2D) randomly-textured slab made of a weakly absorbing material, the maximum absorption enhancement, is equal to $4n^2$, where n is the refractive index of the material [26]. The absorption enhancement is defined as the ratio of absorption in the textured slab to the single pass absorption of a flat equivalent slab. The $4n^2$ limit, proposed by Yablonovitch and Cody [26], is calculated using statistical or ray optics and therefore it is well known as Lambertian or bulk limit. The bulk limit does not hold for wavelength-scale structures, where some of the basic assumptions of the conventional optics are no longer applicable. In 2010, Yu et al. [27, 28] used temporal coupled-mode theory (TCMT) to calculate the maximum absorption enhancement in a nano-scale structure. It was reported that the light trapping limit for grating structure (the so-called nanophotonic limit) can exceed the bulk limit of $4n^2$, but for a narrow angular and spectral range. In chapter 5 of this thesis we extend the work of Yu et al and describe the nanophotonic limit based on the number of resonances that are excited by a particular diffraction order.

Thin-film solar cells are often textured on top and bottom surface. Sometimes top and bottom interfaces have different texturing. Investigating the maximum absorption enhancement in a double side textured structure has not yet studied in sufficient detail. In this thesis we also use the result of TCMT to calculate the nanphotonic limit for a double side corrugated thin-film slab.

1.7. OBJECTIVES

Within this thesis, we aimed at obtaining better understanding about light behaviour inside a periodically textured thin film. This can be used to evaluate the quality and performance of a grating from light trapping perspective. The following questions has

been answered in this thesis:

1. How to distinguish between the different types of resonance (particularly guided and non-guided resonances) in a periodically textured thin film solar cell?
   (a) What is the contribution of each resonance to the total absorption?
   (b) How does the contribution of resonances in total absorption change under oblique incidence?
   (c) How the absorption peaks match with the density of the modes in the absorber?
2. What is the maximum absorption enhancement achievable using periodic texturing?
   (a) How much is the contribution of each resonance in light trapping limit for grating structure?
   (b) What is the ratio between top and bottom grating periods in a double interface textured thin film to achieve maximum absorption enhancement over a large wavelength range?

1.8. OUTLINE OF THE THESIS

This thesis is structured in six distinct chapters. In Chapter 1, a general introduction is given to address the main optical challenge in thin film silicon solar cells and to motivate the need for light trapping. This chapter also describes the main focus of this thesis and the urge to understand the light behaviour inside a periodic waveguide thin film. Chapter 2 provides the mathematical background and the frame work which has been used throughout the thesis. This chapter presents some practical details and calculation techniques which have been used to obtain our results. In Chapter 3, a semi analytical approach is introduced to calculate the contribution of guided and non-guided resonances to total absorption for a grating waveguide structure under normal incidence. In this approach, we use Fourier expansion to calculate the energy spectral density of the electric field inside the absorber. In this way, the weight of each resonance to the total absorption is defined for a large wavelength range and for both TM and TE polarization. Additionally, the proposed mathematical model is supported by numerical and rigorous calculations, using a Maxwell equation solver based on the finite element method. This approach is extended for oblique incidence in Chapter 4. In this chapter it is explained how the variation of tangential and normal components for TM electric field under oblique incidence influences the accuracy of numerical calculation. The correlation between the density of modes and the absorption peaks due to guided mode excitation is also thereby presented in chapter 5 focuses on calculating the maximum absorption enhancement achieved by each type of resonance in a waveguide structure with symmetric and asymmetric gratings. In this chapter a different approach is introduced to count the number of resonances in a grating waveguide structure, at each frequency. Then, TCMT is used to calculate the maximum absorption enhancement for each diffraction order. This approach is extended for a thin film with double side texturing. Chapter 6 provides the conclusion of the thesis.

1.9. CONTRIBUTION TO THE RESEARCH FIELD

There is a common method to understand if an absorption peak is due to the excitation of a guided mode. In such method, a resonance is identified as the intersection of a guided-mode-line of a flat-equivalent waveguide (with the same optical thickness as the grating structure) with the centre of a Brillouin zone of the grating. Applying this method is very difficult for waveguide with thickness much larger than the wavelength. Additionally, the method is not reliable when

- Grating height is comparable with the thickness of the wave-guide;
- The structure is illuminated with TM polarized light.

In this work we provided with a different approach to calculate the weight of each diffraction order into total absorption. Our proposed method can be used to calculate the absorption for each diffraction order, and to distinguish between guided and non-guided resonances regardless of waveguide thickness, polarization, grating properties (height, period, duty cycle), incident angle and wavelength range. Decomposing the total absorption to its components can be used as a tool for grating designers to assess the performance of a new grating or to better understand how manufacturing errors influence the optical performance of the structure. Additionally, using this method allows us to observe the energy transfer between different modes. Knowing the maximum achievable absorption enhancement using periodic texturing is another fundamental question in thin-film solar cell society. In this thesis we have provided a closed formula to calculate the maximum absorption enhancement for each diffraction order for an ideal 1-D grating structure. This formula is based on counting the total number of resonances at each frequency that could be excited by a particular diffraction order. Based on this equation we know how the position of maximum absorption enhancement changes according to variation in grating pitch and refractive index. Another achievement is that we know now how to achieve the maximum absorption in a wide range of wavelengths in a double side textured thin film: the period of top interface should be an aliquant part of the period of bottom interface. This is one of the key parameters in designing double side textured thin-film solar cells.

2

TECHNICAL FRAMEWORK AND MATHEMATICAL BACKGROUND

This chapter describes the mathematical techniques used in this thesis. The purpose of this chapter is to allow readers of this thesis to fully replicate and challenge the conclusions drawn here.

2.1. TECHNIQUES USED IN THIS THESIS

In this chapter we briefly describe how the guided modes of a multilayer thin film structure is calculated using pole method [29] . The dependency of the guided modes frequency to the optical thickness of the thin film is also shown in this chapter. Then we investigate the evolution of guided resonance when a shallow grating is introduced on top of the thin film. We use a conformally textured structure because due to technological processes most of the real thin film solar cells are textured conformally. To calculate the optical thickness of the thin film endowed with a shallow grating two approaches are introduced, effective index and equivalent thickness. We then show that using the effective index or the equivalent thickness are not reliable methods when the grating height is large and, thus, a different method is introduced. Further, we use the Fourier coefficients of the electric field inside the absorber to calculate the contribution of guided and non-guided resonance in total absorption. This approach employs finite element method to calculate the electric field inside the absorber using Maxwell equations. Knowing optical thickness of the grating structure is not required in this method.

2.2. COMSOL MODELLING

The absorption of light in a dielectric is proportional to the square of electric field inside the absorber via:

$$A = \epsilon_0 n \kappa \omega \int_S |E(x,y)|^2 dx dy \tag{2.1}$$

where n and are real and imaginary parts of the refractive index, respectively, ϵ_0 is the dielectric constant of vacuum, and ω is the angular frequency. The integral is over the entire volume of the absorber. Thus, knowing the electric field is necessary to calculate the absorptance spectrum inside a dielectric absorber. In this thesis we use COMSOL Multiphysics, a finite element analysis (FEA) solver, as a modelling tool to calculate the electric field in a thin film absorber. COMSOL has different modules for different applications. Since we are interested in understanding the light behaviour inside a thin film endowed with a wavelength-scale grating we use the Wave Optics Module which uses FEA to solve Maxwell equations in a complex structure. In this thesis, Frequency Domain Electromagnetic Field Modelling is employed to rigorously calculate the electromagnetic field inside the absorber. We use periodic boundary condition (Floquet periodicity) to deal with the periodicity of the structure. The structure is excited with plane waves either TE- or TM-polarized under different incidence angles (0, 10, 30 and 60 degrees). The absorber is made of nc-Si:H, therefore we need to consider material dispersion. In this respect, we use wavelength-dependent n and k data of nc-Si:H in our calculation [30]. The absorptance spectrum is calculated within the wavelength range between 400 nm to 1200 nm with the step of 1 nm using a frequency sweep in COMSOL. The maximum element size (meshing size) in the structure is chosen to be 10 nm to have at least 8 sampling points per wavelength in material. One of the objectives of this thesis is to distinguish between the guided and non-guided resonances in a periodically textured thin-film solar cell. In chapter 3 and chapter 4 we describe how to distinguish between the guided and non-guided resonances using the electric field inside the structure. But, first, let see how to calculate the guided modes of a flat thin film.

2.3. GUIDED MODES OF A MULTILAYER THIN FILM STRUCTURE

One of the methods to calculate the guided modes in a flat multilayer thin film is to use the poles resonance method [29, 31, 32] , also known as the *pole method*. In this method, the reflectance in a multilayer stack is defined recursively [29] and the guided modes are calculated by finding zeroes in the denominator of the reflectance formula. For a multilayer structure the recursive relation for reflectance is [29]:

$$r_{j+1} = \frac{f_{(j+1,j)} + r_j e^{-2i\phi_j}}{1 + f_{(j+1,j)} + r_j e^{-2i\phi_j}} \tag{2.2}$$

where is the ratio of the up going electric field to down going component; is the Fresnel coefficient at interface and it is calculated as follows:

$$f_{(j+1,j)} = \frac{\overline{n}_{j+1} - \overline{n}_j}{\overline{n}_{j+1} + \overline{n}_j} \tag{2.3}$$

and

$$\phi_j = \frac{(2\pi)\cos d_j \alpha_j n_j}{\lambda} \tag{2.4}$$

there, λ ,n_j , and d_j are the wavelength, the real part of refractive index, and the thickness of the j^{th} layer, respectively, and α_j is the angle of refraction within the j^{th} layer. Fur-

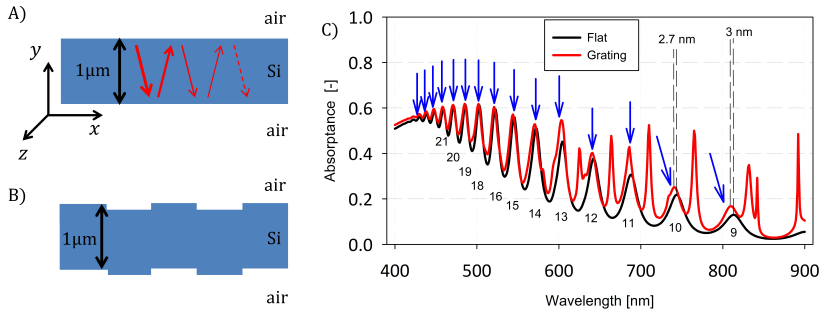

Figure 2.1: shows a 1 μm thick flat film and partial reflection of light inside the structure; B) Shows a shallow grating wave-guide with a total thickness of 1 μm at every point. The top and bottom gratings have the same period (600 nm), filling factor (0.5) and height (20 nm); Black line in C) represents the absorption in the flat film. The numbers below each peak indicate the related Fabry-Perot (FP) mode number. The red line shows the absorption in grating structure. Blue arrows indicate the FP resonance peaks in the grating structure.

thermore, $\overline{n}_j$ is the effective refractive index defined as $\overline{n}_j = \cos\alpha_j n_j$ for the s-component and $\overline{n}_j = n_j/\cos\alpha_j$ for the p-component [1]. Note that knowing the thickness of each layer is very important in calculating the guided modes of a multi-layer structure (equation 2.4). This holds true for the pole method or any other method which is used to calculate the guided modes of a thin film. As long as the structure is flat, measuring the thickness of the film is trivial. However, when working with a textured structure, the thickness needs to be redefined. To elaborate more on this, let us compare two structures. Consider a flat slab made of c-Si with a physical thickness of d equal to 1 μm (Figure 2.1 (A)). The optical thickness of this structure is equal to d time the refractive index n. In next step (Figure 2.1 (B)), we perturb the top and bottom interfaces with height and depth of 20 nm respectively. In this way the perturbation is very small and the physical thickness of the structure is unchanged. Both structures are simulated in COMSOL environment, illuminated by TE polarization (E_z) under normal incidence. Black and red curves in Figure 2.1 (C) show the absorption for the flat and textured slabs, respectively. The numbers below each black peak indicate the Fabry-Perot (FP) mode number of the flat structure and the blue arrows indicate the FP resonance peaks in the grating structure. The FP peaks in the textured structure is slightly shifted with respect to black curve. For example, the last FP peak in the flat structure (mode number 9) is located at 814 nm, whereas the last FP in the grating structure is located at 811 nm. This blue shift indicates that the optical thickness of the grating structure has been changed even though the physical thickness is unchanged.

The peaks position in flat structure can be calculated via:

$$\lambda_q = \frac{2dn}{q} \tag{2.5}$$

where d and n are the structure thickness and the real part of material's refractive index, q is the mode number, which is an integer larger than zero. According to equation 2.5 a

[1] Polarized light with its electric field paralle (perpendiclar) to plane of incidence is refered to as the p-component (s-component). TM (TE) polarized light is commonly also as p-component (s-component).

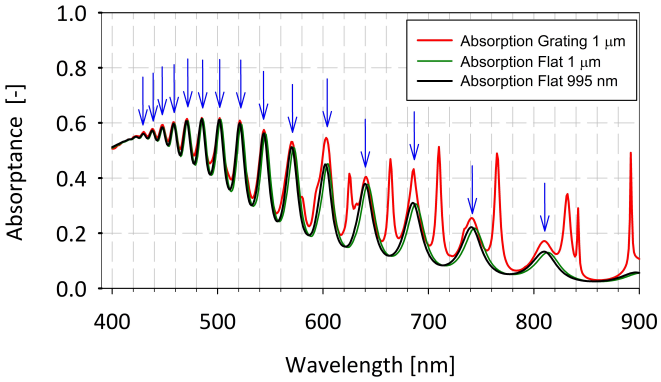

Figure 2.2: The red line represents the absorption in the grating structure. The green and black lines show absorption in flat structures with thickness of 1μm and 995 nm, respectively. The absorption due to FP resonance in the grating structure is pointed by the blue arrows. The position of these resonances is aligned with absorption peak positions in the film with thickness 995 nm. This means that the optical thickness of the grating structure is 5 nm thinner than its physical thickness.

small shift in FP peak position is associated with a change in thickness or refractive index of the film. Since the total thickness influences the absorption, this FP shift provides information about the equivalent thickness of the grating structure. To compensate for this shift, we propose two different approaches:

1. To focus on the flat structure and adjust its thickness such that it has the same FP peak position as the grating structure (*Equivalent thickness*).

2. To focus on the grating structure and adjust the grating parameters (height, duty cycle...) such that its FP peak position matches with the FP peak position in the flat structure (*Effective index*).

2.3.1. EQUIVALENT THICKNESS

The wavelength shift ($\Delta\lambda = \lambda_{max}^{grating} - \lambda_{max}^{flat}$) at the FP peak has a linear relation with the variation in thickness ($d\Delta = d_{equivalent} - 1000mn$) or change of refractive index ($\Delta n = n_{eff}(\lambda_{\max}^{grating}) - n_{Si}(\lambda_{\max}^{grating})$), but it has an inverse relation with the FP mode number (q):

$$\lambda \pm \Delta = d\Delta \pm \frac{2n}{q} \tag{2.6}$$

Therefore, the shift is more visible in longer wavelength (smaller q) that in short wavelength range (Figure 2.1 (C)). For this reason, we choose the $\Delta\lambda$ of the last FP peak position in Figure 2.1 (C) (mode number 9) to calculate the equivalent thickness.
Assuming that the refractive index and the mode number is unchanged within the range of $\Delta\lambda$, the $\Delta d = -5$nm, which consequently suggests the equivalent thickness of grating

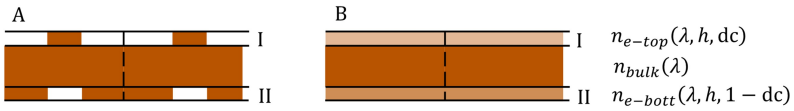

Figure 2.3: A) shows top and bottom grating layers for two periods. The layers are marked with I and II respectively. In B) the grating layers are translated to two uniform layers with different effective refractive indexes. The effective refractive depends on the grating height, filling factor and the wavelength of the light.

structure to be 995 nm. This means that, to calculate the guided modes in the grating structure, d_j in equation 2.4 should be equal to 995 nm rather 1000 nm. Figure 2.2 compares the absorption in grated and flat slabs (red and green lines, respectively) with thickness of 1μm with the absorption in a flat structure with thickness of 995 nm (black line). It is evident that the FP peaks in red and black lines are exactly aligned with each other. This shows that the equivalent flat thickness of the grating structure is 995 nm. It is interesting to note that notwithstanding the physical thickness of grating structure is 1 μm at any point, its optical thickness is smaller and provides a higher absorption than a thicker flat structure. In fact the grating structure exhibit additional absorptance peaks (to be discussed later)

2.3.2. EFFECTIVE INDEX

The 0^{th} order of diffraction does not *feel* the periodicity of the grating. In other words, for the 0^{th} order of diffraction the grating layer can be *seen* as a uniform medium with an effective refractive index. [33] The effective index depends on the height and the duty cycle of the grating and the wavelength of the light in the absorbing medium. [34] This concept can be used to explain the small FP shift in the grating structure with respect to the flat structure. Figure 2.3 (A) and (B) show how the top and bottom grating layers can be translated into a uniform material with an equivalent refractive index which depends on the grating parameters.

The effective medium approximation can be applied to calculate the effective refractive index of each layer if $\lambda >> L$, where L is the grating period and λ is the wavelength in vacuo. Since we are considering a wavelength-scale grating, this theory fails to predict the effective index correctly and cannot be applied [33, 34]. For a fixed grating height and a specific wavelength, the variation of duty cycle can change the effective index in top and bottom layers and consequently alter the FP peak positions. Therefore, we use numerical approach to change the effective refractive index of each layer. In our approach, the last FP peak position in the grating structure is observed, while the duty cycle is changed from 0.1 to 0.9 with the step of 0.1. The red dots in Figure 2.4 represent the variation of the last FP peak in grating structure with respect to different values of duty cycle. The position of the peak follows a reciprocal movement. This is because we change concurrently both top and bottom gratings and, thus, the effective refractive index of the top and bottom layers are complementary with of each other; so, they are identical for dc = 0.5. The red dashed line crosses the brown line (the last FP peak position in flat structure) when the duty cycle is at around 0.25 and 0.75, which means that for these two values of duty cycle the optical thickness of the grating structure is equal

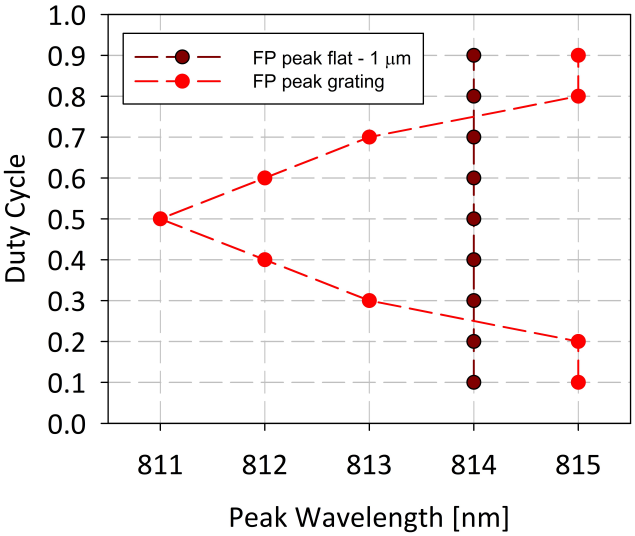

Figure 2.4: Red dashed line represents the movement of the last FP peak position (i.e. peak 9 in Fig.2.1) in the grating structure with respect to the variation of the grating duty cycle. The red dots show the calculation points. The brown dots indicate the position of the last FP resonance of a flat structure with thickness of 1mum. The FP peak position in the grating and at structures would be aligned where the dashed Red line crosses the dashed Brown line.

to the physical thickness of the flat structure. In Figure 2.5, the absorption pattern of a 1 μm thick flat film is compared with the absorption in grating structures with duty cycle of 0.25 and 0.75. As it can be observed from this figure, all the FP resonances for grating and the flat structure are aligned with each other.

Although, an *optically* thicker film, provides a larger FP absorption, the huge FP enhancement at 750 nm is hard to explain using equivalent thickness or refractive index approximation. The large enhancement in FP absorption at around 750 nm is probably due to the coupling between a FP resonance and one of the guided modes of the grating structure. So far, we were able to calculate the equivalent thickness or effective index of the grating structure because we chose not to perturb the flat structure much, by using a very shallow grating (grating height = 20 nm). If the grating height increases, then it is almost impossible to keep track of the changes in absorption. For example, Figure 2.6 shows absorption in a grating structure with grating height equal to 300 nm. The physical thickness of the structure is 1 μm (i.e. from the peak of the top grating to the pit of the bottom grating), identical to the thickness of flat structure (black curve). One can see that there is no correlation between red and black curves. Therefore, we have no mean to calculate the optical thickness of the structure with large grating (300 nm height) and consequently, calculating the guided modes of the structure is not reliable. Based on what is discussed, it is clear that the reliability of defining an equivalent flat structure for a grating waveguide does strongly depend on the grating parameters. Basically, when the grating height is large, neither thickness nor refractive index approximation is reliable

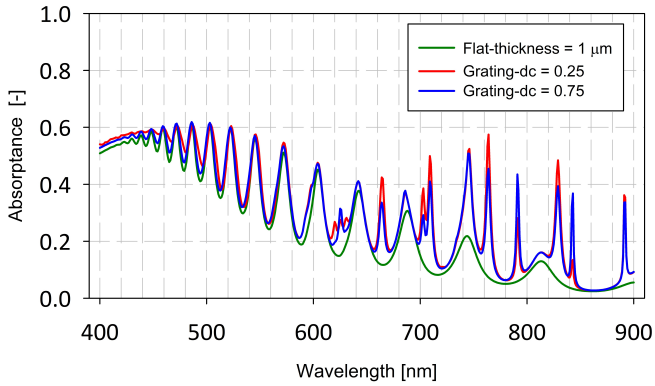

Figure 2.5: The red and blue lines represent the absorption in a 1μm thick grating structure with grating duty cycle equal to 0.25 and 0.75 respectively. The FP peak positions of these two structures are aligned with the FP peak positions of a flat structure with the same thickness. Value of the grating duty cycle can change the optical thickness of the grating structure by altering the effective refractive index of the grating layers.

anymore. Therefore, a different approach, independent of grating parameters or optical thickness of the structure, needs to be employed to associate an absorptance peak with a diffraction order. In this thesis we propose to decompose the total absorption into the absorptions related to each diffraction order. This semi-analytical method is based on the fact that electric field inside a periodically textured structure is also periodic and therefore can be decomposed using a Fourier series approach.

2.4. CALCULATING TOTAL ABSORPTION USING THE ELECTRIC FIELD SPECTRUM

Any periodic function can be decomposed into weighed sum of simple oscillating functions [35]. In a mathematical form, periodic function $f(x)$ can be written as:

$$f x = \sum_{q=-\infty}^{+\infty} c_q e^{\frac{i(2\pi q)x}{L}} \tag{2.7}$$

where is the q^{th} Fourier coefficient and L is the period [2]. $f(x)$ can be replaced with plane wave electric field inside the absorber, but we need to take into account that electric field is a function of position, wavelength and incidence angle. Therefore, the Fourier series of the electric field becomes:

$$E\left(x, y, \lambda_0, \theta_i\right) = \sum_{q=-\infty}^{+\infty} c_{(y,q,\lambda_0,\theta_i)} e^{j\left(\frac{2\pi}{\lambda_0}\sin\theta_i \pm q\frac{2\pi}{L}\right)} \tag{2.8}$$

where and are incidence wavelength in vacuo and angle, respectively. The argument of the exponential part in equation 2.8 is basically the algebraic sum of grating vector and

[2] It is importan to mention that we are working with wavelength scale structures which mean $L \approx \lambda_0$

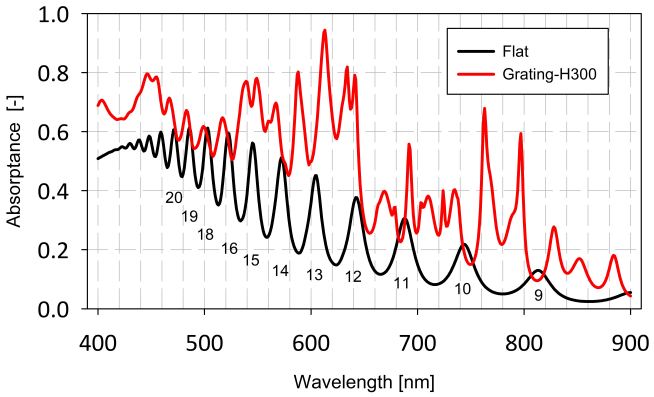

Figure 2.6: Comparing the absorption in a flat (black) and grating structure (red). The structures have identical physical thickness (1 um), the grating has a height of 300 nm with duty cycle 50 %.

the x component of propagation vector in incident medium. So far, we have not made any link between the Fourier series of the electric field and the absorption of light in the absorber.
The absorption of light in a dielectric is calculated using equation 2.1. Since we are studying a 1-D grating, the electric field does not depend on z axis (see Figure 2.1). Thus, equation 2.1 can be reduced to:

$$A_l = \varepsilon_0 n \kappa \omega \int_s |E(x,y)|^2 dxdy \tag{2.9}$$

where A_l is the absorption per unit length and the integral is over the cross section of the structure. To express equation 2.9 in Fourier terms, next step is to obtain $|E(x,y)|^2$ by multiplying both sides of equation 2.8 to its complex conjugate:

$$E\left(x,y,\lambda_0,\theta_i\right) E\left(x,y,\lambda_0,\theta_i\right)^* = \sum_{q=-\infty}^{+\infty} c^*_{(y,q,\lambda_0,\theta_i)} c_{(y,q,\lambda_0,\theta_i)} e^{\left(j\frac{2\pi}{\lambda_0}\sin\theta_i \pm q\frac{2\pi}{L}\right)} e^{\left(-j\frac{2\pi}{\lambda_0}\sin\theta_i \pm q\frac{2\pi}{L}\right)} \tag{2.10}$$

which is equal to:

$$\left|E\left(x,y,\lambda_0,\theta_i\right)\right|^2 = \sum_{q=-\infty}^{+\infty} \left|c_{(y,q,\lambda_0,\theta_i)}\right|^2 \tag{2.11}$$

To derive equation 2.9, both sides of equation 2.11 needs to be multiplied by and integrated over one period of the structure:

$$\epsilon_0 n \kappa \omega \int_s \left|E\left(x,y,\lambda_0,\theta_i\right)\right|^2 dxdy = \epsilon_0 n \kappa \omega \int_s \sum_{q=-\infty}^{+\infty} \left|c_{(y,q,\lambda_0,\theta_i)}\right|^2 dxdy \tag{2.12}$$

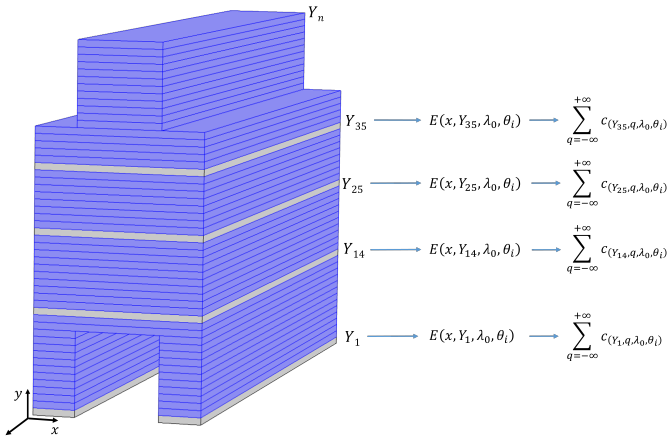

Figure 2.7: the grating structure is divided into many thin sub-layers. Within one sub-layer, the electric field is considered to be invariant along the y-axis. The number of sub-layers influence the accuracy of the calculation.

The left-hand side of the equation 2.12 is total absorption per unit length in the dielectric at frequency ω (wavelength λ_0). The right-hand side, however, represents the total absorption for all the components of electric field spectrum (diffraction orders). Additionally, since each $\left|c_{(y,q,\lambda_0,\theta_i)}\right|^2$ is a number, the integral on the right side of equation 2.12 is the surface area of the cross section of one period of the grating (area marked as c-Si in Figure 2.8) :

$$A_{total}(\lambda_0,\theta_i) = \epsilon_0 n\kappa\omega \sum_{q=-\infty}^{+\infty} \left|c_{(y,q,\lambda_0,\theta_i)}\right|^2 s = \sum_{q=-\infty}^{+\infty} A_q(\lambda_0,\theta_i) \tag{2.13}$$

where A_q is the absorption by the q^{th} diffraction order. From equation 2.8 to equation 2.13 we have done only analytical calculations assuming that that the electric field inside the absorber is a continuous and known function. In reality, the electric field has to be either measured or calculated rigorously. In both scenarios, the electric field is known only at the measurement or calculated points. For any point between two adjacent measurement / calculation points, the electric field is assumed to be unchanged. In other word the electric field is discretized and thus equation 2.13 needs to be modified according to a discreet electric field.

2.5. DIVIDING THE STRUCTURE INTO SUB LAYERS

Every Fourier coefficient in equation 2.12 has a dependency on y. In other words, for each y in the absorber, there is an infinite number of coefficients. This means that to be able to calculate total absorption, we need to slice the structure into many thin sub layers along y direction (see Figure 2.7). Then the electric field at each sub-layer would depend on x and it can then be transformed into its Fourier components.
The electric field is considered to be invariant within one thin sub-layer along y axis. Therefore, to obtain a higher accuracy more sub-layers are needed. The thickness of

each sub-layer is defined such that, for the shortest wavelength-in-material ($\lambda = \lambda_0/n$) within the spectral range of interest, there are at least 10 sub-layers along one wavelength (see Chapter 4). Note that for perpendicular incidence having five sub-layers are sufficient to reach accurate calculation (see Chapter 3). Since, in this thesis, we are interested in wavelength range between 400 nm to 1200 nm, the thickness of sub-layers is defined to be 10 nm and 5 nm for normal and oblique incidence, respectively. The reason for this difference in the thickness of sub-layers under normal and oblique incidence is described explicitly in section 4.2).

2.6. CALCULATING THE ELECTRIC FIELD IN GRATING STRUCTURE USING COMSOL

In Chapter 3 and 4 we study two grating structures with two different grating heights. The results presented in those chapters are obtained by applying our method to calculate the contribution of each diffraction order in total absorption. The field is calculated using COMSOL Multiphysics which is a modelling software based on finite element method. Figure 2.8 illustrates the geometry and the boundary condition used to calculate the electric field. Figure 2.8 (A) shows the structure with large grating (height 300 nm) whereas Figure 2.8 (B) represent the shallow grating with height of 20 nm. The duty cycle (50%) and the period (600 nm) of the grating are the same for both structures.The top and bottom media are assumed to be very thick and thus no energy is reflected from top and bottom boundaries.

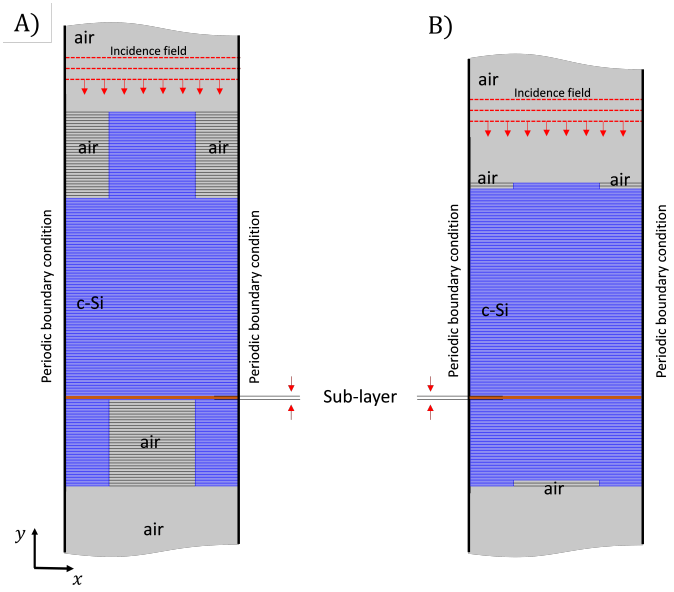

Figure 2.8: Unit cell configuration for two grating structures with the period of 600 nm and the duty cycle of 50%. The unit cell consists of two material, air and nc-Si:H: A) the grating height is 300 nm; B) grating height is 20 nm.

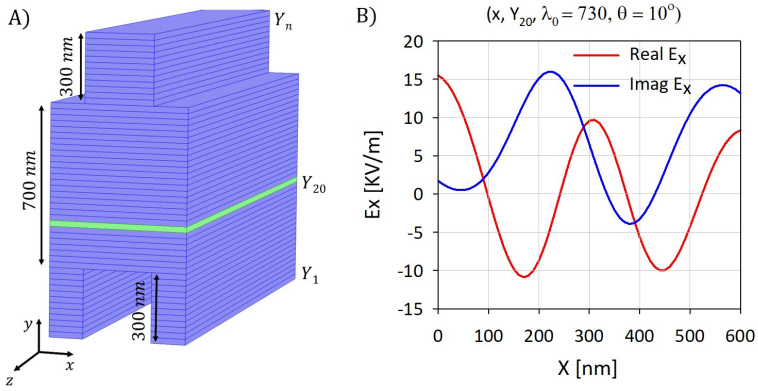

Figure 2.9: A) One period of the grating structure, divided into N thin sub-layers with thickness YN. B) Intensity of the E_x component of the total electric field in the 20^{th} sub-layer, indicated in green in A), at λ_0 = 730 nm and at 10° angular incidence

For the left and right boundaries, Floquet periodicity is enforced and the incidence wavelength range is between 400 nm and 1200 nm. For the absorber, we need to consider material dispersion, thus we use wavelength-dependent n and κ data of nc-Si:H in our calculation [30]. As it has been shown in Figure 2.8, the structure is divided into many sub-layers. Using these inputs, we can rigorously calculate each component of electric field (E_x, E_y, E_z) inside the absorber. Then, we can extract the real and imaginary parts of each component at the boundary of each sub-layer (sub-boundary). Figure 2.8 (A) shows one period of large grating and its sub-layers. The real and imaginary parts of the electric field in the 20^{th} sub-layer (indicated in green) at λ_0 = 730 nm and at 10° angular incidence is presented in in Figure 2.9 (B). For our Fourier analysis we need to have the complex electric field, therefore, the input for equation 2.12 is the complex electric field.

2.7. APPLYING FOURIER TRANSFORM AND CALCULATING THE ABSORPTION

With the electric field calculated in COMSOL, we can use equation 2.12 or 2.13 to calculate the absorption for each diffraction order. The electric field calculated by COMSOL is a discrete set of data whereas equation 2.13 is for a continuous function. Therefore, equation 2.13 needs to be adjusted:

$$A_{total}(\lambda_0,\theta_i) = \epsilon_0 n\kappa\omega \sum_{q=-\infty}^{+\infty} \left|c_{(y,q,\lambda_0,\theta_i)}\right|^2 s = \sum_{q=-\infty}^{+\infty} A_q(\lambda_0,\theta_i) \tag{2.14}$$

where Δy is the thickness of each sub-layer and Δx is the size of meshing in x direction in COMSOL which is set to 2.5 nm. Now, using equation 2.14 and the electric field calculated by COMSOL, we can calculate the contribution of each diffraction order in total absorption without knowing the optical thickness of the grating structure. Calculation sequence is presented in Figure 2.10. Each step is labelled by a number. Each row repre-

sents actions in one sub-layer; summing the absorption at each sub-layer (vertical sum) results in total absorption for each diffraction order in one unit cell. Our purpose is to arrive at row 4, where absorption for each diffraction order is shown. At the end, total absorption (row 5) should be equal to the absorption calculated directly by COMSOL. In Chapter 3 and 4 we show that in fact this is the case and thus the accuracy of our method is reasonably high.

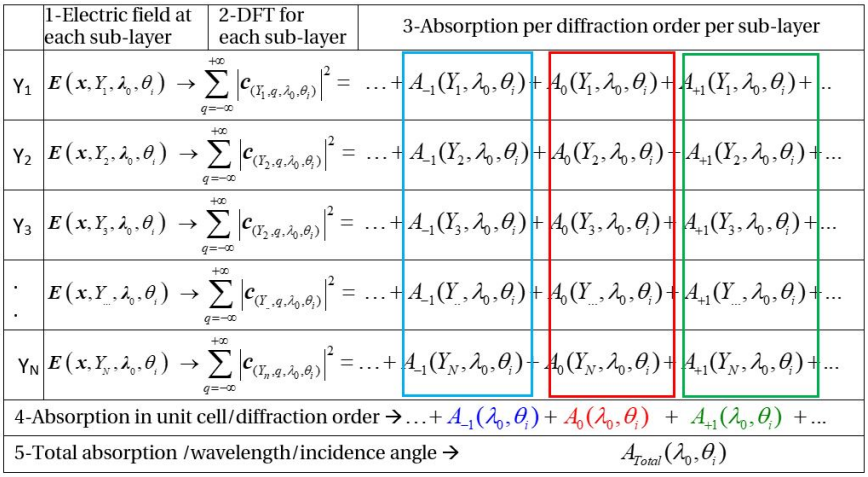

Figure 2.10: Decomposing total absorption into absorption by each diffraction order in a grating structure. Each row represents sequence of actions for one sub-layer. Summing through columns provides absorption for one unit cell.

2.8. THE DENSITY OF MODES (DOM)

It has been previously addressed that one of the main goals of light trapping is to enhance the light absorption as much as possible. For weakly absorbed, long-wavelenght photons, the longer light-matter interaction time is , the higher the absorption is. This indicates that at any absorption peak the group velocity is probably small. The group velicity has inverse relation with the density of optical modes withn the frequency $[\omega, \omega+\Delta\omega]$.To confirm this, we need to calculate the density of the mode (DOM) [3] in the structure at absorption peak because DOM is the inverse of group velocity. Thus, the DOM should be large at an absorption peak. The DOM can be calculated using the complex transmission confidents of the structure [36].

$$DOM(\omega) \equiv \frac{d\kappa}{d\omega} = \frac{1}{d}\frac{y'x - x'y}{x^2 + y^2} \tag{2.15}$$

where x and y are the real and imaginary parts of the transmission coefficient [37] respectively and the prime denotes differentiation with respect to ω. The transmission

[3] The density of modes is the number of solutions to maxwell equations for a particular frequency and for a especific waveguide (boundary condition).

coefficients can be calculated numerically at the same time as the electric field. Therefore, we can check whether or not a peak in absorption matches with a peak in DOM. In section 4.3.2.1 the DOM is calculated for a large grating structure. The DOM peaks match with the absorption peaks in the structure.

2.9. TEMPORAL COUPLED-MODE THEORY (TCMT)

Presence of grating on top of a dielectric wave-guide can be seen as a gate which lets the incident light to couple into one of the resonances of the system. According to the reciprocity principle, each resonance can also couple out and escape from the wave-guide via grating. The time evolution of a resonance with amplitude a and resonant angular frequency ω_0, can be described as follows using the temporal coupled mode theory [27, 28, 38, 39].

$$\frac{d}{dt}a = a\left(\mathrm{j}\omega - \frac{1}{2}\left(\mathrm{N}\gamma_\mathrm{e}+\gamma_\mathrm{i}\right)\right) + j\sqrt{\gamma_e}S \tag{2.16}$$

where S is the amplitude of an external source, $j = \sqrt{-1}$, and are described as external coupling and internal loss rate, respectively. N is the number of output ports which is equal to the number of reflection orders of the grating. Replacing $a(t) = a(\omega)\exp(j\omega t)$ [4] in equation 2.16, the absorption spectrum can be calculated as:

$$A(\omega) = \gamma_i \frac{|a(\omega)|}{|S(\omega)|} = \frac{\gamma_e\gamma_i}{\frac{1}{4}\left(\mathrm{N}\gamma_\mathrm{e}+\gamma_\mathrm{i}\right)^2 + (\omega-\omega_0)^2} \tag{2.17}$$

For high frequencies, material absorption is very large and thus $\gamma_i >> \gamma_e$. This means that most of the incident energy is absorbed by the material and has very small chance to escape the structure. For low frequency however, the material is weakly absorbing and thus absorption rate is much lower than the coupling rate. In this case, $\gamma_e >> \gamma_i$ is called over coupling regime. It has been shown [28] that upper limit for total absorption in over coupling regime can be calculated as:

$$A_T = \frac{2\pi}{\Delta\omega \mathrm{N}} \sum_m \gamma_{i,m} \tag{2.18}$$

where the summation is over all resonances, m, in the frequency range of $[\omega, \omega+\Delta\omega]$ and $\gamma_{i,m}$, being the absorption rate for the m^{th} resonance. In an isotropic bulk material with absorption coefficientα, the absorption rate, γ_i , is identical for all resonances and can be given by:

$$\gamma_i = \alpha v = \alpha\frac{c}{n} \tag{2.19}$$

where is the light velocity inside the material and n is real part of the refractive index. For a thick structure where $d >> \lambda$, each resonance can be approximated as a propagating plane wave in bulk structure [28]. Therefore, total absorption can be given as:

[4] $a(t)$ represents an oscillating function with amplitude $a(\omega)$. This function can closely represent an electromagnetic field which oscillates with angular frequency ω and has the amplitude of " a". This is the simplest way to represent an oscillating field [27, 28, 38].

$$A_T = \frac{2\pi\gamma_i}{\Delta\omega} \cdot \frac{M}{\mathrm{N}} \tag{2.20}$$

where M is the total number of resonances in the structure. Dividing both sides of equation 2.20 by $\alpha.d$ (one pass absorption), the maximum enhancement factor is derived as:

$$F = \frac{A_T}{\alpha d} = \frac{2\pi\gamma_i}{\alpha d\Delta\omega} \cdot \frac{M}{\mathrm{N}} \tag{2.21}$$

This equation, which was first provided by Yu et al [27], is the main result of temporal coupled-mode theory for obtaining maximum absorption enhancement in grating structures. Each diffraction order could excite different set of resonances. Therefore, by counting the number of resonances that are excited by the q^{th} diffraction order, we can decompose the total enhancement factor based on grating diffraction orders as following:

$$F = \frac{2\pi\gamma_i}{\alpha d\Delta\omega \mathrm{N}} \sum_q M_q = F_0 + F_1 + F_2 + ... \tag{2.22}$$

Parameters M_q and N are strongly dependent on few parameters such as grating period, system dimension, number of interfaces and the wavelength of light. Thus, they have to be calculated separately according to the structure. Chapter 5 describes the details for calculating the maximum number of resonance excited by each diffraction order. That chapter also investigates the number of resonances in a structure with double side texturing.

2.10. COUNTING THE NUMBER OF RESONANCES IN A PERIODIC STRUCTURE

As we just addressed, the outcome of equation 2.21 depends on both M and N. The number of channels (N) is the reflection orders from all open interfaces in the structure. An open interface is defined as an interface that allows light to get in or get out of the structure. For example, if the absorber is attached on a reflector, like in most solar cells architectures, then there will be only one open interface (the top one). The number of resonance (M) is the maximum number of modes that are supported by the structure. In structures with 2-D grating M depends on the lattice type, lattice constant at each interface and the thickness of the structure. Therefore, in structures with 2-D grating, the maximum absorption enhancement needs to be calculated case by case. However, for 1-D grating, M depends on the texturing period at each interface and the thickness of the structure. Therefore, it is possible to derive a closed formula for maximum absorption enhancement in 1-D grating structure. Detailed mathematical calculation to obtain total number of resonances for each diffraction order in a 1-D grating structure is presented in Chapter 5. There, we also study the influence of thickness, period and number of textured interfaces on the total number of resonances.

3

DISTINGUISHING BETWEEN NON GUIDED MODES: NORMAL INCIDENT

This chapter is based on the following publication:

H. Ahmadpanahi, R. Vismara, O. Isabella and M. Zeman, "Distinguishing Fabry-Perot from guided resonances in thin periodically-textured silicon absorbers," Opt. Express **26**, A737-A749 (2018).

Abstract: Periodic texturing is one of the main techniques for light-trapping in thin-film solar cells. Periodicity allows for the excitation of guided modes in the structure and, thus, largely enhances absorption. Understanding how much a guided resonance can increase the absorption is therefore of great importance. There is a common method to understand if an absorption peak is due to the excitation of a guided mode, using dispersion diagrams. In such graphs, a resonance is identified as the intersection of a guided-mode-line of a uniform waveguide (with the same optical thickness as the grating structure) with the centre of a Brillouin zone of the grating. This method is unfortunately not reliable when the grating height is comparable with the thickness of the wave-guide, or when the thickness of the wave-guide is much larger than the wavelength. In this work, we provide a novel approach to calculate the contribution of a guided resonance to the total absorption in a periodic wave-guide, without using the dispersion diagram. In this method, the total electric field in the periodic structure is described by its spatial frequencies, using a Fourier expansion. Fourier coefficients of the electric field were used to calculate the absorption of each diffraction order of the grating. Rigorous numerical calculations are provided to support our theoretical approach. This work paves the way for a deeper understanding of light behaviour inside a periodic structure and, consequently, for developing more efficient light-trapping techniques for solar cells applications.

3.1. INTRODUCTION

Semiconductor materials fail to absorb low energy photons efficiently, especially in case of indirect band gap. This means that the quantum efficiency of a semiconductor device drops dramatically close to the materials band gap. In some applications, such as photovoltaics (PV), the absorption of every single photon is important for improving the device conversion efficiency. In materials with a low absorption coefficient near their band-gap, a low-energy photon has to travel a relatively large distance before it is absorbed. Therefore, one can either choose the absorber thickness to be (much) larger than the penetration depth of photons at a specific wavelength, or to deploy light management techniques to increase light capturing. Although increasing the absorber thickness might increase light absorption, it does not necessarily improve the efficiency of corresponding semiconductor devices, since photo-generated charge carriers have to be collected at the contacts. Moreover, in applications like solar cells material cost represents almost 40% of the final cell cost [40]. Additionally, it is very impractical to use thicker layer to absorb, for example, a photon with wavelength 1200 nm using crystalline silicon (c-Si). In that case, an absorber thickness of almost 1 meter would be required [41]. Therefore, it is more practical, economic and efficient to employ light management techniques to absorb a wide range of wavelength using the thinnest possible absorber. Depending on the application, there are many different approaches for light management. In this article, we limit ourselves to light management techniques applied to thin-film hydrogenated nano-crystalline silicon (nc-Si:H) solar cells. This material was chosen because its technology is well developed, its efficiency does not vary much from cell to module, and its indirect band gap makes it a useful test bed for assessing the quality of light management techniques [42]. Light management covers a wide range of techniques that aim to maximize the in-coupling and absorption of solar radiation in the absorber layer [17]. This can be achieved by: (i) efficiently using the solar spectrum, employing multi-junctions [23, 43–45] or spectrum splitters [46–48]; (ii) enhancing light in-coupling by applying anti-reflection (AR) coatings [49–51] or sub-wavelength textures [52, 53]; (iii) using low optical loss back reflectors to avoid light dissipation [54–59]; (iv) minimizing absorption is supporting layers [60–63] (v) promoting light scattering or diffraction by deploying wavelength-scale random [54, 55, 64] or periodic [27, 64–67] texturing, respectively. Random texturing allows the excitation of all modes in the absorber, whereas periodic texturing gives the possibility to excite discrete resonances such as guided modes. Since most of the energy of a guided mode is confined inside the guiding layer [68] for relatively long distances, guided mode excitation leads to a large enhancement of the absorption. In case of a periodic grating, each diffraction order can excite a resonance in the thin film, which is identified by a peak in the absorption diagram. Therefore, understanding the origin of absorption peaks is instrumental in developing more effective light trapping techniques [68–74]. In thin films endowed with gratings, the most common method to identify the origin of a resonance is to check, in a dispersion diagram, the crossing point between the wave-guided modes of a flat wave-guide and the centers of Brillouin zones of the grating. Where such an intersection occurs, the excitation of a guided mode is triggered, resulting in a particular absorption peak [74]. In this contribution, such technique is called the intersection method, and presents a number of shortcomings. The dispersion diagram of a waveguide strongly depends on the thickness, material, interface pro-

file, and the surrounding material of the waveguide. Usually, the effective waveguide thickness increases due to the penetration of electromagnetic fields – to a finite extent – into the surrounding media. This influences the accuracy of the dispersion diagram. Moreover, applying texturing leads to distortion of the mode diagram of a flat waveguide. If the grating height is large with respect to the waveguide thickness, the distortion could be significant, and the intersection method cannot predict the guided resonance. The issue is particularly evident for TM polarization [75]. Additionally, if the absorber supports many number of modes in a wide range of wavelengths, as in the case of thin-film solar cells, guided mode lines in the dispersion diagram become very dense. It thus become challenging to trace a guided mode using the intersection method. Finally, if an absorption peak is the result of multiple mode excitations, this method fails to define the contribution of each resonance in total absorption. In this article we provide a different method to overcome the limitations of intersection method and to deliver a deeper understanding of light behavior inside a periodic wave-guide. In this method, Fourier expansion is employed to decompose the electric field inside the absorber and to calculate the contribution of each resonance in enhancing the total absorption in a thin-film, for the entire wavelength range of interest. This article is organized as follows: in section 3.2, we describe the limitation of the intersection method more explicitly and we define the framework of our new approach. In section 3.3, we describe the theory used to derive the absorption of each diffraction order. In section 3.4, we provide the simulation results obtained by applying the theory and eventually in the final section we draw our conclusion.

3.2. METHODOLOGY

Consider a flat 1 μm thick nc-Si:H film, illuminated with TE-polarized light under normal incidence and in the wavelength range between 400 nm and 900 nm (Figure 3.1 (A)). In the uniform film of Figure 3.1 (A), partially reflected light bounces between the two flat interfaces and, in case of constructive interference, a Fabry-Perot (FP) resonance occurs. Absorption in this structure is shown by the green-dashed line Figure 3.1 (C). To increase the optical performance, one can apply an AR coating or a sub-wavelength texture to the top surface, to increase light in-coupling, and simultaneously prevent light dissipation by adding a good back reflector at the back side. According to reciprocity principle, increasing light in-coupling raises the chance of light out-coupling as well. The presence of a back reflector strongly enhances absorption, but only for specific wavelengths (where constructive interference occurs). Moreover, based on Snell's law, the angle of refraction inside the structure can never exceed the critical angle (of total internal reflection). Therefore, as long as the system is optically flat and the direction of illumination is perpendicular to the surface, light can never be trapped inside the film. From light management perspective, the motivation for adding the periodicity is to confine the incident energy in the absorber, by exciting the guided modes of a structure such as the one illustrated in Figure 3.1 (B). Both flat and textured structures are surrounded by air and are made of nc-Si:H. The textured structure has the same physical thickness as the flat film, and it is illuminated under the same conditions. The optimized grating period for thin-film applications is usually defined by the material band-gap [76], which is around 1100 nm for nc-Si:H.

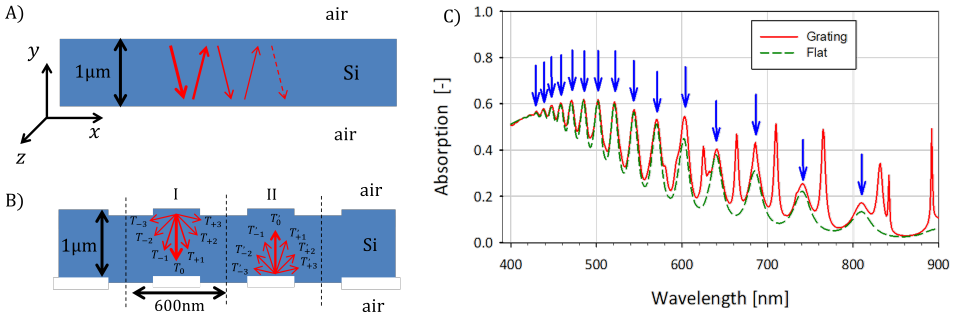

Figure 3.1: A) 1 μm thick nc-Si:H film and partial reflection of light inside the structure. B) A nc-Si:H waveguide, endowed with conformal gratings and characterized by a total thickness of 1 μm at every point. Region I and II show light scattering from each interface. T_i and T_i' are the transmission and reflection from the top and bottom interfaces, respectively. C) Absorption in the flat film (dashed–green line), and in the grating structure (red line). Blue arrows indicate FP resonance peaks.

In this work, we aim to track different guided modes and study their contribution to total absorption. To make our model as simple as possible, we avoid exciting an excessive amount of modes by choosing a grating period of 600 nm. Additionally, to study the evolution of guided modes with respect to FP resonances, we want to avoid disturbing the guided modes of the flat structure. Thus, a shallow grating with a height of only 20 nm was initially chosen. Later, investigation of taller structures (300 nm) will be also carried out. The duty cycle (dc) of the grating is fixed to 0.5. The absorption in the shallow grating structure is shown by the solid-red line in Figure 3.1 (C) and exhibits a clear enhancement with respect to the flat structure. Intuitively, two different types of peaks can be recognized in this curve: the first is very similar to the peaks in the green-dashed curve (flat case). These peaks, indicated by blue arrows, are associated with FP resonances in the grating structure, because their peak positions are the same as the ones of FP resonances in the flat structure. The second types of peaks are sharp and narrow, occurring where there is low absorption in the green-dashed curve. These peaks are most probably the result of the excitation of guided modes via the grating. This hypothesis can be verified using the intersection method. Figure 3.2 (A) shows the dispersion diagram of the flat structure in Figure 3.1 (A), in the wavelength range between 700 nm and 850 nm. Open circles indicate the intersection of a guided mode (blue line) and the center of one Brillouin zone (grey horizontal lines). The wavelength of each intersection Figure 3.2 (A) corresponds with absorption peaks in Figure 3.2 (B). It is apparent that this method can, to some extent, confirm that a particular absorption peak is matched with one of the grating orders. However, it does not provide any information about the relative weight of an excited mode in total absorption coupling [77]. This is important because, in a grating structure such as the one of Figure 3.2 (B), the field scatters into many discrete angles after passing through the first interface. T_i and T_i' are the transmission and reflection from the top and bottom interfaces, respectively. The region which is marked by I shows scattering from the first interface. Scattered field from top surface (T_i in region I) travels through the film and reaches the second interface. Due to the periodicity of the bottom surface, each diffraction order of top surface can further diffract into all available

diffraction orders (T_i' in region II). For example, T_{+2} from the top interface can produce all T_i' orders when it reaches the second interface. This multiple scattering allows the energy to couple from one mode to another, creating an absorption peak which is the result of multiple mode excitations. If the height of grating is small (with respect to the wave-guide thickness), the presence of the grating can be seen as a small perturbation in the refractive index or in the geometry of the wave-guide [78]. This means that the dispersion diagram of the perturbed wave-guide is very similar to the one of flat wave-guide. If the grating height is large, the dispersion diagram of the grating wave guide might differ significantly from the one of flat structure, and the intersection method does not provide reliable result. All these suggest that a different method or tool is needed to enable the analysis of thin-film structures endowed with grating. This can help to have a better understanding of light trapping and absorption in the area of thin-film solar cells.

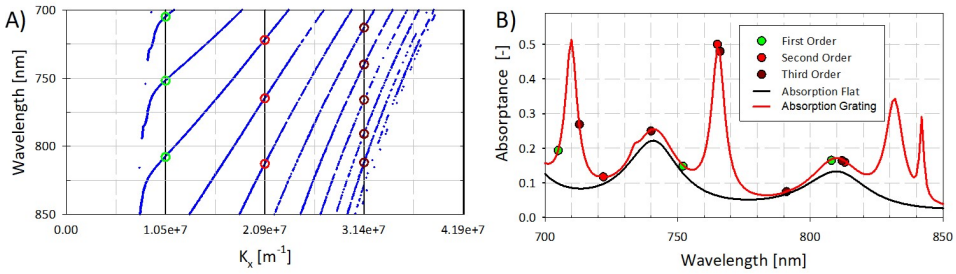

Figure 3.2: A) Dispersion diagram of the flat structure. Vertical axes show the wavelength of light and horizontal axis represents the order of Brillouin zones and the corresponding value of k_x. Blue lines show the position of guided modes in the flat structure, while the open circles indicate where they intersect with the centers of Brillouin zones. B) Absorptance spectra between 700 nm and 850 nm. Circles on the grating absorption (red) curve correspond to intersections between the centers of Brillouin zones of the grating and a guided mode of the flat structure in (A).

3.3. THEORETICAL BACKGROUND

Absorption in a dielectric with volume V is proportional to the integral of the squared magnitude of the electric field over the volume of the material. Since we are modelling a 1-D grating, the integral over a surface S can be considered:

$$A = \epsilon_0 n \kappa \omega \int_S |E(x,y)|^2 dx dy \tag{3.1}$$

where n and κ are real and imaginary parts of the refractive index, respectively, ϵ_0 is the dielectric constant of vacuum, and ω is the angular frequency. The grating vector (periodicity) is along the x direction, while the y axis is along the thickness of the film (see Figure 3.3 (A)). Since the structure is periodic, the electric field inside the film can be expanded using a Fourier expansion [79]. Generally, this can be done by diving the grating structure into many small sub-layers along the y direction (horizontal lines marked with Y_i in Figure 3.3 (A)). For shallow gratings, we only consider the uniform part of the structure (light blue region in Figure 3.3 (A)). For large grating structures, however, the

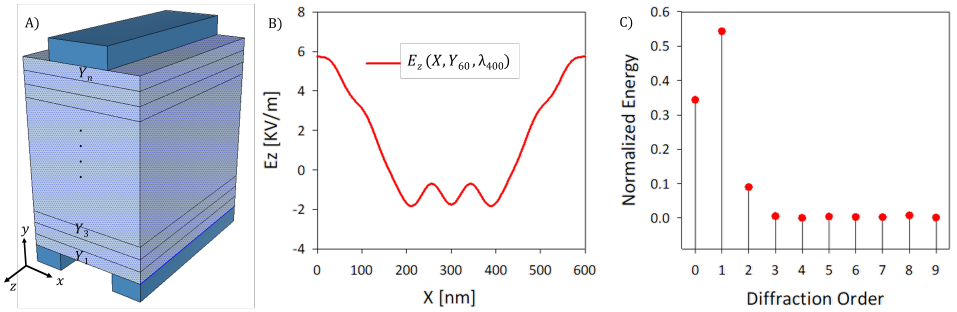

Figure 3.3: A) One period of the grating structure. The light blue region is the uniform part of the film, which is divided into i thin sub-layers, each with thickness Y_i. B) Intensity of the TE-polarized electric field in the 60^{th} sub-layer, at $\lambda_0 = 400nm$. C) First 10 orders of energy spectral density for the electric field, in sub-layer 60 at $\lambda_0 = 400nm$. The energy is normalized by the total energy in one sub-layer.

top and bottom grating rims are also taken into account. The structure (large grating) is divided into top, middle and bottom parts. Top and bottom parts are shown in dark blue color in Figure 3.3 (A), and middle part is shown in light blue color. Each part is then divided into many thin sub-layers. The number of sub-layers is defined such that for the shortest wavelength-in-material ($\lambda = \lambda_0/n$) within the spectral range of interest, there are at least five sub-layers along one wavelength. In this way, for each wavelength there are at least 5 sampling points in the material. For each wavelength and polarization, the electric field can be then described as:

$$E(x, y, \lambda_0, \theta_i) = \sum_{q=-\infty}^{+\infty} c_{(y,q,\lambda_0,\theta_i)} e^{j\left(\frac{2\pi}{\lambda_0}\sin\theta_i \pm q\frac{2\pi}{L}\right)} \tag{3.2}$$

where, $j = \sqrt{-1}$ q and L are grating order and periodicity, respectively, $c_{(y,q,\lambda_0,\theta_i)}$ is the q^{th} Fourier coefficient of the electric field with wavelength λ_0 in the sub layer for the incidence angle equal to . Figure 3.3 (B) shows the TE polarized electric field profile for the60^{th} sub-layer at 400 nm. Multiplying Equation 3.2 by its complex conjugate and integrating over one period (i.e. applying Parseval's theorem), we arrive to the energy of the electric field in one sub-layer [80].

Figure 3.3 (C) illustrates the energy spectrum of the electric field up to 10 orders, for $\lambda_0 = 400nm$ in the 60^{th} sub-layer. In other words, such diagram exactly shows how the total energy in the 60^{th} sub-layer is distributed within different diffraction orders of grating. The symmetry of the electric field implies a symmetry in energy distribution, that is $T_{-i} = T_{+i}$. Therefore, the total energy in T_i is actually equal to $T_{-i} + T_{+i}$. For example, in Figure 3.3 (C), the first diffraction order contains 55% of the total energy, meaning that $T_{-1} = T_{+1} = 27.5\%$ of the total energy. Summing the energy of all sub-layers, we end up with the total electric energy stored in one period of the grating (L):

$$\int_0^y \int_0^L |E(x, \lambda_0, \theta_i)|^2 dx dy = \sum_{\mathbf{i=y_1}}^{\mathbf{i=y_n}} \sum_{\mathbf{q=-\infty}}^{\mathbf{q=+\infty}} \int_0^L \left|c_{i,q,\lambda_0,\theta_i}\right|^2 dx \tag{3.3}$$

The left-hand side of equation 3.3 represents the total electric energy in one period, while

the right-hand side of this equation describes the distribution of energy per each diffraction order in one period. Multiplying both sides of equation 3.3 by $\epsilon_0 n\kappa\omega$ yields:

$$\epsilon_0 n\kappa\omega \int_0^y \int_0^L |E(x,\lambda_0,\theta_i)|^2 dxdy = \epsilon_0 n\kappa\omega \sum_{\mathbf{i=y_1}}^{\mathbf{i=y_n}} \sum_{\mathbf{q=-\infty}}^{\mathbf{q=+\infty}} \int_0^L \left| c_{i,q,\lambda_0,\theta_i} \right|^2 dx \tag{3.4}$$

Where the left-hand side is the total absorption, while the right-hand side represents the total absorption in terms of diffraction orders. $|c_{(y,q,\lambda_0,\theta_i)}|^2$ is a function of θ_i, which implies that each Fourier component of electric field varies based on the incidence angle. Therefore, for each incidence angle, equation 3.4 needs to be applied. In this work, θ_i is considered to be zero and thus further on we omit the sub-index of θ_i. The electric file inside the absorber is the input for equation 3.4. This means that the electric field distribution inside the absorber has to be calculated separately using a rigorous electromagnetic simulation tool at optical frequencies. This rigorously-calculated electric filed then is used to calculate the Fourier coefficients.

3.4. RESULTS AND DISCUSSION

Equation 3.4 is used to study the absorption pattern of the structure of Figure 3.1 (B), with two different grating heights: 20 nm (shallow structure, H20) and 300 nm height (large structure, H300). COMSOL Multiphysics was employed, to rigorously calculate the electric field inside these architectures. Both structures are excited under normal incidence, and the absorption is calculated (for TM and TE polarization) in the wavelength range 400 nm – 1100 nm. For each wavelength, the calculation is done according to the real and imaginary parts of nc-Si:H refractive index at corresponding wavelength. We use red lines in Figure 3.4 (A) to Figure 3.4 (D) display absorption values directly computed by COMSOL in one period of the model. For $\lambda_0 > 460$ nm, the absorption coefficient of nc-Si:H decreases, hence the incident radiation can penetrate deeper into the film. For this reason, it is mostly absorbed in the middle part of the structure. Absorption in large grating structure for TM polarized light is presented in Figure 3.4 (D). The small difference between computed (by COMSOL) and calculated (with equation 3.4 absorption – for $\lambda_0 < 420$ nm – can be attributed to meshing in COMSOL. In fact, the TM-polarized electric field is discontinuous at the nc-Si:H / air interface, hence great variation of the field in that area can be expected. This is not the case for TE-polarized light, hence such difference is not observed in Figure 3.4 (C). Nevertheless, for solar cell applications the main focus is on longer wavelengths, for which the absorption calculated by equation 3.4 very well matches with the rigorous calculation done by COMSOL. It can be observed that the absorption by the E_y component of the TM-polarized electric field is much stronger in the large structure, with respect to the shallow structure (Figure 3.4 (B)). This indicates that the energy content in higher diffraction orders is greater for tall grating than for shallow ones. The reason is explicitly discussed in the section “TM polarization”.

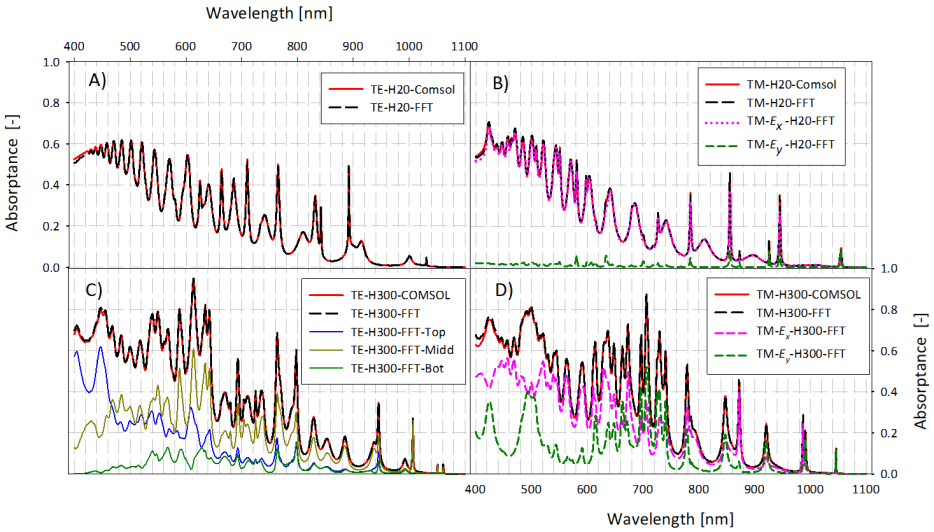

Figure 3.4: A) absorption for TE-polarized light and B) absorption for E_x and E_y components of TM-polarized light, in the shallow structure. Red lines represent light absorption calculated directly by COMSOL, while black lines show light absorption in the uniform part of the model. C) and D) represent light absorption - in the architecture endowed with large gratings - for TE and TM polarizations, respectively. Solid–red and dashed–black lines show the total absorption calculated by COMSOL and equation 3.4, respectively. Blue, grey and green colored curves in C) represent absorption in the top, middle, and bottom parts of the large structure (see Figure 3.3 (A)), for TE-polarized light. Dashed pink and green colored curves in D) show absorption in the large structure for E_x and E_y components of TM-polarized light, respectively.

3.4.1. TE POLARIZATION (E_z COMPONENT)

Figure 3.5 (A) illustrates one period of the grating structure as well as the orientation of the incident and transmitted electric field outside and inside this structure, respectively. Inside the absorber in Figure 3.5 (A) one can see the direction of oscillation and propagation of one of the diffracted plane waves inside the absorber (in time domain), before it reaches the bottom surface. Total field inside the structure is the sum of transmitted field from top interface and scattered field from the second interface. For TE polarization, the electric field of the incident wave is perpendicular to the plane of incidence and the electro-magnetic field propagates along y direction. The transmitted field has its electric field along z direction, but its wave vector gains x component and falls in the (x, y) plane. Figure 3.5 (B) presents the total absorption in the uniform part of the shallow structure when it is excited by TE polarized light. Each color in the graph represents the total absorption by one of the gratings order. As it has been addressed before, the shallow grating is not able to diffract the incident energy efficiently. This means that the incident field is not perturbed much by the grating structure and most of the incident energy does not feel the grating. This is the reason why the zeroth diffraction order (yellow) has the largest contribution in total absorption in Figure 3.5 (B). It is important to notice that not all the diffraction orders could excite a guided mode resonance. The diffraction angle for each grating order is given by $\beta_q = \sin^{-1}\left(\frac{\sin(\theta_i)}{n} \pm \frac{q \cdot \lambda_0}{n \cdot L}\right)$, where m is

the diffraction order, n is the refractive index, L is grating period, λ_0 is the wavelength and is the angle of incidence.

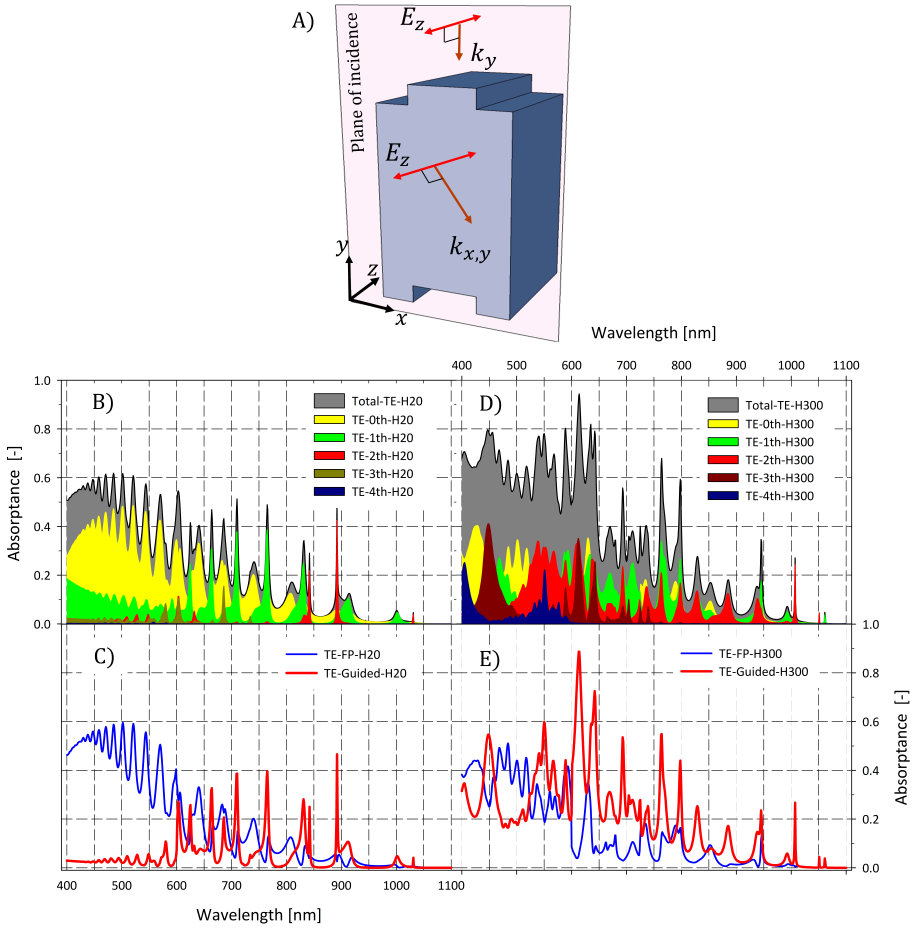

Figure 3.5: A) orientation of incident and transmitted electric field for one period of the grating structure for TE polarization. B) Each color indicates the total absorption for different diffraction order in the uniform part of the shallow grating structure. C) Absorption by each diffraction order in large grating structure is represented by different colors. Total absorption for TE polarization is shown in grey. D) and E) present total FP (blue lines) and guided resonance (red lines) triggered by the absorption of TE polarized light, for shallow and large structure respectively.

The diffraction angle decreases as the incident wavelength decreases. A diffraction order could excite a guided mode resonance only if its diffraction angle is larger than material's critical angle at that wavelength. Therefore, depending on the wavelength, one diffraction order can contribute to FP and guided resonance. For the grating structure in Figure 3.1 (B) for wavelengths shorter than 600 nm, the first diffraction order contributes to FP resonances because its angle of diffraction is smaller than the critical angle of nc-Si:H in this wavelength range. Therefore, the sharp absorption peaks in green color in Figure

3.5 (B) are due to the excitation of guided modes via the first diffraction order only for wavelengths longer than 600 nm. Diffraction angle for higher diffraction orders ($m \geq 2$) is larger than critical angle for entire wavelength range of our interest. The zeroth diffraction order ($\beta_q = 0$) is always a FP resonance. When the grating height is increased, incidence energy could better "feel" the grating. As a result, light absorption corresponded to zero diffraction order decreases significantly and large amount of incidence energy diffracted to higher orders. This can be observed in Figure 3.5 (C), where the absorption by the zeroth order is not more significant than higher orders for $\lambda < 700nm$. For longer wavelengths, first and second orders have larger shares in total absorption. According to the gratings equation, the diffraction angle of a grating does not depend on the grating height. Thus, even for large grating structure, the first diffraction order counts as FP resonance for wavelength shorter than 600 nm. In Figure 3.5 (D) and E, total absorption is distinguished by its resonance type. Blue lines represent the absorption by FP resonance in shallow and large grating structures, respectively. Interestingly, FP absorption is smaller in large structure than in shallow structure. Instead, absorption triggered by guided mode in large structure (red lines) is obviously higher than in shallow structure. As we mentioned before, large structure diffracts the incident energy more efficient.

3.4.2. TM POLARIZATION

Inside the grating structure, the electric field of TM-polarized light can be described as the superposition of two orthogonally oscillating electric fields, E_x and E_y. The E_x component represents a plane wave propagating along the $\mp y$ direction. When the diffraction angle is smaller than the critical angle, the components of electric filed can be seen as a FP resonance, created by partially reflected energy from top and bottom interfaces.

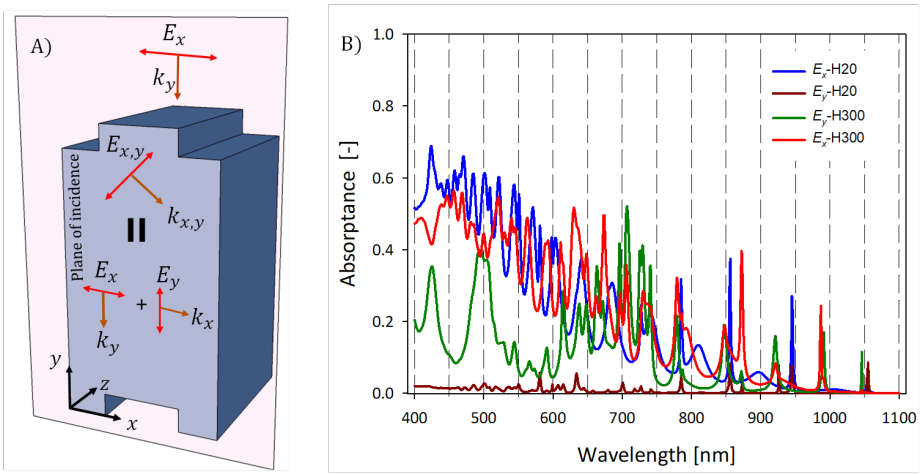

Figure 3.6: : A) Grating structure and orientation of the electric field before and after reaching the top interface, for TM-polarized illumination. The electric field vector inside the film can be decomposed in to two orthogonally oscillating electric fields, along the x and y. B) Total absorption by both components of the TM-polarized electric filed, for large and shallow grating structures.

The E_y component, on the other hand, represents a plane wave propagating along the

$\mp x$ direction (parallel to the grating vector). The Pointing vector inside the waveguide is defined as , and represents the direction of propagation of electromagnetic energy [79]. For TM polarization, the magnetic field oscillates along the z axis, thus:

$$\overrightarrow{S}_m = S_{x,m} \cdot \hat{x} + S_{y,m} \cdot \hat{y} = \pm E_{y,m} \cdot H_{z,m} \hat{x} \mp E_{x,m} \cdot H_{z,m} . \hat{y} \tag{3.5}$$

where the sub index m is the diffraction order, while $\hat{x}$ and $\hat{y}$ are unit vectors in the x and y directions, respectively. Equation 3.5 shows that, for a particular diffraction order, a larger value of E_y leads to a larger energy flux in the x direction. In addition, in a plane wave the electric field and propagation vectors are always perpendicular to each other. This means that the zeroth diffraction order (with propagating vector along y) has $E_y = 0$. The E_x and E_y components contributes differently in total absorption. In Figure 3.6 (B) the total absorption due to each components of TM polarized light for shallow and large gratings are shown. We would like to emphasize that the only difference between large and shallow structure is their grating height. Therefore, any difference in their absorption patterns is directly linked to the different grating height. For example, in Figure 3.6 (B) a significant increase in absorption of the E_y component in the large structure is observed, while E_x absorption does not change dramatically for shallow and large structures.

TM POLARIZATION (E_x COMPONENT)

We first study the light absorption by the x component of the electric field, in the *large* and *shallow* structure. Figure 3.7 illustrates the absorption of the E_x component of the $TM-$polarized electric field by each diffraction order, in structures endowed with *shallow* and *large* gratings, calculated using Equation 3.4. For $\lambda_0 < 600nm$, the correlation between the peaks of the 0^{th} diffraction order and the notches in the 1^{st} diffraction order (Figure 3.7 (A)) indicates a strong light coupling between these two orders.

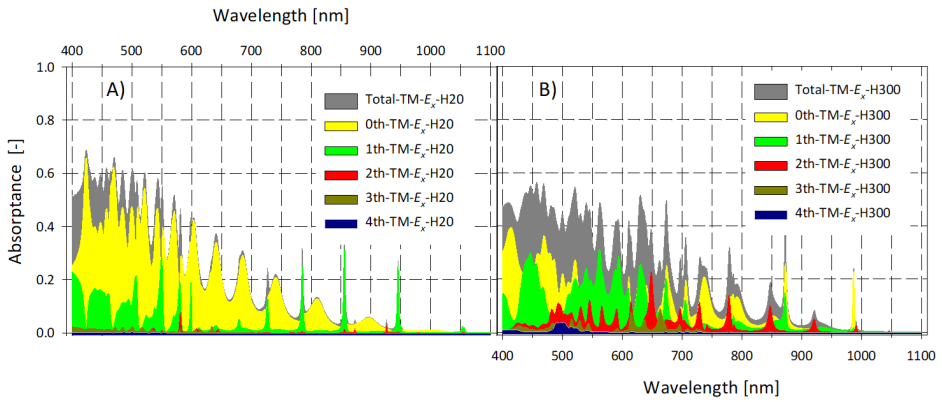

Figure 3.7: :Total absorption of the Ex component for each diffraction order: inside the uniform part of the shallow grating structure (A), and inside the entire large grating structure (B), for TM-polarized illumination.

In this wavelength range, the diffraction angle of the 1^{st} order is smaller than the critical angle of nc-Si:H, thus first and zero diffraction orders can be considered as FP resonance. For the *shallow* structure it is clear that the contribution of the 0^{th} diffraction

order to the total absorption is very large, even at longer wavelengths.This situation indicates FP resonances due to (i) the already addressed low efficiency of the grating and (ii) the propagation vector aligned to the y axis. For $\lambda_0 > 700nm$, the absorption peaks by the 1^{st} diffraction order can be considered as guided resonance, since in this range the diffraction angle of the 1^{st} order is larger than the critical angle. In the large structure, absorption by higher diffraction orders is highly enhanced, while zeroth order triggered absorption is clearly lower (Figure 3.7 (B)). This implies that larger gratings interact more strongly with the incident radiation, thus diffracting more energy into higher orders.

TM POLARIZATION (E_y COMPONENT)

Absorption by each diffraction order for the E_y component of the TM-polarized electric field for the shallow and large structure, calculated with equation 3.4, is presented in (A) and Figure 3.8 (B), respectively. In section "TM polarization", it was discussed that the Ey component has no 0^{th} diffraction order. In Figure 3.8 one can clearly see that the absorption by the 0^{th} diffraction order is zero. All of the absorption peaks in Figure 3.8 with $\lambda_0 > 600nm$ are directly connected to the excitation of guided modes, because their diffraction angles are larger than the critical angle. It is important to clarify that for $\lambda_0 < 500nm$, the sum of absorption by the first 4 diffraction orders of E_y does not yield the total absorption, since orders greater than 4 were not included, because – at short wavelengths – resonance peaks start overlap and cover each other, becoming indistinguishable. This creates an overall flat absorption profile, which does not give much information about the behavior of light inside the structure. Finally, total absorption by TM polarization in the shallow and large structure is decomposed into FP and guided resonance absorption (Figure 3.8 (C)). Blue and black dashed lines represent total FP absorption in structures with large and shallow gratings, respectively. Going from shallow to large grating, FP absorption is unaffected (for TM-polarized light). However, absorption triggered by guided resonances (solid lines in Figure 3.8 (C)) are dramatically higher for the large structure, especially $\lambda_0 > 600nm$. The sudden jump in guided resonance absorption at $\lambda_0 = 600nm$ is attributed to the contribution of 1st diffraction order to guided resonance.

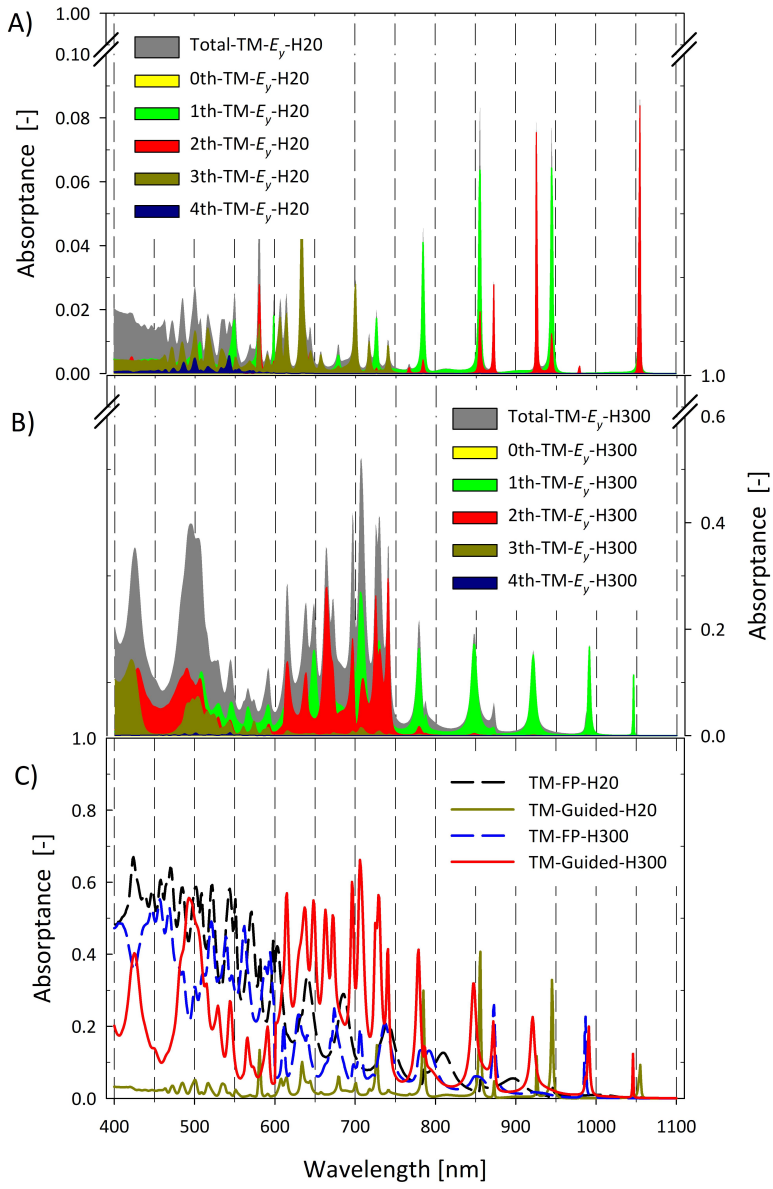

Figure 3.8: :(A)–(B) Contribution of each diffraction order, for the Ey component of the electric field, to total absorption. (C) Total FP (dashed lines) and guided resonance (continuous lines) triggered absorption, for shallow and large structure.

3.5. CONCLUSIONS

We have provided a different approach to calculate the contribution of different resonances to total absorption, without using a dispersion diagram. In this approach, Fourier expansion is employed to calculate the energy spectral density of the electric field inside a textured structure. This approach is supported by numerical and rigorous calculations, using a software based on the finite element method. We were able to track the origin of each absorption peak, (guided resonance or FP). Using our technique, we were also able to define accurately the relative weight of each resonance in total absorption, for every point in the wavelength range of interest. This method can be used for a large wavelength range and it is not limited by film thickness or grating profile. This approach is also not limited to solar cell applications and can be used to understand the light behavior in any multilayer structure with periodic texturing.

4

DISTINGUISHING BETWEEN NON GUIDED MODES: OBLIQUE INCIDENT

This chapter is based on the following publication:
H. Ahmadpanahi, O. El Gawhary, R. Vismara, O. Isabella and M. Zeman, "Assessing light absorption contributions in thin periodically-textured silicon absorbers under oblique illumination," AIP Advances **9**, A737-A749 (2018).

Abstract: Periodic texturing is one of the main techniques to enhance light absorption in thin-film solar cells. The presence of periodicity, such as grating, allows guided mode excitation in the structure, thus enhancing absorption. However, grating efficiency in exciting guided modes is highly dependent on the wavelength and incident angle of light. This is very important especially in solar cell application, where the light source – the sun – is broadband and largely angle-dependent. Nevertheless, most of literature only focuses on the frequency response of periodic texturing, thus neglecting the effect of angular movement of the sun. In this work we use Fourier expansion to calculate the absorption of each Fabry-Perot and diffraction order in an absorptive periodic waveguide. The structure is illuminated with TM and TE polarized light and under three different incident angles. Using this method, we are able to calculate the contribution of a guided resonance to total absorption for different angles of incidence. The work here developed and supported by rigorous numerical calculations can be used to better understand light propagation in a periodic waveguide structure, such as thin-film solar cells.

4.1. INTRODUCTION

Sun is a broadband and largely angle-dependent light source. Its spectrum consists of a wide range of frequencies from UV to IR [81]. To better exploit the solar spectrum for photovoltaic (PV) energy generation, enormous amount of study is dedicated

to multi-junction solar cells [23, 45, 46, 82–89], spectrum splitting [47, 48, 90–92] and different light trapping schemes [54], especially focused on the longer wavelength range [27, 55, 56, 58, 59, 76, 77, 93–95]. However, in very few of these studies the angle of incidence is considered to be not perpendicular to the surface of the solar cell [96–98]. Applications such as concentrator photovoltaic and spectrum splitters only work under normal incidence [99]. Therefore, sun tracking systems are implemented to ensure an optimal system performance. On the other hand, in conventional PV installations, where solar cells are mounted in a fixed position, the angle of incidence changes at every moment. This influences light absorption in the solar cell, especially for solar cells endowed with random or periodic texturing.

4.2. METHODOLOGY

In our previous work, we considered normal incidence in our analysis to distinguish between guided and non-guided absorption resonances in a periodically-textured thin-film solar cell [29]. We note that non-guided modes are also known as leaky modes for which $k_x \leq k_0$, where k_0 is the wave vector in the incident medium. In this contribution, we extend our analysis to the case of oblique incident angles. A simple way to find the guided modes of a multilayer slab, albeit applicable to (mostly) flat interfaces, is to plot the reflection or transmission coefficients using a Fabry-Perot formula for $0 < k_x <$ large values (say, much larger than k_0, where k_0 is computed in the incident medium)[100–102]. Then, every time one comes across a resonance for an incident $k_x > k_0$, that resonance corresponds to a guided mode [103]. However, as we focus on textured slabs, we employ instead a Fourier expansion to decompose the electric field inside a periodically textured thin-film solar cell. Then, the absorption for each wavelength, polarization, incident angle, and diffraction order is calculated using its corresponding Fourier coefficients. As an example, this analysis is done for a thin-film silicon slab in the wavelength range between 400 and 1100 nm, for both TM and TE polarizations and under three different angles of incidence. We assess the contribution of both guided and non-guided modes as well as unveil their relative weight with respect to the total absorptance. In this respect, the goal of our work is not just to distinguish between guided and non-guided resonances but to investigate how the absorption seems to be split among the different modes. It should be mentioned that our analysis is limited to planar incidence. Although conical incidence represents the most general case, its study usually leads to anisotropic effects and coupling between s and p polarization, which make the whole analysis more complex. Without losing generality of our approach [29], let us consider a 1μm thick periodically-textured nc-Si:H thin film. The one-dimensional (1-D) texturing has a period of 600 nm, height of 300 nm and duty cycle of 50%. The structure is surrounded by air and it is illuminated with TE and TM polarized light under oblique incidence (see Figure 4.1). Figure 4.1 also shows two scattering events inside the absorber. In region I, light is scattered into many discrete angles by the front surface of the absorber. In region II, a second scattering event is shown, whereby light is scattered once again, this time by the rear surface. In particular, each transmission order from top surface (T_i) re-scatters into all T_i' diffraction orders promoted by the bottom interface. Therefore, a guided mode can couple to other guided modes or to a Fabry-Perot mode, and vice versa [29]. In order to distinguish between different resonances inside the absorber, we use Fourier expan-

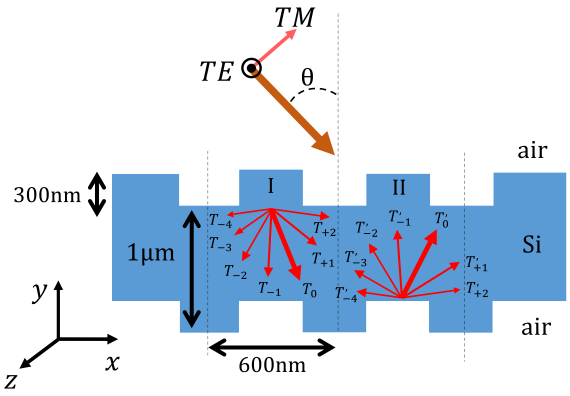

Figure 4.1: A) A 1μm thick nc-Si:H waveguide, endowed with 1-D front and rear gratings and characterized by a total thickness of 1μm at every point. The structure is illuminated under an oblique incident angle with TE (electric field parallel with z axis) and TM (electric field perpendicular to z axis) polarizations. Region I and II show light scattering from each interface. T_i and T_i'i are the transmission and reflection from the front and rear interfaces, respectively.

sion to describe the total electric field inside the absorber, using its Fourier coefficients [104]. This can be done by diving the grating structure into many thin sub-layers, along the y direction, as depicted in Figure 4.2 (A). The thickness of each sub-layer is defined such that, for the shortest wavelength-in-material ($\lambda = \lambda_0/n$) within the spectral range of interest, there are at least 10 sub-layers along one wavelength. Note that for perpendicular incidence having five sub-layers are sufficient to reach accurate calculation [29]. In oblique angle illumination, however, more sub-layers are needed to reach the same accuracy, especially in the top rim of grating and for TM polarization.

In this way, for each wavelength there are at least 10 sampling points in the material. Within one sub-layer, the electric field is considered to be invariant along the y-axis. At each sub-boundary, the field is expressed using Fourier coefficients. Figure 4.2 (B) shows the x-component of electric field (E_x) at the boundary of 20^{th} sub-layer under 10° illumination and at λ_0= 730 nm. Since the incident angle is 10°, the electric field inside absorber is not symmetric. Hence, despite the symmetry of the grating, the Fourier coefficients with the same order may not be equal (i.e. $T_{+i} \neq T_{-i}$). This is illustrated in figure Figure 4.2 (C), where the difference between positive and negative diffraction orders can be clearly observed. For each wavelength, sub-layer and angle of incidence, equation 4.1 is applied [29]. In this way, for each wavelength and angle of incidence, it is possible to express total absorption as function of the contribution of each diffraction order:

$$\epsilon_0 n\kappa\omega \int_0^y \int_0^L |E(x,\lambda_0,\theta_i)|^2 dx dy = \epsilon_0 n\kappa\omega \sum_{\mathbf{i=y_1}}^{\mathbf{i=y_n}} \sum_{\mathbf{q=-\infty}}^{\mathbf{q=+\infty}} \int_0^L \left| c_{i,q,\lambda_0,\theta_i} \right|^2 dx \tag{4.1}$$

where ϵ_0 is the dielectric constant of vacuum, n and κ are real and imaginary parts of the refractive index, respectively, and ω is the angular frequency. $c_{(i,q,\lambda_0,\theta_i)}$ is q^{th} Fourier coefficient of the electric field, with wavelength λ_0, in the i^{th} sub-layer, and for inci-

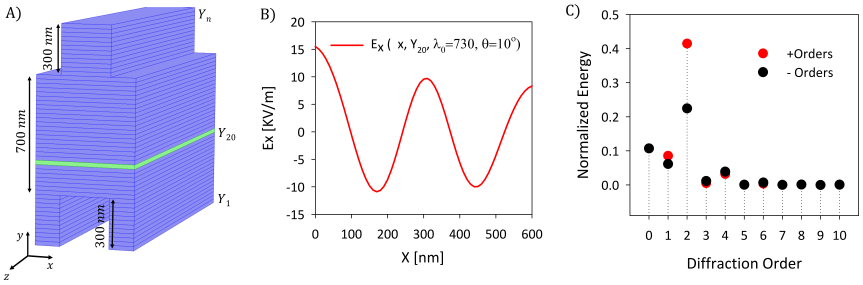

Figure 4.2: One period of the grating structure, divided into N thin sub-layers with thickness Y_N. B) Intensity of the E_x component of the total electric field in the 20^{th} sub-layer, indicated in green in A), at λ_0 = 730 nm and at 10° angular incidence. C) First 20 orders of the energy spectral density of the electric field, in the 20th sub-layer at λ_0 = 730 nm. Energy is normalized to the total energy in one sub-layer. Since the electric field is asymmetric, efficiency of the positive and negative diffraction orders are not equal.

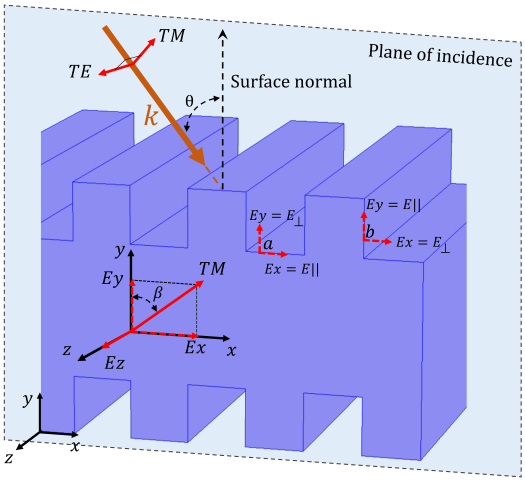

Figure 4.3: Configuration of incidence and diffracted electric field for TE and TM polarized light, with incident and diffracted angles θ and β respectively. E_x and E_y components of the electric field in TM polarization vary by changing the incidence angle.

dence angle θ_i The left-hand side of equation 4.1 represents total absorption, while the right-hand side indicates the contribution of each diffraction order, $\left|c_{i,q,\lambda_0,\theta_i}\right|^2$. In this method, the total electromagnetic field at each point inside the structure needs to be calculated separately, using for example a rigorous electromagnetic simulation tool. This field is then used as an input for equation 4.1. For our analysis, we employed COMSOL Multiphysics [105] to rigorously calculate the total absorption and total electric field inside the absorber, for both TE and TM polarizations and for three different angles of incidence: 10°, 30° and 60°. Then, the real and imaginary parts of the electric field for each sub-layer, polarization and incidence angle are exported to Mathematica [79] for further analysis. The validation of the method, already demonstrated for perpendicular incidence [29], is such that total absorption from equation 4.1 should be equal to the absorption calculated by COMSOL.

4.3. RESULTS AND DISCUSSION

The configuration of incidence and diffracted electric field in the grating structure is illustrated in Figure 4.3. For TE polarized light, the direction of the electric field oscillation does not change inside the absorber. On the other hand, for TM polarized light, the situation is different. The total electric field can be decomposed into E_x and E_y components, whose magnitudes change as function of the incident angle. Figure 4.3 shows all the components of the electric field inside the absorber, for one particular diffraction angle β. The diffraction angle for each grating order is given by the grating equation: $\beta_q = \sin^{-1}\left(\frac{\sin(\theta_i)}{n} \pm \frac{q\cdot\lambda_0}{n\cdot L}\right)$, where q is the diffraction order, n is the refractive index, L is the grating period, λ_0 is the wavelength in *vacuo* and θ_i is the angle of incidence. In general, for every incident angle θ_i, more than one diffraction angle is possible. One of the aims of this work is to distinguish between Fabry-Perot (FP) and guided modes, when the angle of incidence is non-zero ($\theta_i \neq 0$). According to the grating equation, a diffraction order could excite a guided mode resonance only if its diffraction angle is larger than material's critical angle (θ_c) at that wavelength. Therefore, depending on the incident wavelength and angle, a diffraction order could contribute to both FP and guided resonances. Fabry-Perot modes correspond to an incident plane wave (in air) endowed with a real k_x while the guide modes are Fabry-Perot resonances that correspond to an incident plane wave with an imaginary k_x.

4.3.1. TE POLARIZATION (E_z COMPONENT)

Total absorption in the grating structure for TE polarized light is calculated by means of equation 4.1 for three different incident angles, and illustrated in Figure 4.4 Panels (A), (C) and (E) show absorption for 10°, 30° and 60° angles of incidence, respectively. The oblique incidence implies that $\beta_{+q} \neq \beta_{-q}$. Thus, absorption for the $+q^{th}$ and $-q^{th}$ orders may not be equal. However, for ease of presentation, total absorption by both $+q^{th}$ and $-q^{th}$ orders is represented by one color. The nc-Si:H slab can support up to 12 diffraction orders for oblique incident angles, for $\lambda_0 < 450$ nm. Nevertheless, for the sake of clarity, Figure 4.4 only presents the first four diffraction orders. As addressed before, not all diffraction orders can excite a guided mode resonance. For $\theta_i = 10°$, β_{-1} is larger than critical angle (θ_c) when $\lambda \geq 496$ nm, whereas β_{+1} can excite a guided mode for $\lambda \geq 705$

nm. For $\theta_i = 10°$, for all higher diffraction orders ($q \leq -2$ and $q \geq 2$), the diffraction angle is larger than the critical angle in the entire wavelength range of interest. Despite the incidence angle, the 0^{th} diffraction order is always a FP resonance. Total absorption, due to guided or FP resonance for each incident angle, is shown in Figure 4.4 (B), (D) and (F). One can observe that in TE polarization case total absorption is directly linked to guided resonance absorption. When the incidence angle decreases, the guided resonance absorption decreases significantly and so does the total absorption. It is noteworthy that the method presented in equation 4.1 is validated for TE polarization, given the excellent superposition of COMSOL- and FFT-computed spectra for all simulated angles of incidence.

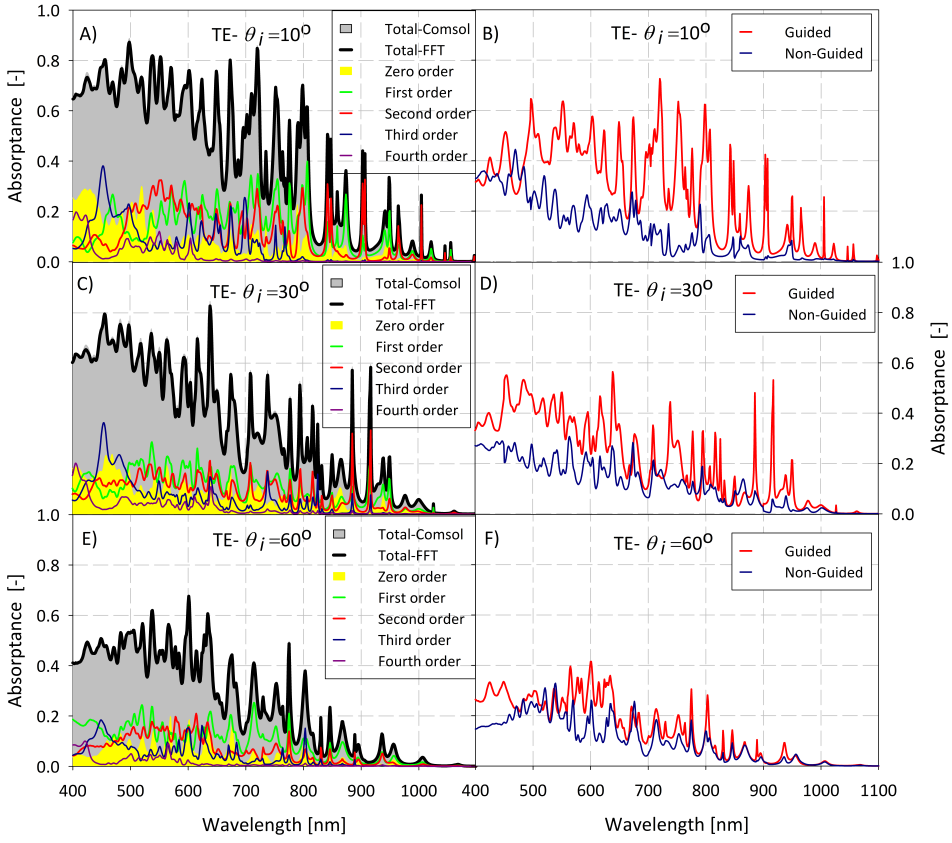

Figure 4.4: A), C) and E) Each color represent the absorption in grating structure by TE polarized light for a different diffraction orders and incidence angle. B). D) and F) present the absorptance ascribed to Fabry-Perot (blue lines) and guided resonance (red lines), triggered by the absorption of TE polarized light and for different incidence angles.

4.3.2. TM POLARIZATION

TM-polarized light can be described as the superposition of two orthogonally oscillating electric fields, E_x and E_y. E_x represents a plane wave propagating along the $\pm y$ direction. On the other hand, E_y indicates a plane wave propagating along the $\pm x$ direction (parallel to the grating vector). Top and bottom rims of the grating create a non-uniform surface. In other words, depending on x and y coordinates, E_x or E_y can be parallel or perpendicular to the grating surface (locations "a" and "b" in Figure 4.3). Therefore, under TM-polarized illumination, for any non-zero incident angle, there is a component of the electric field which is perpendicular to the grating surface (i.e. not continuous at the air/nc-Si:H boundary). This discontinuity of the electric field at the interface induces slight error in our calculation using equation 4.1, mostly located at the short wavelengths.

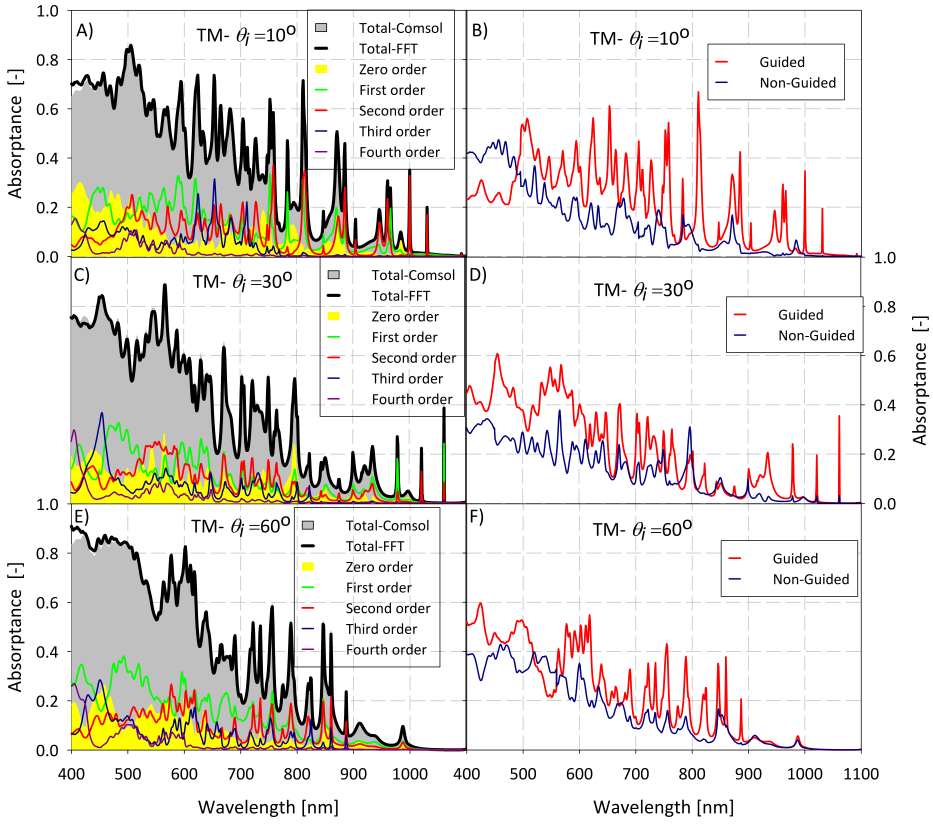

Figure 4.5: A), C) and E) show absorption in grating structure for each diffraction order when it is illuminated using TM polarization with θ_i = 10°, 30° and 60° oblique incidence, respectively. Diagrams B), D) and F) show the contribution on absorptance of guided and Fabry-Perot (FP) resonances for each incidence angle.

The gap between the grey area and the black line in Figure 4.5 clearly show this mismatch, which is largest at shorter wavelengths and decreases for larger wavelengths.

The reason is that the absorption coefficient of nc-Si:H is very high at short wavelengths, hence almost all incident energy is absorbed by the top rim of the grating (i.e. where the surface is highly non-uniform). Therefore, in this spectral range the discontinuity of the electric field has the maximum influence on our calculations. By decreasing further the thickness of sub-layers (not shown here), this mismatch can be significantly reduced. Each color in Figure 4.5 (A), (C) and (E) represent the absorption for a particular diffraction order, under TM polarized light. In Figure 4.5, the total TM polarized light, sum of E_x and E_y components, is shown. The contribution of each of those components in total absorption is presented in Figure 4.6. For the sake of clarity, absorption for the $+q^{th}$ and $-q^{th}$ orders are once again plotted together. Interestingly, the result is that in TM polarization case total absorption increases slightly by increasing the angle of incidence. Conversely, guided resonance absorption at shorter wavelengths increases as the incidence angle increases.

TM POLARIZATION (E_x AND E_y COMPONENTS)

As it has been addressed before, TM polarized light can be decomposed into two orthogonally polarized components, E_x and E_y. It is interesting to look at the electric components of TM polarized light, that is, to see how E_x and E_y contribute to the total absorption at each incident angle. Graphs (A), (C), (E) and (B), (D), (F) in Figure 4.6 show the absorptance under different incident angles for E_x and E_y components, respectively. Each color in Figure 4.6 shows total absorption for the $+q^{th}$ and $-q^{th}$ orders combined. It is important to notice that absorption for the 0^{th} order diffraction of the E_y component is zero. As it has been addressed before, E_y can be seen as a plane wave propagating along the x-axis.In plane waves, the electric field and propagation vectors are always perpendicular to each other [36]. Therefore, the 0^{th} diffraction order (with propagating vector along y) has $E_y = 0$. For $\theta_i = 10°, 30°$ and $60°$, all the absorption peaks at $\lambda_0 > 705, > 905$ and > 560 nm are directly connected to the excitation of guided modes, because their diffraction angles are larger than their respective critical angles. Without the presence of the grating, the structure would be a flat thin film. Such a structure can be seen as a 1-D photonic crystal consisting of only one layer (This is very extreme assumption, the only similarity is that thin film also show band gap). One of the properties of photonics crystals is their band gap structure. Inside a band-gap, the density of the modes (DOM) is low and thus waves in range of frequencies are forbidden and cannot be transmitted through the material. At the edge of the band gap, however, the DOM is very large [106] and, consequently, the group velocity is very low, meaning that energy travels slowly and therefore the interaction time between light and the film is enhanced. The presence of grating at the film interface breaks the photonics band gap and creates more resonances. A higher number of resonances ultimately indicates a larger DOM which leads to higher absorption. The DOM in the structure for TE polarized light with 10° incidence angle is presented by gray curve in Figure 4.7. The DOM for this structure was carried out by computing complex transmission coefficients in COMSOL Multiphysics and then plugging them in Equation 7 of reference [106]. The mode density augments at the photonics band edge. This means that the edge of each absorption peak (absorption by one diffraction order and not the total absorption) should correspond with a peak in DOM. In Figure 4.7, for sake of visibility, the DOM peaks are re-scaled to one. This information

can be used in thin film solar cells design.

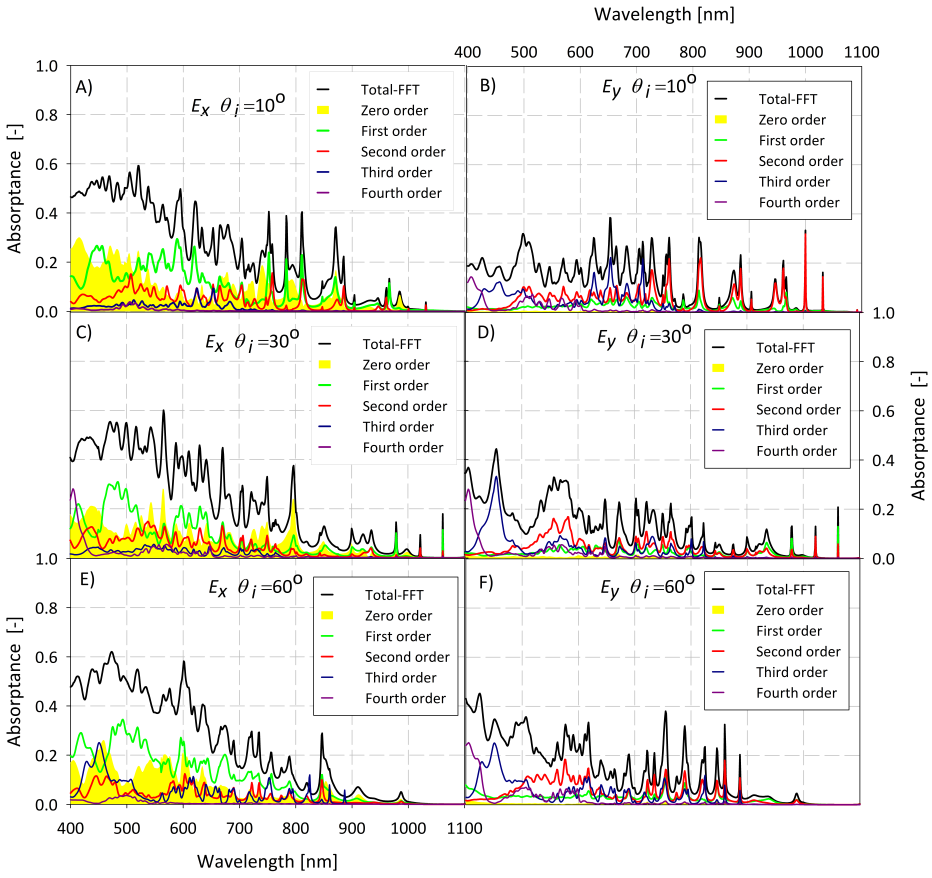

Figure 4.6: : Left (right) panels show total absorptance spectra for each diffraction order of the E_x (E_y) component for the three studied incident angles.

If the thickness of the thin film is defined, then the band gap of the structure is defined as well. To enhance the absorption, the grating shall be designed in such a way that efficiently excites the modes at the edge of the band gap, where the mode density is higher.

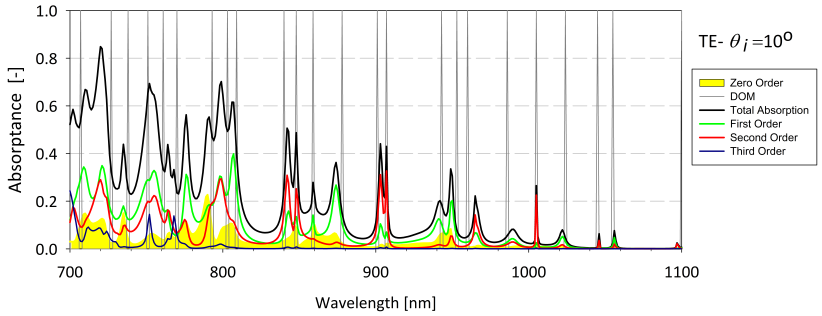

Figure 4.7: :Density of the modes (DOM) overlaid on the absorptance calculated for the grating structure in case of TE-polarized light with 10° angle of incidence. Most of the peaks in the DOM match with the edge of absorption peaks in the structure.

4.4. DISCUSSION AND CONCLUSION

In conclusion, we would like to emphasize that we have employed a Fourier expansion approach to calculate the spectral energy density of the electric field inside a periodically-textured nc-Si:H slab, under oblique incidence and for both TE and TM polarizations for 1D grating. Numerical and rigorous calculations were provided to support our approach. Our proposed method can be used to calculate the absorption for each diffraction order, and to distinguish between FP and guided resonances regardless of grating height, incident angle and wavelength range. With the right meshing, it is possible to achieve a very good accuracy even at short wavelengths. This work was triggered by the limitation of intersection method [28, 72, 107]. As we describe in our previous work [29], it is very challenging to track guided modes in a highly textured structure using the dispersion diagram of a flat structure with the same optical thickness as the grating structure. The optical thickness of a grating structure largely depends on the grating properties such as height, duty cycle and grating profile. For a wavelength-scale structure, it is even more challenging to define one optical thickness for all diffraction orders. In the method hereby proposed, tracking of guided modes is possible without knowing the optical thickness or the dispersion diagram. Another reason for this work is that adding texturing to a flat structure might behave as an antireflection layer and thus enhance the absorption by enhancing the light coupling into FP resonance rather than guided modes. Our proposed method enables tracking the distribution of incidence energy within different resonances. Although our method is not a grating design tool, it can be used to assess the performance of a new grating design or of an existing one. This is because in our method we rely on the computed electric field inside the structure, rather than the grating profile. However, this method can be used by grating designers to evaluate the impact of their design on the performance of the entire system, or to better understand how manufacturing errors influence the optical performance of the structure. Another application of our method is to calculate the absorption enhancement (total absorption over one pass absorption) for a particular diffraction order. Since the absorption for each resonance is known, we are able to calculate the absorption enhancement for that resonance without using the Temporal Coupled-Mode Theory (TCMT) [40]. Our method

can be used for any grating period, wavelength range or incidence angle. However, for grating structures with curved or non-rectangular surfaces, this method probably does not provide accurate result in the non-uniform part of the structure. In this situation, the thickness of sub-layers in the non-uniform part of the structure has to be very thin (depending on the wavelength, grating profile and polarization) to achieve accurate results. In the uniform region, however, this method can be fully trusted. The same principle can be applied for 2D grating structures to evaluate the optical performance of a real solar cell. In this situation, in each sub-layer a 2-D Fourier transform needs to be employed for each component of electric field (E_x, E_y and E_z). Our approach is also not limited to solar cell applications and can be used to understand the light behavior in different multilayer structures with periodic texturing.

5

NANO-PHOTONICS ABSORPTION LIMIT IN DOUBLE SIDE TEXTURED SLABS

This chapter is based on the following publication:

Hamed Ahmadpanahi, Robin Vismara, Olindo Isabella, and Miro Zeman, "Understanding the nano-photonics absorption limit in both front-side and front/rear-side textured slabs", Opt. Express **27**, A1173-A1187 (2019).

Abstract: Surface texturing is one of the main techniques to enhance light absorption in solar cells. In thin film devices, periodic texturing can be used to excite the guided resonances supported by the structure. Therefore, total absorption is enhanced largely due to the excitation of these resonances. Although the maximum absorption enhancement limit in both bulk and photonic structures is known already, the weight of each resonance type in this limit is not yet clear. In this contribution, we extend the temporal couple-mode theory, deriving a closed formula to distinguish the contribution of Fabry-Perot and wave-guided modes within the absorption limit for 1-D grating structures. Secondly, using this analytical approach we can clearly address cases of bulk and thin absorber thicknesses. Our results, supported by rigorous electromagnetic calculation, show that absorption enhancement in a 1-D grating structure can be much higher than the nano-photonic limit ($2\pi n$) reported by Yu et al. Thirdly, beyond the framework put forward by Yu et al., we extended our theory to describe the absorption enhancement in double side textured slabs. We have found that when the periods of top and bottom gratings are aliquant, absorption is enhanced in a wider frequency range. We provide rigorous numerical calculations to support our theoretical approach.

5.1. INTRODUCTION

The performance of solar cells is strongly linked to their light absorption capabilities [33]. Therefore, a significant amount of research has been dedicated to different light management techniques, in order to improve light absorption in the device active layer [17, 108]. Light management is mostly focused on (i) the effective use of solar spectrum [43, 44, 46–48, 109, 110], (ii) maximizing the number of photons reaching the absorber layer [61–63, 111], (iii) keeping the solar radiation energy inside the absorber long enough, until it is absorbed by the material. The first aspect can be achieved by employing spectrum splitters and multi-junction devices [112–115]. The second aspect is accomplished by applying anti-reflection coatings and by minimizing light absorption in non-active layers [49, 51, 53, 116–118]. The third aspect, usually referred to as light trapping or optical path enhancement, is attained by altering the propagation direction of light such that total internal reflection inside the absorber occurs [119]. This is possible only if one or both surfaces of the absorber are textured. After hitting an interface with random texturing, incident light is scattered into propagation directions with a wide angular range [64, 120, 121]. The greater the scattering angle, the larger the optical path length enhancement. Optical path length enhancement is defined as l/d , with d representing the absorber physical thickness and $l = d/\cos\theta$, where θ is the scattering angle [122]. In 1982, Yablonovitch elaborated that in a weakly absorbing slab with a 2-D Lambertian scattering interface, an optical path length enhancement of $4n^2$ can be achieved (where n is the refractive index of the absorber material) [123]. The angular intensity distribution (AID) of a Lambertian scatterer obeys Lambert's cosine law [124] and has an isotropic angular response, independently of the light incident angle. In defining the limit, the material absorption is considered to be very small, because the angular intensity distribution (AID) follows Lambert's cosine law only if the slab is transparent (weakly absorbing). Furthermore, the thickness of slab is considered to be much larger than the incidence wavelength, and thus the light path can be defined in the framework of geometric optics. The $4n^2$limit which is based on statistical ray optics, is nowadays commonly referred to as the Yablonovitch limit or Lambertian limit. The Lambertian limit holds for any angle of incidence from to (acceptance angle) with zero being the normal and grazing to the slab surface. By decreasing the acceptance angle of the cell from π to 2α, it is possible to increase the optical path enhancement from $4n^2$ to $4n^2/\sin 2\alpha$ [26, 125]. The limit of $4n^2/\sin 2\alpha$, commonly employed in concentrator photovoltaic, is valid for bulk structures and can easily be calculated using geometrical optics. On the other hand, when the texturing size or the absorber layer thickness is comparable to the wavelength, wave effects of light become prominent [126]. Thus, some of the basic assumptions leading to conventional limit are no longer applicable. In 2010, Yu et al. showed that – in the wave optics regime – the light absorption enhancement factor can go far beyond the conventional Lambertian limit, using wavelength-scale grating structures [27, 28]. This limit, which is called nano-photonics limit, was derived using statistical temporal coupled mode theory and can be calculated using:

$$F = \frac{2\pi\gamma_{\mathrm{i}}}{\alpha d\Delta\omega}\frac{M}{N} \tag{5.1}$$

where M and N are the total number of resonances and reflection (leaking) orders sup-

ported by the structure in the frequency range $\Delta\omega$, respectively; d is the absorber thickness; γ_i is the decay rate and it is linked to the material absorption coefficient α via , where c is the speed of light in vacuum and n is the real part of material refractive index. At each frequency range, M and N are strongly dependent on grating symmetry, arrangement of unit cell and thickness of the absorber. In a grating structure, each diffraction order can excite at least one resonance within the frequency range $\Delta\omega$, if $2\pi/L < \Delta\omega/c$ (L is the grating period). Therefore, the total number of resonances is the sum of resonances excited by different diffraction orders. Generally speaking, each diffraction order has different efficiency, meaning that the energy of incident light is not distributed uniformly among them. Consequently, each diffraction order has a different contribution to total absorption. For this reason, calculating the maximum absorption enhancement factor for each diffraction order is of great importance in grating design [77, 78, 127], especially for thin-film solar cells – where the absorber thickness is too small to efficiently absorb photons with energy close to the absorber band gap [41]. Among all different materials used in thin-film solar cells, (nano)-crystalline silicon is a good bench mark to study different light trapping schemes, due to its low absorption coefficient in the near infrared part of the spectrum [42]. In this paper, we apply the statistical temporal coupled mode theoretical approach (developed by Yu et al.) to calculate the maximum enhancement factor for each type of resonance in a grating structure. The maximum absorption enhancement for 2-D grating structure varies according to the dimensions (lattice constant) and arrangement of unit cell (hexagonal, square, triangle). Therefore, for 2-D grating, it is not possible to come down a closed formula independent of grating arrangement and unit cell dimensions. For this reason, in this article we only deal with one dimensional (1-D) grating structures. For our analysis, we consider normal incidence and only one polarization. Total number of resonances is then multiplied by two in order to consider two polarizations. This work is divided in two parts: first, we investigate the case of texturing at one surface. We then extend our calculations for double side textured structures.

5.2. CONTRIBUTION OF GUIDED AND NON-GUIDED MODES

Consider a periodically corrugated dielectric slab with thickness d and periodicity L, made of (nano)-crystalline silicon. The slab is placed on a perfect mirror and it is illuminated from above under normal incidence (Figure 5.1 (A). The incident plane wave, after hitting the air-Si interface, scatters into many distinct propagating directions inside the slab. The scattered waves bounce along the z and x directions, exciting resonances. In such a structure, the value of the wave-number of resonances inside the film is not continuous, but is described by the following equation:

$$k_{(p,q)} = n\frac{\omega_{(p,q)}}{c} = \sqrt{\left(p\frac{2\pi}{d}\right)^2 + \left(q\frac{2\pi}{L}\right)^2} \begin{cases} p = \pm 1, \pm 2, \ldots \pm\infty \\ q = 0, \pm 1, \ldots \pm\infty \end{cases} \tag{5.2}$$

where, ω is the angular frequency of light. Each p and q pair correspond to one resonance. The index $p(q)$ refers to resonances excited in the $z(x)$ direction, due to the thickness of the slab, d (period of the grating, L). Any frequency lower than $\omega_{(\pm 1,0)}$ (cut off frequency) cannot propagate inside the structure. In a frequency range $[\omega, \omega + \Delta\omega]$,

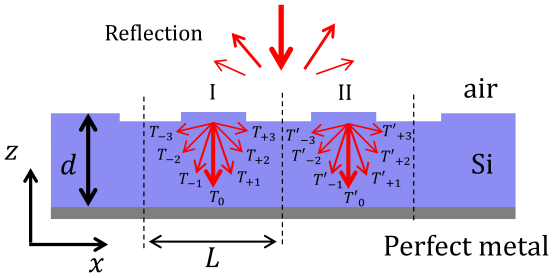

Figure 5.1: Light scattering in a Si-based periodically textured structure with thickness d and period of L. The two regions, marked I and II, represent the first (T_i) and second (T'_i) scattering of the incident plane wave inside the structure, respectively. The structure is placed on a flat silver. First and second scattering both occur at Si-air interface.

the total number of resonances supported by a 1-D structure with asymmetric grating, can be calculated as [42]:

$$M = P \cdot \psi \cdot \frac{d}{d\omega}\left(\frac{\text{area of circle with radius} \quad k = \omega \cdot n/c}{\text{area of a resonance}}\right) \cdot \Delta\omega = \ldots$$
$$\ldots = P \cdot \psi \cdot 2\pi \cdot \frac{n^2\omega}{c^2}\left(\frac{L}{2\pi}\right)\left(\frac{d}{2\pi}\right)\Delta\omega \tag{5.3}$$

where c is the speed of light in vacuo, is the total number of polarizations that is taken into account (for polarized light, TE or TM, for non-polarized light). In this work, we only consider one polarization, therefore throughout this article. is grating symmetry coefficient and have only two values, for asymmetric and for symmetric grating. In this context, an asymmetric grating is characterized by a grating whose cross-sectional period does not have mirror symmetry. According to reference [126] under normal incidence the number of resonances in symmetric grating is half of that of asymmetric grating. Because a symmetric grating cannot couple a normal incidence, which has an even modal amplitude profile, to resonances with odd modal amplitude profile. However, if the modal amplitude of the incidence beam is not symmetric (oblique incidence), then even a symmetric grating can couple some part of the incidence energy to resonances with odd modal amplitude. In this work we are considering normal incidence, therefore, we follow the approach in [126]. Equation 5.3 describes the total number of resonances supported by the structure (the dots enclosed by the red circle in Figure 5.2 within the frequency range $[0,\omega]$, and does not provide any information about the type of resonance. We use the same method as in equation 5.3 to count the number of resonances with different origin. We also use k_G and k_d instead of $2\pi/L$ and $2\pi/d$, respectively, to ease the writing. In Figure 5.2 a random resonance occupies an area equal to $(q\cdot k_G)\cdot(p\cdot k_d)$. Each diffraction order in k–space occupies a minimum area of $(q\cdot k_G)\times(1\cdot k_d)$, for example the red rectangle in Figure 5.2 represents the minimum area that a second order diffraction resonance occupies $(2k_G\cdot k_d)$. Now, for a particular q^{th} (diffraction order) we can change the value of p and calculate the total area – in k–space – that all resonances for a particular diffraction order can occupy. Of course, any p and q pair must be chosen such that equation 5.2 is held. For example, the grey rectangle in Figure 5.2 shows the total area

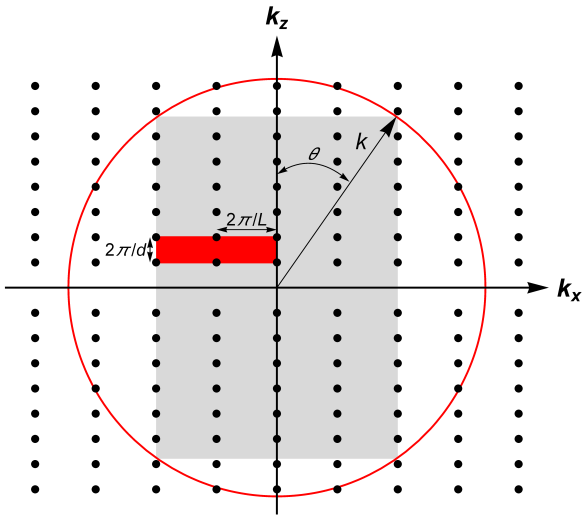

Figure 5.2: Resonances (black dots) in a waveguide endowed with a 1-D grating with period L. The grey region represents the maximum area (in reciprocal k–space) that can be occupied by all the second diffraction orders in the frequency range $[0, \omega]$. $\theta = \arcsin(2 \cdot k_G / k)$ is the angle showing the direction of the k vector inside the material, when pointing at the highest second order resonance

(in the reciprocal or k–space) that can be possibly occupied by second diffraction order, below frequency $\omega = (k \cdot c)/n$. This area is equal to $4 \cdot q \cdot k_G \cdot k \cdot \cos\theta$, where $q = 2$ (second diffraction order), $k = (n \cdot \omega)/c$, and $\theta = \arcsin q \cdot k_G / k$.Using the same concept as equation 5.3, and using the normalized frequency $s = L/\lambda$, one can calculate the number of resonances for the qth diffraction order, within the frequency range $[\omega, \omega + \Delta\omega]$:

$$M_q = 4\psi \frac{n^2 s}{c\sqrt{(ns)^2 - q^2}} \cdot \frac{d}{2\pi} \Delta\omega \tag{5.4}$$

Using equation 5.4 , one can count all guided resonances, but not pure Fabry-Perot (FP) resonances (i.e. those dots which are located on the k_z axis in Figure 5.2 , indicated with $k_{(p,0)}$). FP resonances are only defined by the optical thickness of the film and the wavelength of incident light ($q = 0$ in equation 5.2). In the frequency range between $[\omega, \omega + \Delta\omega; \omega > \omega_{(1,0)}]$ the number of pure FP resonance can be calculated by:

$$M_{\mathrm{FP}} = \frac{d}{d\omega}\left(2\frac{k}{k_d}\right) = 2\frac{n}{k_d c}\Delta\omega \tag{5.5}$$

According to equation 5.3, any frequency lower than cut-off frequency cannot propagate inside the structure. Therefore, equation 5.4 is valid only for $\omega > \omega_{(1,0)}$. Now that we can count all the resonances and distinguish their origin (guided or Fabry-Perot), the total enhancement factor for each type of resonance can be calculated, using equation 5.1 If we determine M_q using equation 5.4 and then substitute the obtained value in equation 5.1 ,we can calculate the total enhancement factor for q^{th} diffraction order as:

$$F_q = 4\frac{ns}{\sqrt{(ns)^2 - q^2}} \cdot \frac{1}{2 \cdot \psi \cdot \lfloor s \rfloor + 1} \tag{5.6}$$

where $N = 2 \cdot \psi \cdot \lfloor s \rfloor + 1$ is the number of channels (reflection orders) for this structure, and $\lfloor x \rfloor$ represents the largest integer that is smaller than x. Equation 5.6 shows the enhancement factor for a particular guided resonance, when $\sqrt{(L/d \cdot n)^2 + (q/n)^2} < s$. The enhancement factor for pure FP in an asymmetric grating can calculated by:

$$F_{\mathrm{FP}} = \frac{2}{2 \cdot \psi \cdot \lfloor s \rfloor + 1} \tag{5.7}$$

The numerator indicates that a FP resonance enhances the light path 2 times. Equation 5.7 is only valid for $s > L/(d \cdot n)$, which is the cut-off frequency of the structure. Absorption enhancement due to FP resonance decreases as frequency increases. The symmetry of grating does not affect the total number of excited FP resonance (equation 5.5 has not dependency on Ψ) but it affects absorption enhancement due to FP resonance. As an asymmetric grating could couple a FP resonance into to resonances with odd or even modal amplitude profile, a FP resonance in such a grating structure has more chance to escape the system. This means that for $s \geq 1$, absorption enhancement due to FP resonance is smaller in asymmetric grating than in symmetric one. For normalized frequency $0 \leq s < 1$, equation 5.7 shows identical result for symmetric and asymmetric gratings. The total (cumulative) enhancement factor is obtained by adding the enhancement factor for all diffraction orders and the pure FP resonances:

$$F_{\mathrm{TOT}} = F_{\mathrm{FP}} + \sum_{q=1}^{q=\infty} F_q \tag{5.8}$$

Using equation 5.8, we propose the weight of Fabry-Perot contribution to the enhancement factor (W_{FP}) as:

$$W_{FP} = \frac{F_{FP}}{F_{Total}} \tag{5.9}$$

We shall use this aggregated metric in the remainder of this contribution to quantitatively distinguish the impact of Fabry-Perot resonances on total absorption enhancement factor.

5.3. EXTENDING THE TEMPORAL COUPLE-MODE THEORY TO DIFFERENT THICKNESSES

According to equation 5.2, the wavenumber must reach the minimum value $k_{min} = \sqrt{(2\pi/d)^2 + (q2\pi/L)^2}$,in order to excite the lowest mode ($p = 1$) of the q^{th} diffraction order. Therefore, the normalized frequency must be $s > \sqrt{(L/(n \cdot d))^2 + (q/n)^2}$to excite the first guided resonance of the q^{th} diffraction order. Here the thickness of the film comes into account. In fact, the larger is the optical thickness $(n \cdot d)$ of the film with respect to the grating period ($L/(n \cdot d) \to 0$), the closer the system behaves like in the

bulk regime, and vice versa. Thus, only in the range $\sqrt{\left(L/(n\cdot d)\right)^2+\left(q/n\right)^2} < s$ equation 5.4 counts the guided modes. This clearly shows that the slab thickness has an impact on the maximum absorption enhancement. For example, equation 5.6 indicates that, if $s \to q/n$, then $F_q \to \infty$. However, the condition $s > \sqrt{\left(L/(n\cdot d)\right)^2+\left(q/n\right)^2}$ must be respected. Therefore, only for a film with very large optical thickness ($L/(n\cdot d) \to 0$) the enhancement factor can be infinitely large. The result of equations 5.6 to 5.8 for an overall thick slab slab (d = 1 mm) is presented in Figure 5.3 (B). The black curve represents the cumulative absorption enhancement in a film with the physical thickness of 1 mm $L/(n\cdot d) = 1.5\times10^{-4}$ with $n = 4$, endowed with 1-D asymmetric texturing. At $s = q/n$, a new diffraction order appears. Therefore, a peak in the guided mode enhancement (grey curve) and in the total enhancement (black curve) is observed. Since the diffraction angle decrease as frequency increases, the enhancement drops dramatically until $s = (q+1)/n$, where a new peak appears. At $s = 1$, the number of channels (reflection orders) increases from 1 to 3 and therefore the enhancement drops suddenly. In Figure 5.3 (C) we present W_{FP} related to the structure shown in Figure 5.3 (A). For $s < 0.25$ (considering $s = q/n$, with $n = 4$ and $q = 1$), no diffraction order exists and all the absorption enhancement is due to FP resonance, therefore, $F_{TOT} = F_{FP}$ and W_{FP}= 100%. At s =0.25 the first diffraction order arises. The absorption is significantly enhanced due to presence of such first diffraction order (see the black curve at $s = 0.25$ in Figure 5.3 (B)), whereas F_{FP} does not change (see the blue curve in Figure 5.3 (B), for $0 < s < 1$, F_{FP} does not vary). As $F_{TOT} = F_{FP} + F_{q=\pm1}$, where $F_{q=\pm1} >> F_{FP}$, W_{FP} drops suddenly.

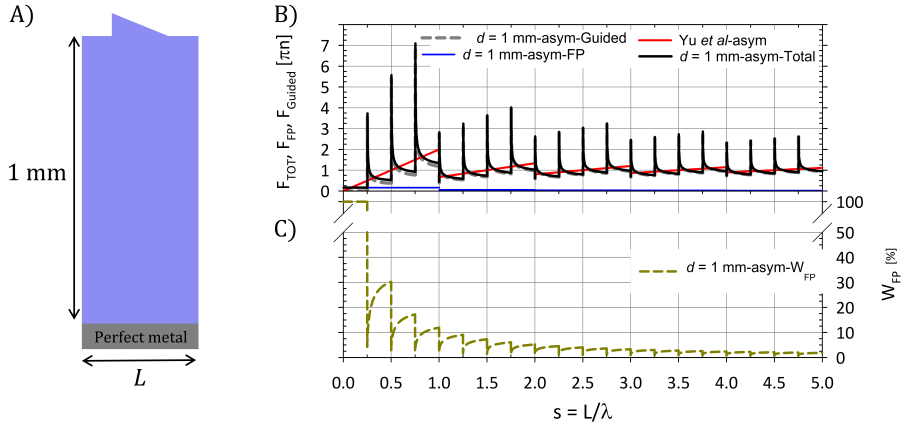

Figure 5.3: A schematic presentation of a thick structure with asymmetric grating. B) Absorption enhancement achievable in a thick Si film with 1D asymmetric periodic texturing (d = 1 mm). The maximum enhancement achieved by the guided and FP resonances are shown by dashed grey and solid blue lines, respectively. Their sum results in the total enhancement (black line). The red curve represents the maximum enhancement factor calculated by Yu et al. C) represents the W_{FP} for the structure shown in A).

$F_{q=\pm1}$ decreases as the normalized frequency increases and, therefore, W_{FP} grows rapidly until reaches its maximum (around 30%) at $s \to 0.5$. For $s = 0.5$ another diffraction order arises and thus W_{FP} drops again. This sequence repeats: for s approaching q/n, W_{FP} is

peaks and for $s = q/n$ the W_{FP} is minimum. So far, only asymmetric grating has been considered. The number of channels are also influenced by the symmetry of the grating and becomes $N_{sym} = \lfloor s \rfloor + 1$. Therefore, the maximum enhancement achieved by symmetric grating would be half of asymmetric one. Figure 5.4 (B) shows the absorption enhancement in a symmetric grating structure with thickness of 1 mm (identical to the structure in Figure 5.3 (A)). One can clearly see that the maximum absorption enhancement is half of the one for asymmetric grating (Figure 5.3 (B)). For a film with $d \to \infty$, the maximum theoretical enhancement tends to infinite for both symmetric and asymmetric gratings. Thus for an infinitely thick structure the symmetry of the grating profile does not play any role in defining maximum absorption enhancement. In Figure 5.4 (C) the W_{FP} related to the structure shown in Figure 5.4-A is presented. Comparing Figure 5.4 (C) and Figure 5.3 (C), one can observe that in a structure with symmetric grating (Figure 5.4 (A)) the W_{FP} is larger than in a structure with asymmetric grating (Figure 5.3 (A)). This is due to the fact that a structure with symmetric grating has smaller F_{FP} than a structure with asymmetric grating, while both structures have the same F_{FP}. Therefore, W_{FP} is larger in structure endowed with symmetric grating.

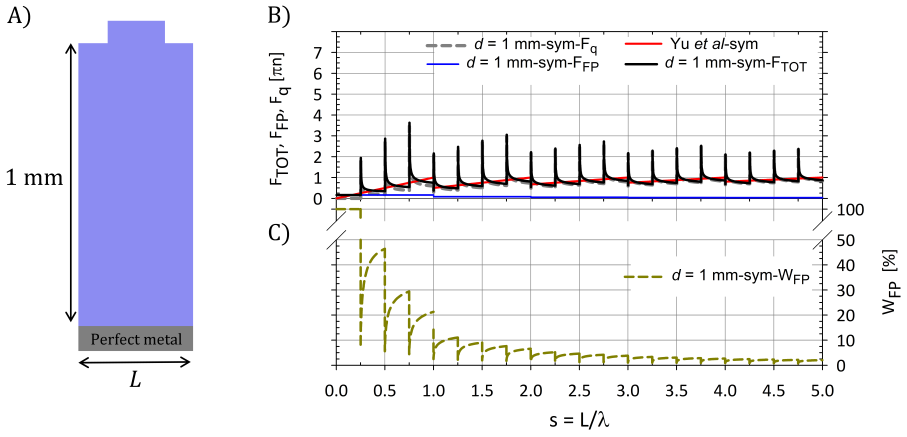

Figure 5.4: A schematic presentation of a thick structure with a symmetric grating. B) Absorption enhancement in a thick Si slab with thickness-to-period ratio $L/(n \cdot d) = 1.5 \times 10^{-4}$ ($d = 1$ mm) endowed with a symmetric grating. C) represents the W_{FP} for the structure shown in A).

5.3.1. MAXIMUM ENHANCEMENT FREQUENCY (BULK)

The maximum enhancement frequency for bulk structures (i.e. the frequency at which the enhancement is maximum) occurs when the denominator in equation 5.6 tends to zero, i.e. $s \to q/n$. On the other hand, for $s \geq 1$ the number of channels increases, which results in a drop of enhancement. From these two conditions, we can conclude that s_{max} can be calculated using equation below:

$$s_{\max} = \lim_{q \to n^-} \frac{q}{n} \tag{5.10}$$

The refractive index n can be any positive real number, whereas q can only be an integer. Therefore, depending on whether n is an integer or not we get two situations: a) if n is an integer the maximum frequency occurs for $q = n–1$; b) if n is not an integer, s_{max} occurs for $q = \lfloor n \rfloor$. In this work, since we assume $n = 4$ for both symmetric and asymmetric structures, the maximum enhancement occurs at $s = 0.75$, where the third diffraction order has the largest propagation angle and there is only one channel (reflection order).

5.3.2. MAXIMUM ENHANCEMENT IN THIN FILM

So far, we have discussed the case of a film with a very large thickness. As mentioned earlier, when L/d increases, the lowest frequency to excite the first resonance for a diffraction order is increased. Therefore, the peaks in equation 5.6 do not occur at $s = q/n$, but rather at $s = \sqrt{(L/(n \cdot d))^2 + (q/n)^2}$. This situation is illustrated in Figure 5.5 (B) where the absorption enhancement for an asymmetric grating structure with thickness of 1 μm is shown (Figure 5.5 (A)).

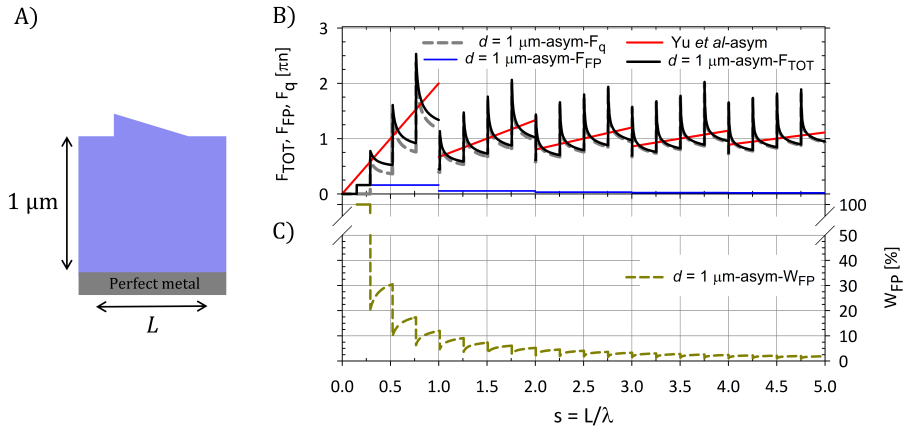

Figure 5.5: A) Represents one period of a 1000-nm thick Si film endowed with asymmetric grating B) Shows the absorption enhancement in the structure shown in A). Dashed grey and solid blue lines represent the enhancement due to guided and FP resonances, respectively, while the solid black curve is their sum. The red line is the limit calculated by Yu et al. for a symmetric grating structure. C) Represents the W_{FP} for the structure shown in A).

The maximum absorption enhancement occurs at around $s = 0.76$ rather than 0.75. Additionally, since the structure is thin, its cut off frequency occurs at higher frequency. This can be observed in Figure 5.5 (B) where $F_{FP} \neq 0$ for $s \geq 0.15$ rather than $s = 0$. Although, changing the thickness influences the cut-off frequency, it does not affect the W_{FP} much. In Figure 5.5 (C) the W_{FP} is only slightly shifted to the right with respect to Figure 5.3 (C), but its maximum and minimum values remains unchanged. The absorption enhancement is lower for a thin film with a symmetric grating. The graph in Figure 5.6 (B) presents the absorption enhancement achieved in a 1000-nm thick film with a symmetrical grating (Figure 5.6 (A)). Although symmetric gratings have much lower maxima than asymmetric gratings, it still higher than what is predicted by Yu et al., but

for a small frequency range. The graph in Figure 5.6 (C) illustrates the W_{FP} related to the structure shown in Figure 5.6 (A).

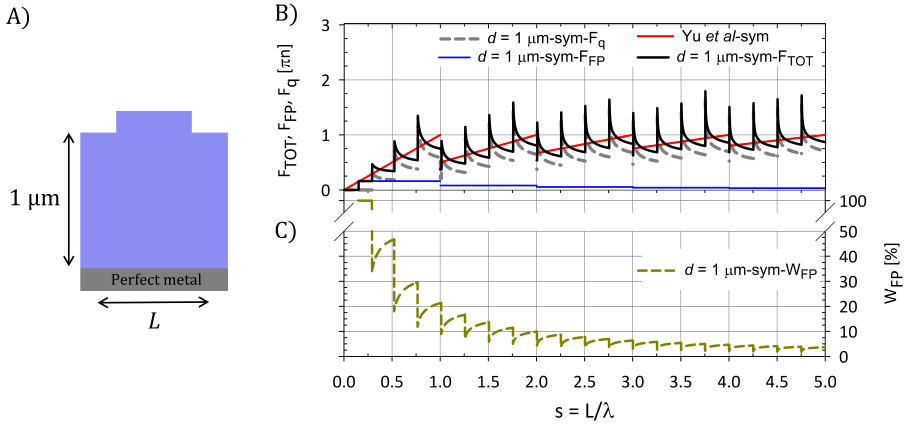

Figure 5.6: A) Schematic presentation of a 1000-nm thick Si film endowed with symmetric grating. B) Shows the absorption enhancement in the structure shown in A). Dashed grey and solid blue lines represent the enhancement due to guided and FP resonances, respectively, while the solid black curve is their sum. The red line is the limit calculated by Yu et al. for a symmetric grating structure. C) represents the W_{FP} for the structure shown in A).

As it has been elaborated earlier, changing the thickness does not influence the maximum or minimum values for W_{FP}, but theW_{FP} is shifted to left or right for decreasing of increasing the thickness, respectively. To test our theoretical analysis, we rigorously calculate the absorption enhancement using a symmetric and an asymmetric grating structure shown in Figure 5.7 (A) and 5.8 (A) respectively. Both gratings have a duty cycle of 50%, height $h = 20$ nm and period of $L = 600$ nm. The structures have a thickness of $d = 1000$ nm. We use TE polarized light under normal incidence within the wavelength range [750 nm, 1100 nm] ($0.54 < s < 0.8$). We use COMSOL Multiphysics, a finite element analysis (FEA) solver, as a modelling tool to rigorously calculate the electromagnetic field inside the absorber. Periodic boundary condition is used to calculate the electric field in the periodic structure. The electric field is then decomposed into its spatial components, using Fourier expansion to calculate the absorption enhancement for each diffraction order [99].

Since Si is a dispersive material, in this simulation we use wavelength-dependent $n(\lambda)$ and $\kappa(\lambda)$data of nc-Si:H [**?**]. The wavelength-dependent absorption coefficient, α , can be calculated using $\kappa(\lambda)$ via $\alpha(\lambda) = 4\pi\kappa(\lambda)/\lambda$. The wavelength-dependency of α implies that γ_i is also a function of wavelength. The electric field inside the structure is calculated for each wavelength, using the wavelength-dependent n and k data. The result for symmetric grating is illustrated in Figure 5.7 (B). Each color represents the absorption enhancement for one diffraction order. There are peaks well beyond both the asymmetric and symmetric 1-D nano-photonic limit ($2\pi n$ and πn, respectively), and one even exceeding the 2-D Lambertian bulk limit ($4n^2$). This example shows that for a

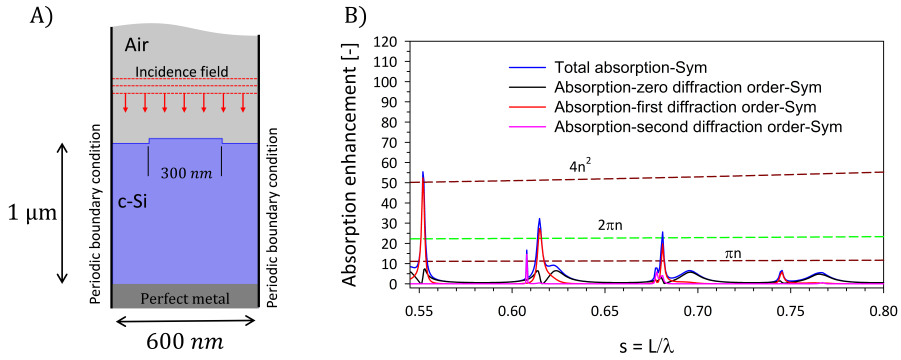

Figure 5.7: A) shows one period of a 1 μm thick Si slab endowed with a symmetric grating. The grating has a period of 600 nm, duty cycle 50% and height of 20 nm. The structure is excited using normal incidence plane wave. The electric field inside the Si slab is calculated using COMSOL multyphysics. B) Shows the absorption enhancement in the structure shown in A), total absorption at each wavelength is divided by the one pass absorption [99] at corresponding wavelength, to calculate the enhancement. Absorption enhancement for each grating order is also presented in different color.

limited frequency range, the enhancement can significantly exceed the nano-photonic limit. Comparing Figure 5.6 (B) and Figure 5.7 (B) one can realize that the absorption enhancement is larger than what is predicted by our theoretical model. One of the reasons is that the analytical approach does not consider the multiple scattering in the structure. It counts each resonance only for the first scattering event (T_i). Whereas, in the rigorous calculation, multiple scattering events are taken into account (T_i and T_i'). Therefore, the simulation shows a higher absorption enhancement. In Figure 5.8 (A), one period of a 1 μm thick Si slab endowed with an asymmetric grating is shown. The only difference between Figure 5.7 (A) and Figure 5.8 (A) is the symmetry of the grating; other specifications are identical. In Figure 5.8 (B) one can see the absorption enhancement for each diffraction order for the structure shown in Figure 5.8 (A). Here, similar to Figure 5.7 (B), the peaks exhibit values well beyond both the asymmetric and symmetric 1-D nano-photonic limit ($(2\pi n$ and πn, respectively), and the 2-D Lambertian bulk limit ($4n^2$). The absorption enhancement at $s = 0.55$ and 0.62 are almost double in Figure 5.8 (B) with respect to Figure 5.7 (B).

5.4. ABSORPTION ENHANCEMENT IN DOUBLE SIDE TEXTURED SLAB

So far, we discussed the case of a single grating structure on a flat mirror. In real thin film solar cells, however, both interfaces might be corrugated, due to manufacturing processes. Now, let us consider a Si slab with thickness of d, having each interface textured with a different periodicity, L_{top} and L_{bot} respectively. In Figure 5.9 light scattering from top (T_i) and bottom (T_i') interfaces of a double side textured slab is shown. Texturing the second interface with different periodicity allows the light to be re-scattered with different angular distribution, thus exciting more resonances.

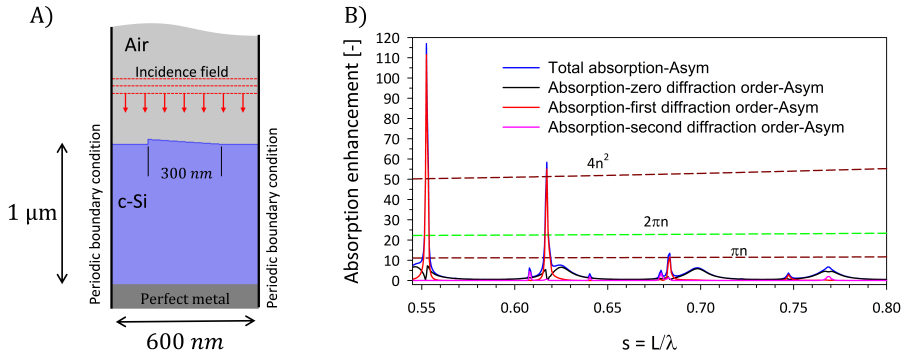

Figure 5.8: A) shows one period of a 1 μm thick Si slab endowed with a symmetric grating. The grating has a period of 600 nm, duty cycle 50% and height of 20 nm. The structure is excited using normal incidence plane wave. The electric field inside the Si slab is calculated using COMSOL multyphysics. B) Shows the absorption enhancement in the structure shown in A), total absorption at each wavelength is divided by the one pass absorption [99] at corresponding wavelength, to calculate the enhancement. Absorption enhancement for each grating order is also presented in different color.

5

The scale of the structure in Figure 5.9 is only for presentation purposes and it is not related to our calculation. Attempting to find the maximum absorption enhancement achievable in such an optical system entails to extend the temporal coupled-mode theory as put forward by Yu et al. [27, 28], since it handles only one side texturing. Therefore, we suggest that the total number of resonances M_{double} is the sum of resonances excited by the top (M_t) and bottom gratings (M_b). The total number of resonances in a 1-D structure with double side periodic texturing in the frequency range $[\omega, \omega + \Delta\omega]$ can be thus calculated as:

$$M_{double} = 2\pi \frac{n^2\omega}{c^2}\left(\psi_{top}\frac{L_{\text{top}}}{2\pi} + \psi_{bot}\frac{L_{\text{bot}}}{2\pi}\right)\left(\frac{d}{2\pi}\right)\Delta\omega \tag{5.11}$$

where L_{top} and L_{bot} are the periodicity of the top and bottom interfaces, respectively .ψ_{top} and ψ_{bot} are the symmetry coefficient for top and bottom gratings respectively. To count the number of resonances based on the diffraction order, we need to use Equations 5.4 for top and bottom grating separately. Doing so, we arrive at:

$$M_{\text{t,b}} = 4\frac{n^2}{c}\cdot\frac{d}{2\pi}\left(\psi_{top}\frac{s_{\text{t}}}{\sqrt{(ns_{\text{t}})^2 - q_{\text{t}}^2}} + \psi_{bot}\frac{s_{\text{b}}}{\sqrt{(ns_{\text{b}})^2 - q_{\text{b}}^2}}\right)\Delta\omega \tag{5.12}$$

where $s_t = L_{top}/\lambda$ and $s_b = L_{bot}/\lambda$ are the normalized frequency of the top and bottom interfaces, respectively; and q_t and q_b are the q^{th} diffraction order of the top and bottom gratings, respectively. If the solar cell is placed on a mirror, then the number of leakage channels (N) only depends on the periodicity of the top interface. If the mirror is not present, N is the sum of channels from top and bottom interfaces. Combining Equations 5.1 and 5.12 , we can obtain the enhancement factor per diffraction order:

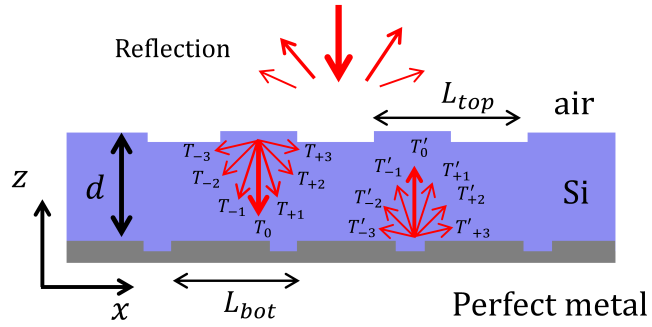

Figure 5.9: Light scattering in a double side periodically textured Si-based slab. The periods of top and bottom gratings are indicated as L_{top} and L_{bot} respectively. The structure has a thickness d. The first and second scattering of the incident plane wave inside the structure, is indicated by T_i and (T'_i respectively. The structure is placed on a grating made of a perfectly reflecting metal. Here, second scattering occurs at the Si-metal interface.

$$F_{\mathrm{t,b}} = \frac{4n}{2\psi_{top}\lfloor s_{\mathrm{t}}\rfloor + 1}\left(\psi_{top}\frac{s_{\mathrm{t}}}{\sqrt{(ns_{\mathrm{t}})^2 - q_{\mathrm{t}}^2}} + \psi_{bot}\frac{s_{\mathrm{b}}}{\sqrt{(ns_{\mathrm{b}})^2 - q_{\mathrm{b}}^2}}\right) \tag{5.13}$$

This equation is a linear sum of the enhancement achieved by the top and bottom surfaces. If we plot the enhancement from top or bottom gratings individually, a graph very similar to Figure 5.3 or Figure 5.4 can be obtained, depending on the symmetry of the grating. Note that for double side texturing top and bottom gratings could have different symmetry. However, since normalized frequency is directly linked to the grating period, the plot for the bottom grating might be shifted to the right or left with respect to the plot for the top grating. The amount of shift depends on the ratio between L_{top} and L_{bot}. If $L_{top}/L_{bot} > 1$, there is a shift toward high frequencies. On the other hand, for $L_{top}/L_{bot} < 1$, a shift toward low frequencies occurs. For $L_{top}/L_{bot} = 1$, no shift is observed. The L_{top}/L_{bot} ratio can be defined according to the applications. In thin film solar cell, it is desirable to increase the absorption in a wide range of frequencies close to the band gap of the material. Therefore, the L_{top}/L_{bot} ratio should be smaller than one. L_{top} should be smaller than the band gap wavelength. On the other hand, L_{bot} should be larger than L_{top}, to ensure maximum excitation of modes. Figure 5.10 (A) schematically shows a slab with double side texturing, the top and bottom gratings are symmetric but they have different periods. The structure in 5.10 (A) is only used for presentation purposes; the scale of top and bottom grating is exaggerated and it is not used for our calculation.

In Figure 5.10 (B) one can see the cumulative enhancement factor calculated for a double side textured film with a thickness of 1000 nm. The period of top and bottom symmetric gratings are 600 nm and 660 nm respectively. Since$L_{top}/L_{bot} < 1$ the red curve is shifted to the left with respect to the blue curve. As it can be seen in Figure 5.10 (B), the solid black line has more peaks than either blue or red curves. The structure in Figure 5.11 (A) shows a 1μm thick slab endowed with asymmetric grating on top and bottom inter-

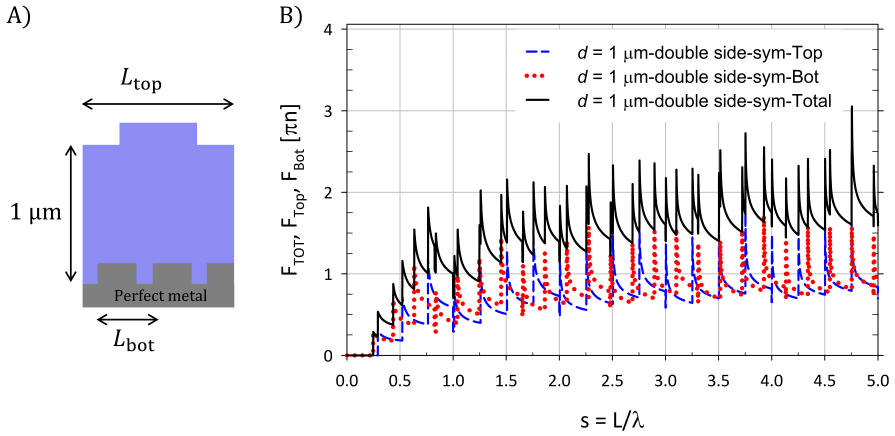

Figure 5.10: A) schematically shows a 1μm thick slab endowed with symmetric grating on two interfaces. The scale of top and bottom grating is exaggerated only for purpose of visualization; B) reports the absorption enhancement from top (blue) and bottom (red) symmetric gratings in a 1000-nm thick Si film. The ration for L_{top}/L_{bot} is equal to 0.909. Total enhancement is shown in black line.

faces. The top and bottom gratings have different periods, the scale of top and bottom grating is exaggerated and it is not used for our calculation. Figure 5.11 (B) represents the absorption enhancement in a structure with double side texturing with asymmetric grating. Apart from the grating symmetry, the structure is identical to the one we used for Figure 5.10 (A). In conformal texturing ($L_{top}/L_{bot} = 1$), peaks resulting from the excitation of modes by top and bottom grating overlap, creating larger peaks ($F_{t,b} = 2F_q$). However, the absorption is not enhanced spectrally. In solar cell application, it is desirable to design top and bottom gratings such that none of the peaks from top and bottom gratings overlap. Therefore, L_{top} should be an aliquant part of L_{bot}, or vice versa [76, 128]. In this way, no multiple of the top grating vector ($q_{top} \cdot k_{top}$) is equal to a multiple of the bottom grating vector ($q_{bot} \cdot k_{bot}$). In other words, none of the diffraction angles from top surface matches with bottom diffraction angles.

5.5. CONCLUSIONS

Leveraging the temporal coupled-mode theory, we have used an alternative method to calculate total number of resonances with same $|k_x|$ in the frequency range $[\omega, \omega + \Delta\omega]$ supported by a grating structure. Our results allow for calculating the maximum absorption enhancement for each diffraction order in 1-D grating structure. We discussed the influence of grating symmetry as well as the film thickness in absorption enhancement. We have shown that in a 1-D grating structure, the absorption can be enhanced much

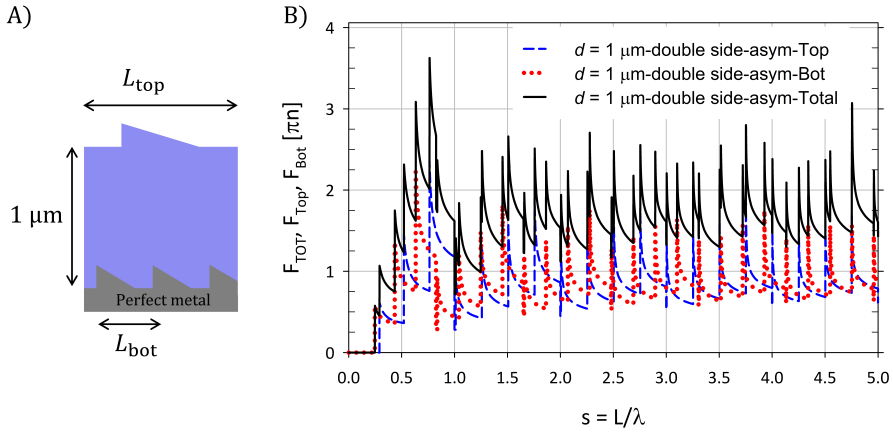

Figure 5.11: A) Schematically shows a 1μm thick slab endowed with asymmetric grating on two interfaces. The scale of top and bottom grating is exaggerated only for purpose of visualization; B) reports the absorption enhancement from top (blue) and bottom (red) asymmetric gratings in a 1000-nm thick Si film. The ration for L_{top}/L_{bot} is equal to 0.909. Total enhancement is shown in black line.

more than $2\pi n$ in multiple frequencies (Figure 5.7). The maxima in cumulative absorption enhancement depends on the grating period, slab thickness and absorber refractive index (see Equation 5.6). For $n = 4$, the absolute maximum occurs when the third diffraction order is active. Furthermore, we have also shown that weight of Fabry-Perot resonances on the total enhancement factor can be computed. In all treated cases, such weight stays below 50% for symmetric and below 30% for asymmetric grating. Moreover, it has been shown that weight of Fabry-Perot resonances on the total enhancement factor does not change with the thickness of the slab. We have also shown that for achieving even higher absorption enhancement within a larger frequency range a double-side grating-textured absorption slab should be considered [128, 129], in which L_{top} should be an aliquant of L_{bot}, or vice versa (see Equation 5.13). This last result further extends the temporal coupled-mode theory as proposed by Yu et al. Finally, we did not consider 2-D gratings in this work, because it is not possible to derive a closed formula independent of grating arrangement and unit cell dimensions. Nevertheless, we expect similar trends in 2-D case. Meaning that, in higher normalized-frequency, the value for absorption enhancement in 2-D structure, would reach the 2-D bulk limit of $4n^2$, but for low frequencies we expect higher absorption enhancement.

6

CONCLUSION

This thesis focusses on a deeper understanding of light behaviour inside a periodically textured thin Si film. The result of the thesis is not limited to solar cell application but it can be used to understand the light behaviour in any periodic textured thin film. Introducing a semi analytical approach to calculate the contribution of each resonance in total absorption is one of the achievements of this thesis. It has been addressed in Chapter 3 and 4 that it is very challenging to track guided modes in a highly textured structure using the dispersion diagram of a flat structure with the same optical thickness as the grating structure. The optical thickness of a grating structure largely depends on the grating properties such as height, duty cycle and grating profile. For a wavelength-scale structure, it is even more challenging to define one optical thickness for all diffraction orders. In the method we have proposed, tracking of guided modes is possible without knowing the optical thickness or the dispersion diagram of the grating structure. This approach calculates the spectral energy density of the electric field inside a periodically-textured nc-Si:H slab using Fourier expansion. The electric field distribution inside the absorber has to be calculated separately using a rigorous electromagnetic simulation tool at optical frequencies. This rigorously-calculated electric filed then is used to calculate the Fourier coefficients. Our proposed method can be used to calculate the absorption for each diffraction order, and to distinguish between guided and non-guided resonances regardless of grating height, incident angle and wavelength range. Chapter 3 and 4 have shown explicitly that using this method one can calculate the weight of each resonance in total absorption. Tracking the distribution of incidence energy within different resonances provides a tool to assess the performance of a new grating design or of an existing one. This is because in our method we rely on the computed electric field inside the structure, rather than the grating profile. Additionally, this method can be used by grating designers to evaluate the impact of their design on the performance of the entire system, or to better understand how manufacturing errors influence the optical performance of the structure. In Chapter 4 we discussed that a flat thin film can be seen as a 1-D photonics crystal with a very clear optical gap. Inside the optical gap, the density of modes (DOM) is very low and consequently the absorption. It has been shown in

this chapter that the presence of grating at the film interface breaks the optical gap and creates more resonances. A higher number of resonances ultimately indicates a larger DOM which leads to higher absorption. The correlation between DOM in the absorber with the absorption peaks is illustrated in Chapter 4. The mode density augments at the photonics band edge. This means that the edge of each absorption peak (absorption by one diffraction order and not the total absorption) should correspond with a peak in DOM. Our method to calculate the weight of a resonance in total absorption can be used for any grating period, wavelength range or incidence angle. However, for grating structures with curved or non-rectangular surfaces, this method probably does not provide accurate result in the non-uniform part of the structure. In this situation, the thickness of sub-layers in the non-uniform part of the structure has to be very thin (depending on the wavelength, grating profile and polarization) to achieve accurate results. In the uniform region, however, this method can be fully trusted. The same principle can be applied for 2-D grating structures to evaluate the optical performance of a real solar cell. In this situation, in each sub-layer a 2-D Fourier transform needs to be employed for each component of electric field (E_x, E_y and E_z). This approach is also not limited to solar cell applications and can be used to understand the light behaviour in different multilayer structures with periodic texturing. Another application of this method is to calculate the absorption enhancement (total absorption over one pass absorption) for a particular diffraction order. Since the absorption for each resonance is known, we are able to calculate the absorption enhancement for that resonance without using the Temporal Coupled-Mode Theory (TCMT). In Chapter 5, maximum absorption enhancement in a 1-D grating waveguide structure is calculated for each diffraction order. The calculation shows that the nano-photonics limit for a 1-D structure can vary depending on the thickness of the film, however, for a very thick structure, the nano-photonic limit surpasses the 2-D bulk limit ($4n^2$) at multiple frequencies. For bulk structure the maximum enhancement occurs at frequency:

$$s_{\max} = \lim_{q \to n^-} \frac{q}{n}$$

where $q$is diffraction order, n is the refractive index and s is the normalized frequency. For example, if $n = 4$, the absolute maximum occurs at frequency where the third diffraction order is excited. In this chapter the influence of grating symmetry in absorption enhancement is also discussed. The result shows that for a thick structure there is no difference between structures with symmetric or asymmetric gratings in maximum absorption enhancement value. Theoretically, the absorption in thick grating structures can be enhanced to infinity, therefore the symmetry of the grating does not play any role. However, for thin structures the role of grating symmetry become more visible. The symmetry of the grating influences the peak height and not the peak positions. Thus, for thin structures, the maxima in cumulative absorption enhancement occur when the normalized frequency is:

$$s = \sqrt{\left(L/(n \cdot d)\right)^2 + \left(q/n\right)^2}$$

where L is grating period and d is the thickness of the slab. Chapter 5 also reports the case study of double side texturing in thin films. In conformal texturing ($L_{top}/L_{bot} = 1$),

peaks resulting from the excitation of modes by top and bottom grating overlap, creating larger peaks ($F_{t,b} = 2F_q$). However, the absorption is not enhanced spectrally. To have high absorption enhancement within a larger frequency range in a double-side grating-textured slab, $L_{top}1$ should be an aliquant of $L_{bot}1$, or vice versa. In this way, no multiple of the top grating vector ($q_{top} \cdot k_{top}$) is equal to a multiple of the bottom grating vector ($q_{bot} \cdot k_{bot}$). In other words, none of the diffraction angles from top surface matches with bottom diffraction angles. Chapter 5 did not consider 2-D gratings structures, because the number of resonances for 2-D gratings highly depends on the dimensions (lattice constant) and arrangement of unit cell (hexagonal, squared, triangular, etc.). Therefore, for 2-D grating it is not possible to derive a close formula independent from grating arrangement and unit cell dimensions.

6.1. OUTLOOK OF THE THESIS:

There is still plenty of room to dig deeper in light behaviour in grating structures. In this thesis, for example, 2-D grating structure were not investigated. The work presented in Chapter 3 and 4 can be extended for 2-D grating. In general, the concept of using Fourier series to decompose total absorption to its components can be used for 2-D grating structures as well. However, the approach slightly changes depending on the lattice constant and lattice arrangement (hexagonal, squared, triangular, etc.). One of the challenges in 2-D grating structure is that regardless of the polarization of incidence light, Fourier transform has to be done for three components of electric field. Another challenge is that Fourier transform has to be modified according to the grating lattice. For example, for a hexagonal lattice, Hexagonal Discrete Fourier transform (HDFT) has to be implemented. In Chapter 5, the maximum absorption enhancement in 1-D grating structure is presented. In this chapter we did not consider 2-D grating structure because the maximum absorption enhancement in structure with 2-D grating strongly depends on the arrangement of unit cell and thus it is not possible to derive a closed equation to calculate the maximum absorption enhancement for 2-D grating. However, it should be still possible to derive a closed formula for each lattice arrangement. Additionally, to derive equation 2.19 in Chapter 2 we have assumed that is identical for all resonances. This assumption does not hold for thin films where the absorber can be seen as an anisotropic media. In this situation varies for each resonance.

REFERENCES

[1] Miltos Tsoskounoglou, George Ayerides, and Efi Tritopoulou. The end of cheap oil: Current status and prospects. *Energy Policy*, 36(10):3797–3806, 2008.

[2] Alexander Tsatskin and Oded Balaban. Peak oil in the light of oil formation theories. *Energy Policy*, 36(6):1826–1828, 2008.

[3] Ugo Bardi. Peak oil: The four stages of a new idea. *Energy*, 34(3):323–326, 2009.

[4] A brief history of solar energy. \T1\textquotedblright,https://www.solarunitedneighbors.org/news/brief-history-solar-energy-2/. November 19, 2015.

[5] A Chodos. April 25, 1954: Bell labs demonstrates the first practical silicon solar cell. *APS News-This month in Physics history*, 2009.

[6] Pierpaolo Spinelli, VE Ferry, J Van de Groep, M Van Lare, MA Verschuuren, REI Schropp, HA Atwater, and A Polman. Plasmonic light trapping in thin-film si solar cells. *Journal of Optics*, 14(2):024002, 2012.

[7] Simone Zanotto, Marco Liscidini, and Lucio Claudio Andreani. Absorption enhancement and light trapping regimes in thin-film silicon solar cells with a photonic pattern. In *Conference on Lasers and Electro-Optics: Applications*, page JTuB3. Optical Society of America, 2010.

[8] Harry A Atwater and Albert Polman. Plasmonics for improved photovoltaic devices. *Nature materials*, 9(3):205, 2010.

[9] Vivian E Ferry, Luke A Sweatlock, Domenico Pacifici, and Harry A Atwater. Plasmonic nanostructure design for efficient light coupling into solar cells. *Nano letters*, 8(12):4391–4397, 2008.

[10] Mary D Archer and Martin A Green. *Clean electricity from photovoltaics*, volume 1. World Scientific, 2001.

[11] Olindo Isabella, Janez Krč, and Miro Zeman. Modulated surface textures for enhanced light trapping in thin-film silicon solar cells. *Applied Physics Letters*, 97 (10):101106, 2010.

[12] Bennett W Schneider, Niraj N Lal, Simeon Baker-Finch, and Thomas P White. Pyramidal surface textures for light trapping and antireflection in perovskite-on-silicon tandem solar cells. *Optics express*, 22(106):A1422–A1430, 2014.

[13] Piotr Kowalczewski, Marco Liscidini, and Lucio Claudio Andreani. Light trapping in thin-film solar cells with randomly rough and hybrid textures. *Optics express*, 21 (105):A808–A820, 2013.

[14] S Mokkapati, FJ Beck, A Polman, and KR Catchpole. Designing periodic arrays of metal nanoparticles for light-trapping applications in solar cells. *Applied Physics Letters*, 95(5):053115, 2009.

[15] Sourav Kanti Jana, Alessia Le Donne, and Simona Binetti. Enhancement of silicon solar cell performances due to light trapping by colloidal metal nanoparticles. *Journal of Physics and Chemistry of Solids*, 73(2):143–147, 2012.

[16] E Wang, TP White, and KR Catchpole. Resonant enhancement of dielectric and metal nanoparticle arrays for light trapping in solar cells. *Optics express*, 20(12): 13226–13237, 2012.

[17] M Zeman, O Isabella, S Solntsev, and K Jäger. Modelling of thin-film silicon solar cells. *Solar Energy Materials and Solar Cells*, 119:94–111, 2013.

[18] Corsin Battaglia, Ching-Mei Hsu, Karin Söderström, Jordi Escarré, Franz-Josef Haug, Mathieu Charrière, Mathieu Boccard, Matthieu Despeisse, Duncan TL Alexander, Marco Cantoni, et al. Light trapping in solar cells: can periodic beat random? *ACS nano*, 6(3):2790–2797, 2012.

[19] Celine Pahud, Olindo Isabella, Ali Naqavi, Franz-Josef Haug, Miro Zeman, Hans Peter Herzig, and Christophe Ballif. Plasmonic silicon solar cells: impact of material quality and geometry. *Optics Express*, 21(105):A786–A797, 2013.

[20] Klaus Jäger, Marinus Fischer, René ACMM van Swaaij, and Miro Zeman. Designing optimized nano textures for thin-film silicon solar cells. *Optics Express*, 21(104): A656–A668, 2013.

[21] Piotr Kowalczewski, Angelo Bozzola, Marco Liscidini, and Lucio Claudio Andreani. Light trapping and electrical transport in thin-film solar cells with randomly rough textures. *Journal of Applied Physics*, 115(19):194504, 2014.

[22] Mika Kambe, Akira Takahashi, Naoki Taneda, Kunio Masumo, Takuji Oyama, and Kazuo Sato. Fabrication of a-si: H solar cells on high haze sno 2: F thin films. In *2008 33rd IEEE Photovoltaic Specialists Conference*, pages 1–4. IEEE, 2008.

[23] Julien Bailat, Luc Fesquet, Jean-Baptiste Orhan, Y Djeridane, B Wolf, P Madliger, J Steinhauser, S Benagli, D Borrello, L Castens, et al. Recent developments of high-efficiency micromorph tandem solar cells in kai-m pecvd reactors. In *Proc. 25th Eur. Photovoltaic Solar Energy Conf./5th World Conf. Photovoltaic Energy Convers.*, pages 2720–2723, 2010.

[24] Olindo Isabella, Folkert Moll, Janez Krč, and Miro Zeman. Modulated surface textures using zinc-oxide films for solar cells applications. *physica status solidi (a)*, 207(3):642–646, 2010.

[25] Baojie Yan, Laura Sivec, Guozhen Yue, Chun-Sheng Jiang, Jeffrey Yang, and Subhendu Guha. Effect of dual-function nano-structured silicon oxide thin film on multi-junction solar cells. In *2011 37th IEEE Photovoltaic Specialists Conference*, pages 002560–002565. IEEE, 2011.

[26] Eli Yablonovitch and George D Cody. Intensity enhancement in textured optical sheets for solar cells. *IEEE Transactions on Electron Devices*, 29(2):300–305, 1982.

[27] Zongfu Yu, Aaswath Raman, and Shanhui Fan. Fundamental limit of nanophotonic light trapping in solar cells. *Proceedings of the National Academy of Sciences*, 107(41):17491–17496, 2010.

[28] Zongfu Yu, Aaswath Raman, and Shanhui Fan. Fundamental limit of light trapping in grating structures. *Optics express*, 18(103):A366–A380, 2010.

[29] SA Shakir and AF Turner. Method of poles for multilayer thin-film waveguides. *Applied Physics A*, 29(3):151–155, 1982.

[30] Martin A Green and Mark J Keevers. Optical properties of intrinsic silicon at 300 k. *Progress in Photovoltaics: Research and Applications*, 3(3):189–192, 1995.

[31] F-J Haug, K Söderström, A Naqavi, C Battaglia, and C Ballif. Excitation of plasmon and guided-mode resonances in thin film silicon solar cells. *MRS Online Proceedings Library Archive*, 1391, 2012.

[32] O El Gawhary, MC Dheur, SF Pereira, and JJM Braat. Extension of the classical fabry–perot formula to 1d multilayered structures. *Applied Physics B*, 111(4):637–645, 2013.

[33] Philippe Lalanne and Dominique Lemercier-Lalanne. On the effective medium theory of subwavelength periodic structures. *Journal of Modern Optics*, 43(10): 2063–2085, 1996.

[34] Philippe Lalanne and Dominique Lemercier-Lalanne. Depth dependence of the effective properties of subwavelength gratings. *JOSA A*, 14(2):450–459, 1997.

[35] Jean Baptiste Joseph Baron Fourier. *The analytical theory of heat*. The University Press, 1878.

[36] Jon M Bendickson, Jonathan P Dowling, and Michael Scalora. Analytic expressions for the electromagnetic mode density in finite, one-dimensional, photonic bandgap structures. *Physical Review E*, 53(4):4107, 1996.

[37] Max Born and Emil Wolf. *Principles of optics: electromagnetic theory of propagation, interference and diffraction of light*. Elsevier, 2013.

[38] Hermann A Haus. Waves and fields in optoelectronics prentice-hall. *Inc. Englewood Cliffs, New Jersey*, 1984.

[39] Ch Kittel. Introduction to solid state physics, 7th edn., chapter 15, 1995.

[40] Angèle Reinders, Pierre Verlinden, Wilfried Van Sark, and Alexandre Freundlich. *Photovoltaic solar energy: from fundamentals to applications*. John Wiley & Sons, 2017.

[41] Carsten Schinke, P Christian Peest, Jan Schmidt, Rolf Brendel, Karsten Bothe, Malte R Vogt, Ingo Kröger, Stefan Winter, Alfred Schirmacher, Siew Lim, et al. Uncertainty analysis for the coefficient of band-to-band absorption of crystalline silicon. *AIP Advances*, 5(6):067168, 2015.

[42] F-J Haug and C Ballif. Light management in thin film silicon solar cells. *Energy & Environmental Science*, 8(3):824–837, 2015.

[43] Baojie Yan, Guozhen Yue, Laura Sivec, Jeffrey Yang, Subhendu Guha, and Chun-Sheng Jiang. Innovative dual function nc-siox: H layer leading to a> 16% efficient multi-junction thin-film silicon solar cell. *Applied Physics Letters*, 99(11):113512, 2011.

[44] Karin Söderström, Grégory Bugnon, Rémi Biron, Céline Pahud, Fanny Meillaud, Franz-Josef Haug, and Christophe Ballif. Thin-film silicon triple-junction solar cell with 12.5% stable efficiency on innovative flat light-scattering substrate. *Journal of Applied Physics*, 112(11):114503, 2012.

[45] Takuya Matsui, Haijun Jia, Michio Kondo, Kouichi Mizuno, Shigenori Tsuruga, Satoshi Sakai, and Yoshiaki Takeuchi. Application of microcrystalline si 1- x ge x infrared absorbers in triple junction solar cells. In *2010 35th IEEE Photovoltaic Specialists Conference*, pages 000311–000316. IEEE, 2010.

[46] Hiroyuki Sakaki, Tomonori Tanoue, Koji Yokoyama, Dian Chau Sun, Yoshinobu Sekiguchi, and Yoshinori Yukimoto. Design and performances of a triple (gaas, si, and ge)-solar-cell system with multi-layered spectrum splitters. *Japanese Journal of Applied Physics*, 20(S2):127, 1981.

[47] Allen Barnett, Douglas Kirkpatrick, Christiana Honsberg, Duncan Moore, Mark Wanlass, Keith Emery, Richard Schwartz, Dave Carlson, Stuart Bowden, Dan Aiken, et al. Very high efficiency solar cell modules. *Progress in Photovoltaics: Research and Applications*, 17(1):75–83, 2009.

[48] Sinae Kim, Shunsuke Kasashima, Porponth Sichanugrist, Taizo Kobayashi, Tokio Nakada, and Makoto Konagai. Development of thin-film solar cells using solar spectrum splitting technique. *Solar Energy Materials and Solar Cells*, 119:214–218, 2013.

[49] Janez Krc, Franc Smole, and Marko Topic. Advanced optical design of tandem micromorph silicon solar cells. *Journal of non-crystalline solids*, 352(9-20):1892–1895, 2006.

[50] R Bouffaron, L Escoubas, V Brissonneau, JJ Simon, G Berginc, Ph Torchio, F Flory, and Ph Masclet. Spherically shaped micro-structured antireflective surfaces. *Optics express*, 17(24):21590–21597, 2009.

[51] Martin A Green. Solar cells: operating principles, technology, and system applications. *Englewood Cliffs, NJ, Prentice-Hall, Inc., 1982. 288 p.*, 1982.

[52] Jordi Escarre, Karin Söderström, Matthieu Despeisse, Sylvain Nicolay, Corsin Battaglia, Gregory Bugnon, Laura Ding, Fanny Meillaud, Franz-Josef Haug, and Christophe Ballif. Geometric light trapping for high efficiency thin film silicon solar cells. *Solar Energy Materials and Solar Cells*, 98:185–190, 2012.

[53] Stuart A Boden and Darren M Bagnall. Optimization of moth-eye antireflection schemes for silicon solar cells. *Progress in Photovoltaics: Research and Applications*, 18(3):195–203, 2010.

[54] T Söderström, F-J Haug, X Niquille, and C Ballif. Tcos for nip thin film silicon solar cells. *Progress in Photovoltaics: Research and applications*, 17(3):165–176, 2009.

[55] Hitoshi Sai and Michio Kondo. Effect of self-orderly textured back reflectors on light trapping in thin-film microcrystalline silicon solar cells. *Journal of Applied Physics*, 105(9):094511, 2009.

[56] Guozhen Yue, Laura Sivec, Jessica M Owens, Baojie Yan, Jeffrey Yang, and Subhendu Guha. Optimization of back reflector for high efficiency hydrogenated nanocrystalline silicon solar cells. *Applied physics letters*, 95(26):263501, 2009.

[57] K Söderström, J Escarré, O Cubero, F-J Haug, S Perregaux, and C Ballif. Uv-nanoimprint lithography technique for the replication of back reflectors for n-i-p thin film silicon solar cells. *Progress in Photovoltaics: Research and Applications*, 19(2): 202–210, 2011.

[58] Benjamin Lipovšek, Janez Krč, Olindo Isabella, Miro Zeman, and Marko Topič. Modeling and optimization of white paint back reflectors for thin-film silicon solar cells. *Journal of applied physics*, 108(10):103115, 2010.

[59] O Isabella, S Dobrovolskiy, G Kroon, and M Zeman. Design and application of dielectric distributed bragg back reflector in thin-film silicon solar cells. *Journal of Non-Crystalline Solids*, 358(17):2295–2298, 2012.

[60] Takashi Koida, Hiroyuki Fujiwara, and Michio Kondo. Reduction of optical loss in hydrogenated amorphous silicon/crystalline silicon heterojunction solar cells by high-mobility hydrogen-doped in2o3 transparent conductive oxide. *Applied Physics Express*, 1(4):041501, 2008.

[61] Chandan Das, Andreas Lambertz, Juergen Huepkes, Wilfried Reetz, and Friedhelm Finger. A constructive combination of antireflection and intermediate-reflector layers for a-si/ μ c-si thin film solar cells. *Applied Physics Letters*, 92(5):053509, 2008.

[62] Didier Dominé, Peter Buehlmann, Julien Bailat, Adrian Billet, Andrea Feltrin, and Christophe Ballif. Optical management in high-efficiency thin-film silicon micromorph solar cells with a silicon oxide based intermediate reflector. *physica status solidi (RRL)–Rapid Research Letters*, 2(4):163–165, 2008.

[63] Sylvie Faÿ, Jérôme Steinhauser, Sylvain Nicolay, and Christophe Ballif. Polycrystalline zno: B grown by lpcvd as tco for thin film silicon solar cells. *Thin Solid Films*, 518(11):2961–2966, 2010.

[64] Corsin Battaglia, Ching-Mei Hsu, Karin Söderström, Jordi Escarré, Franz-Josef Haug, Mathieu Charrière, Mathieu Boccard, Matthieu Despeisse, Duncan TL Alexander, Marco Cantoni, et al. Light trapping in solar cells: can periodic beat random? *ACS nano*, 6(3):2790–2797, 2012.

[65] O Isabella, A Campa, MCR Heijna, W Soppe, R van Erven, RH Franken, H Borg, and M Zeman. Diffraction gratings for light trapping in thin-film silicon solar cells. In *Conference Record of the 23rd European Photovoltaic Solar Energy Conference*, pages 2320–2324, 2008.

[66] N Senoussaoui, M Krause, J Müller, E Bunte, T Brammer, and Helmut Stiebig. Thin-film solar cells with periodic grating coupler. *Thin solid films*, 451:397–401, 2004.

[67] C Haase and Helmut Stiebig. Optical properties of thin-film silicon solar cells with grating couplers. *Progress in Photovoltaics: Research and Applications*, 14(7):629–641, 2006.

[68] Ali Naqavi, Franz-Josef Haug, Corsin Battaglia, Hans Peter Herzig, and Christophe Ballif. Light trapping in solar cells at the extreme coupling limit. *JOSA B*, 30(1): 13–20, 2013.

[69] Aimi Abass and Carsten Rockstuhl. Analytical model of guided modes in structures with rough surfaces. In *Optical Nanostructures and Advanced Materials for Photovoltaics*, pages PTh2B–3. Optical Society of America, 2015.

[70] F-J Haug, Karin Söderström, Ali Naqavi, and Christophe Ballif. Excitation of guided-mode resonances in thin film silicon solar cells. *MRS Online Proceedings Library Archive*, 1321, 2011.

[71] Karin Söderström, Franz-Josef Haug, Jordi Escarre, Oscar Cubero, and Christophe Ballif. Photocurrent increase in n-i-p thin film silicon solar cells by guided mode excitation via grating coupler. *Applied Physics Letters*, 96(21):213508, 2010.

[72] F-J Haug, T Söderström, O Cubero, V Terrazzoni-Daudrix, and C Ballif. Influence of the zno buffer on the guided mode structure in si/zno/ag multilayers. *Journal of Applied Physics*, 106(4):044502, 2009.

[73] Peter N Saeta, Vivian E Ferry, Domenico Pacifici, Jeremy N Munday, and Harry A Atwater. How much can guided modes enhance absorption in thin solar cells? *Optics Express*, 17(23):20975–20990, 2009.

[74] Ulrich W Paetzold, Stephan Lehnen, Karsten Bittkau, Uwe Rau, and Reinhard Carius. Nanoscale observation of waveguide modes enhancing the efficiency of solar cells. *Nano letters*, 14(11):6599–6605, 2014.

[75] Karin Söderström. Coupling light into thin silicon layers for high-efficiency solar cells. Technical report, EPFL, 2013.

[76] O Isabella, R Vismara, DNP Linssen, KX Wang, S Fan, and M Zeman. Advanced light trapping scheme in decoupled front and rear textured thin-film silicon solar cells. *Solar energy*, 162:344–356, 2018.

[77] F-J Haug, K Söderström, A Naqavi, and C Ballif. Resonances and absorption enhancement in thin film silicon solar cells with periodic interface texture. *Journal of Applied Physics*, 109(8):084516, 2011.

[78] Ali Naqavi, F-J Haug, Christophe Ballif, Toralf Scharf, and Hans Peter Herzig. Limit of light coupling strength in solar cells. *Applied Physics Letters*, 102(13):131113, 2013.

[79] Julius Adams Stratton. *Electromagnetic theory*. John Wiley & Sons, 2007.

[80] Jonathan Y Stein. *Digital signal processing: A computer science perspective*. John Wiley & Sons, Inc., 2000.

[81] Christian A Gueymard. The sun's total and spectral irradiance for solar energy applications and solar radiation models. *Solar energy*, 76(4):423–453, 2004.

[82] Romain Cariou, Jan Benick, Frank Feldmann, Oliver Höhn, Hubert Hauser, Paul Beutel, Nasser Razek, Markus Wimplinger, Benedikt Bläsi, David Lackner, et al. Iii–v-on-silicon solar cells reaching 33% photoconversion efficiency in two-terminal configuration. *Nature Energy*, 3(4):326, 2018.

[83] Florent Sahli, Jérémie Werner, Brett A Kamino, Matthias Bräuninger, Raphaël Monnard, Bertrand Paviet-Salomon, Loris Barraud, Laura Ding, Juan J Diaz Leon, Davide Sacchetto, et al. Fully textured monolithic perovskite/silicon tandem solar cells with 25.2% power conversion efficiency. *Nature materials*, 17(9):820, 2018.

[84] Marko Jošt, Eike Köhnen, Anna Belen Morales-Vilches, Benjamin Lipovšek, Klaus Jäger, Bart Macco, Amran Al-Ashouri, Janez Krč, Lars Korte, Bernd Rech, et al. Textured interfaces in monolithic perovskite/silicon tandem solar cells: advanced light management for improved efficiency and energy yield. *Energy & Environmental Science*, 11(12):3511–3523, 2018.

[85] DT Grant, KR Catchpole, KJ Weber, and TP White. Design guidelines for perovskite/silicon 2-terminal tandem solar cells: an optical study. *Optics express*, 24 (22):A1454–A1470, 2016.

[86] Kevin A Bush, Axel F Palmstrom, J Yu Zhengshan, Mathieu Boccard, Rongrong Cheacharoen, Jonathan P Mailoa, David P McMeekin, Robert LZ Hoye, Colin D Bailie, Tomas Leijtens, et al. 23.6%-efficient monolithic perovskite/silicon tandem solar cells with improved stability. *Nature Energy*, 2(4):17009, 2017.

[87] T Todorov, O Gunawan, and S Guha. A road towards 25% efficiency and beyond: perovskite tandem solar cells. *Molecular Systems Design & Engineering*, 1(4):370–376, 2016.

[88] Hairen Tan, Laura Sivec, Baojie Yan, Rudi Santbergen, Miro Zeman, and Arno HM Smets. Improved light trapping in microcrystalline silicon solar cells by plasmonic back reflector with broad angular scattering and low parasitic absorption. *Applied Physics Letters*, 102(15):153902, 2013.

[89] Karin Söderström, Grégory Bugnon, Rémi Biron, Céline Pahud, Fanny Meillaud, Franz-Josef Haug, and Christophe Ballif. Thin-film silicon triple-junction solar cell with 12.5% stable efficiency on innovative flat light-scattering substrate. *Journal of Applied Physics*, 112(11):114503, 2012.

[90] Carissa N Eisler, Emily D Kosten, Emily C Warmann, and Harry A Atwater. Spectrum splitting photovoltaics: Polyhedral specular reflector design for ultra-high efficiency modules. In *2013 IEEE 39th Photovoltaic Specialists Conference (PVSC)*, pages 1848–1851. IEEE, 2013.

[91] Min Seok Jang and Harry Atwater. Plasmonic rainbow trapping structures for light localization and spectrum splitting. *Physical Review Letters*, 107(20):207401, 2011.

[92] Chetan Singh Solanki and Hemant Kumar Singh. *Anti-reflection and light trapping in c-Si solar cells*. Springer, 2017.

[93] H Iida, N Shiba, T Mishuku, H Karasawa, A Ito, M Yamanaka, and Y Hayashi. Efficiency of the a-si: H solar cell and grain size of sno 2 transparent conductive film. *IEEE Electron Device Letters*, 4(5):157–159, 1983.

[94] K Söderström, J Escarré, O Cubero, F-J Haug, S Perregaux, and C Ballif. Uv-nanoimprint lithography technique for the replication of back reflectors for n-i-p thin film silicon solar cells. *Progress in Photovoltaics: Research and Applications*, 19(2): 202–210, 2011.

[95] Takashi Koida, Hiroyuki Fujiwara, and Michio Kondo. Reduction of optical loss in hydrogenated amorphous silicon/crystalline silicon heterojunction solar cells by high-mobility hydrogen-doped in2o3 transparent conductive oxide. *Applied Physics Express*, 1(4):041501, 2008.

[96] N Rezaei, O Isabella, ZAEP Vroon, and M Zeman. Optical optimization of a multilayer wideband anti-reflection coating using porous mgf2 for sub-micron-thick cigs solar cells. *Solar Energy*, 177:59–67, 2019.

[97] Hele Savin, Päivikki Repo, Guillaume Von Gastrow, Pablo Ortega, Eric Calle, Moises Garín, and Ramon Alcubilla. Black silicon solar cells with interdigitated back-contacts achieve 22.1% efficiency. *Nature nanotechnology*, 10(7):624, 2015.

[98] Daria Freier, Roberto Ramirez-Iniguez, Tahseen Jafry, Firdaus Muhammad-Sukki, and Carlos Gamio. A review of optical concentrators for portable solar photovoltaic systems for developing countries. *Renewable and Sustainable Energy Reviews*, 90:957–968, 2018.

[99] H Ahmadpanahi, R Vismara, O Isabella, and M Zeman. Distinguishing fabry-perot from guided resonances in thin periodically-textured silicon absorbers. *Optics express*, 26(18):A737–A749, 2018.

[100] Omar El Gawhary, Nick J Schilder, Alberto da Costa Assafrao, Silvania F Pereira, and H Paul Urbach. Restoration of s-polarized evanescent waves and subwavelength imaging by a single dielectric slab. *New Journal of Physics*, 14(5):053025, 2012.

[101] Omar El Gawhary, Nick J Schilder, Alberto da Costa Assafrao, Silvania F Pereira, and H Paul Urbach. Restoration of s-polarized evanescent waves and subwavelength imaging by a single dielectric slab. *New Journal of Physics*, 14(5):053025, 2012.

[102] O El Gawhary, MC Dheur, SF Pereira, and JJM Braat. Extension of the classical fabry–perot formula to 1d multilayered structures. *Applied Physics B*, 111(4):637–645, 2013.

[103] Ronald Newbold Bracewell and Ronald N Bracewell. *The Fourier transform and its applications*, volume 31999. McGraw-Hill New York, 1986.

[104] For more information about COMSOL Multiphysics, See: . https://www.comsol.eu/, . Accessed: 17-11-2018.

[105] For more information about Wolfram Mathematica please visit: . http://www.wolfram.com/mathematica/, . Accessed: 17-11-2018.

[106] K. Söderström O. Isabella H. Peter Herzig C. Ballif M. Zeman A. Naqavi, F. J. Haug. Geometrical impact on guided mode excitation in solar cells. In *Renewable Energy and the Environment Optics and Photonics Congress*, page JM5A.21. Optical Society of America, 2012.

[107] Karin Söderström. Coupling light into thin silicon layers for high-efficiency solar cells. Technical report, EPFL, 2013.

[108] Lucio Claudio Andreani, Angelo Bozzola, Piotr Kowalczewski, Marco Liscidini, and Lisa Redorici. Silicon solar cells: toward the efficiency limits. *Advances in Physics: X*, 4(1):1548305, 2019.

[109] Takuya Matsui, Haijun Jia, Michio Kondo, Kouichi Mizuno, Shigenori Tsuruga, Satoshi Sakai, and Yoshiaki Takeuchi. Application of microcrystalline si 1- x ge x infrared absorbers in triple junction solar cells. In *2010 35th IEEE Photovoltaic Specialists Conference*, pages 000311–000316. IEEE, 2010.

[110] H Lee, S Ahn, S Lee, and J Choi. Silicon thin film technology applications for low cost and high efficiency photovoltaics. In *21st International Photovoltaic Science and Engineering Conference, Fukuoka 4A–2I–01*, 2011.

[111] Takashi Koida, Hiroyuki Fujiwara, and Michio Kondo. Reduction of optical loss in hydrogenated amorphous silicon/crystalline silicon heterojunction solar cells by high-mobility hydrogen-doped in2o3 transparent conductive oxide. *Applied Physics Express*, 1(4):041501, 2008.

[112] Simon P Philipps, Frank Dimroth, and Andreas W Bett. High-efficiency iii–v multijunction solar cells. In *McEvoy's Handbook of Photovoltaics*, pages 439–472. Elsevier, 2018.

[113] Volker Steenhoff, Maren Juilfs, Regina-Elisabeth Ravekes, Martin Vehse, and Carsten Agert. Resonant-cavity-enhanced a-ge: H nanoabsorber solar cells for application in multijunction devices. *Nano energy*, 27:658–663, 2016.

[114] Pulin Yeh and Naichia Yeh. Design and analysis of solar-tracking 2d fresnel lens-based two staged, spectrum-splitting solar concentrators. *Renewable energy*, 120: 1–13, 2018.

[115] Alexander Dorodnyy, Valery Shklover, Leonid Braginsky, Christian Hafner, and Juerg Leuthold. High-efficiency spectrum splitting for solar photovoltaics. *Solar Energy Materials and Solar Cells*, 136:120–126, 2015.

[116] Takashi Fujibayashi, Takuya Matsui, and Michio Kondo. Improvement in quantum efficiency of thin film si solar cells due to the suppression of optical reflectance at transparent conducting oxide/si interface by ti o 2/ zn o antireflection coating. *Applied physics letters*, 88(18):183508, 2006.

[117] M-Y Chiu, C-H Chang, M-A Tsai, F-Y Chang, and Peichen Yu. Improved optical transmission and current matching of a triple-junction solar cell utilizing sub-wavelength structures. *Optics Express*, 18(103):A308–A313, 2010.

[118] Jordi Escarre, Karin Söderström, Matthieu Despeisse, Sylvain Nicolay, Corsin Battaglia, Gregory Bugnon, Laura Ding, Fanny Meillaud, Franz-Josef Haug, and Christophe Ballif. Geometric light trapping for high efficiency thin film silicon solar cells. *Solar Energy Materials and Solar Cells*, 98:185–190, 2012.

[119] Ralf B Wehrspohn, Uwe Rau, and Andreas Gombert. *Photon management in solar cells*. John Wiley & Sons, 2015.

[120] HW Deckman, CR Wronski, H Witzke, and E Yablonovitch. Optically enhanced amorphous silicon solar cells. *Applied Physics Letters*, 42(11):968–970, 1983.

[121] HW Deckman and JH Dunsmuir. Applications of surface textures produced with natural lithography. *Journal of Vacuum Science & Technology B: Microelectronics Processing and Phenomena*, 1(4):1109–1112, 1983.

[122] Christian Stefano Schuster. *Diffractive optics for thin-film silicon solar cells*. Springer, 2016.

[123] Eli Yablonovitch. Statistical ray optics. *JOSA*, 72(7):899–907, 1982.

[124] Johann Heinrich Lambert. *Photometria sive de mensura et gradibus luminis, colorum et umbrae*. Klett, 1760.

[125] Patrick Campbell and Martin A Green. Light trapping properties of pyramidally textured surfaces. *Journal of Applied Physics*, 62(1):243–249, 1987.

[126] Eugene Hecht. Hecht optics. *Addison Wesley*, 997, 1998.

[127] Howard R Stuart and Dennis G Hall. Thermodynamic limit to light trapping in thin planar structures. *JOSA A*, 14(11):3001–3008, 1997.

[128] Wei-Chun Hsu, Jonathan K Tong, Matthew S Branham, Yi Huang, Selçuk Yerci, Svetlana V Boriskina, and Gang Chen. Mismatched front and back gratings for optimum light trapping in ultra-thin crystalline silicon solar cells. *Optics Communications*, 377:52–58, 2016.

[129] Ken Xingze Wang, Zongfu Yu, Victor Liu, Yi Cui, and Shanhui Fan. Absorption enhancement in ultrathin crystalline silicon solar cells with antireflection and light-trapping nanocone gratings. *Nano Letters*, 12(3):1616–1619, 2012. doi: 10.1021/nl204550q. URL https://doi.org/10.1021/nl204550q. PMID: 22356436.

SUMMARY

The absorption coefficient of a semiconductor drops significantly for photons with energy smaller than its band gap energy. The band gap of silicon falls in the near infra-red (NIR) part of the spectrum and therefore, red and NIR photons have to travel a large distance in silicon-based solar cells before they are absorbed. This is a common issue for all silicon based solar cells, including the wafer-based devices. But it is more pronounced for thin-film solar cells. To overcome this issue light trapping techniques such as:
are usually implemented in thin-film solar cells. This thesis explores light trapping in thin-film structures with periodic surface texturing. In specific, this thesis studies the weight of absorption by each diffraction order in total absorption. Furthermore, this thesis explores the maximum absorption enhancement in a thin film textured by a 1-D grating. Additionally, the role of grating symmetry and the number of textured interfaces are studied in this thesis. This thesis is focused on a deeper understanding of light behaviour inside a periodically textured Si film. The result of the thesis, however, is not limited to solar cell application and can be used to understand the light behaviour in any periodic textured thin film. Introducing a semi analytical approach to calculate the contribution of each resonance in total absorption is one of the achievements of this thesis. It has been addressed in Chapter 3 and 4 that it is very challenging to track guided modes in a highly textured structure using the dispersion diagram of a flat structure with the same optical thickness as the grating structure. The optical thickness of a grating structure largely depends on the grating properties such as height, duty cycle and grating profile. For a wavelength-scale structure, it is even more challenging to define one optical thickness for all diffraction orders. In the method we have proposed, tracking of guided modes is possible without knowing the optical thickness or the dispersion diagram of the grating structure. To these ends, the following research questions are asked:

1. How to distinguish between the different types of resonance (particularly guided and non-guided resonances) in a periodically textured thin film solar cell?
   (a) What is the contribution of each resonance to the total absorption?
   (b) How does the contribution of resonances in total absorption change under oblique incidence?
   (c) How the absorption peaks match with the density of the modes in the absorber?
2. What is the maximum absorption enhancement achievable using periodic texturing?
   (a) How much is the contribution of each resonance in light trapping limit for grating structure?

(b) What is the ratio between top and bottom grating periods in a double interface textured thin film to achieve maximum absorption enhancement over a large wavelength range?

This thesis is structured in six distinct chapters. In Chapter 1 a general introduction is given to address the main challenge in thin-film silicon solar cells and to motivate the need for light trapping. This chapter also describes the main focus of this thesis and the urge to understand the light behaviour inside a periodic waveguide thin film. This is followed by Chapter 2, which provides the mathematical background and the frame work which has been used throughout the thesis. This chapter presents some practical details and calculation techniques which have been used to obtain our result. In Chapter 3, a semi-analytical approach is introduced to calculate the contribution of guided and non-guided resonances to total absorption of a grating waveguide structure under normal incidence. In this approach, we use Fourier expansion to calculate the energy spectral density of the electric field inside the absorber. In this way, the weight of each resonance in total absorption is defined for a large wavelength range for TM and TE polarization. Additionally, the proposed mathematical model is supported by numerical and rigorous calculations, using a software based on the finite element method. This approach is extended for oblique incidence in Chapter 4. In this chapter it is explained how the variation of tangential and normal components for TM electric field under oblique incidence influences the accuracy of numerical calculation. The correlation between the density of modes and the absorption peaks due to guided mode excitation is also presented in this chapter. Chapter 5 focuses on calculating the maximum absorption enhancement achieved by each type of resonance in a waveguide structure with symmetric and asymmetric gratings. In this chapter a different approach is introduced to count the number of resonances in a grating waveguide structure, at each frequency. Then, temporal coupledmode theory is used to calculate the maximum absorption enhancement for each diffraction order. This approach is extended for a thin film with double-side texturing. Chapter 6 provides the conclusion of the thesis.

SAMENVATTING

De absorptiecoëfficiënt voor een halfgeleider is aanzienlijk kleiner dan de bandafstandsenergie. De band gap van silicium valt in het nabije infrarood (NIR) deel van het spectrum en daarom hebben fotonen in NIR een grote afstand in silicium gebaseerde zonnecellen voordat ze worden geabsorbeerd. Dit is een veel voorkomend probleem voor alle op silicium gebaseerde zonnecellen, inclusief de op wafers gebaseerde apparaten. Maar het is meer uitgesproken voor zonnecellen met dunne film. Om dit probleem te omzeilen, zijn technieken om licht te vangen zoals:
Zijn meestal geïmplementeerd in dunne film zonnecellen. Dit proefschrift onderzoekt lichtstripping in dunne filmstructuren met periodieke oppervlaktetextuur. In het bijzonder bestudeert dit proefschrift het gewicht van absorptie door elke diffractieorde in totale absorptie. Verder onderzoekt dit proefschrift de maximale absorptieverbetering in een dunne film met een 1-D raster. Bovendien worden de rol van raspsymmetrie en het aantal gestructureerde grensvlakken bestudeerd in dit proefschrift.
Dit proefschrift richt zich op een beter begrip van lichtgedrag in een periodiek gestructureerde c-Si film. Het resultaat van het proefschrift is echter niet beperkt tot de toepassing van zonnecellen en kan worden gebruikt om het lichtgedrag in een periodieke dunne textuurfilm te begrijpen. Het introduceren van een semi-analytische benadering om de bijdrage van elke resonantie in totale absorptie te berekenen, is een van de prestaties van dit proefschrift. In hoofdstuk 3 en 4 is aan de orde gekomen dat het een hele uitdaging is om geleide modi in een structuur met een hoge structuur te volgen met behulp van het spreidingsdiagram van een platte structuur met dezelfde optische dikte als de roosterstructuur. De optische dikte van een traliestructuur hangt grotendeels af van de tralie-eigenschappen zoals hoogte, werkcyclus en roostervorm. Voor een golflengteschaalstructuur is het nog uitdagender om één optische dikte voor alle diffraktieopdrachten te definiëren. In de methode die we hebben voorgesteld, is het volgen van geleide modi mogelijk zonder de optische dikte of het verspreidingsdiagram van de roosterstructuur te kennen. Hiertoe worden de volgende onderzoeksvragen gesteld:

1. Hoe onderscheid te maken tussen de verschillende soorten resonantie (met name geleide en niet-geleide resonanties) in een periodiek gestructureerde dunne film zonnecel?
   (a) Wat is de bijdrage van elke resonantie in totale absorptie?
   (b) Hoe verandert de bijdrage van resonanties in totale absorptie onder schuine incidentie?
   (c) Hoe de absorptiepieken overeenkomen met de dichtheid van de modi in de absorber?
2. Wat is de maximaal haalbare absorptieverbetering met behulp van periodieke texturering?

(a) Hoeveel bedraagt de bijdrage van elke resonantie in de limiet voor lichtgrit voor de roosterstructuur?

(b) Wat is de verhouding tussen de bovenste en onderste roosterperioden in een getextureerde dunne film met dubbele interface om maximale absorptieverbetering over een groot golflengtebereik te bereiken?

Dit proefschrift is gestructureerd in zes verschillende hoofdstukken. In hoofdstuk 1 wordt een algemene inleiding gegeven om de belangrijkste uitdaging aan te gaan in dunne film siliciumzonnecellen en om de noodzaak van lichtinvang te motiveren. Dit hoofdstuk beschrijft ook de belangrijkste focus van dit proefschrift en de drang om het lichtgedrag in een periodieke dunne golfgeleiderfilm te begrijpen. Dit wordt gevolgd door Hoofdstuk 2 voor de wiskundige achtergrond en het kaderwerk dat in de hele scriptie is gebruikt. Dit hoofdstuk bevat enkele praktische details en berekeningsmethoden die zijn gebruikt om ons resultaat te verkrijgen. In Hoofdstuk 3 wordt een semi-analytische benadering geïntroduceerd om de bijdrage van geleide en niet-geleide resonanties aan totale absorptie voor een golfvormende golfgeleiderstructuur onder normale invalshoek te berekenen. In deze benadering gebruiken we Fourier-expansie om de energiespectrale dichtheid van het elektrische veld in de absorber te berekenen. Op deze manier wordt het gewicht van elke resonantie in totale absorptie gedefinieerd voor een groot golflengtebereik voor TM- en TE-polarisatie. Bovendien wordt het voorgestelde wiskundige model ondersteund door numerieke en rigoureuze berekeningen, met behulp van een software die is gebaseerd op de eindige-elementenmethode. Deze benadering wordt in hoofdstuk 4 uitgebreid voor schuine incidentie. In dit hoofdstuk wordt uitgelegd hoe de variatie van tangentiële en normale componenten voor TM elektrisch veld onder schuine inval invloed heeft op de nauwkeurigheid van numerieke berekening. De correlatie tussen de dichtheid van modi en de absorptiepieken als gevolg van begeleide modus-excitatie wordt ook gepresenteerd in dit hoofdstuk. Hoofdstuk 5 richt zich op het berekenen van de maximale absorptie-verbetering bereikt door elk type resonantie in een golfgeleiderstructuur met symmetrische en asymmetrische rasters. In dit hoofdstuk wordt een andere benadering geïntroduceerd om het aantal resonanties in een roostergolfgeleiderstructuur bij elke frequentie te tellen. Vervolgens wordt de temporele koppelmodustheorie gebruikt om de maximale absorptieverbetering voor elke diffractievolgorde te berekenen. Deze aanpak wordt uitgebreid voor een dunne film met dubbelzijdige texturen aan de zijkant. Hoofdstuk 6 geeft de conclusie van het proefschrift.

LIST OF PUBLICATIONS

4. **H. Ahmadpanahi**, R. Vismara, O. Isabella, and M. Zeman, *Understanding the nano-photonics absorption limit in both front-side and front/rear-side textured slabs*, Opt. Express **27**, A1173-A1187 (2019).

3. **H. Ahmadpanahi**, O. El Gawhary, R. Vismara, O. Isabella, and M. Zeman, *Assessing light absorption contributions in thin periodically-textured silicon absorbers under oblique illumination*, AIP Advances **9**, A737-A749 (2018).

2. **H. Ahmadpanahi**, R. Vismara, O. Isabella, and M. Zeman, *Distinguishing Fabry-Perot from guided resonances in thin periodically-textured silicon absorbers*,in Light, Energy and the Environment 2018 (E2, FTS, HISE, SOLAR, SSL), OSA Technical Digest Optical Society of America (2018), paper OT5C.3..

1. **H. Ahmadpanahi**, R. Vismara, O. Isabella, and M. Zeman, *Distinguishing Fabry-Perot from guided resonances in thin periodically-textured silicon absorbers*, Opt. Express **26**, A737-A749 (2018).

ACKNOWLEDGEMENTS

Completing a PhD is a great personal accomplishment, I could not have done this without the help of many others whom I will acknowledge now. My sincerest apologies if I have left you out. The first phase of my PhD started on October 2013, when I joined the Optics research group in the faculty of applied science. I would like to start by expressing my gratitude to Prof. Dr Paul Urbach the head of Optics research group. Whom without his help I would not be able to start my PhD at TU Delft. Paul, thanks for accepting me in your group and providing me with the facilities and the means for research. Another person who has helped me a lot is Dr. Omar El Gawhary. Omar, I really would like to thank you for all of your help. I have learned a lot from you, in physics and mathematics. You have inspired me as a person, by not compromising scientific quality for whatever reason or being eager and available to help. I never forget our philosophical discussions in VSL while eating "panini met kaas en tomaat". Actually, without your support I probably would never have had a chance to do part of my research at VSL. Thank you again, Omar. I also would like to thanks Dr. Aurèle Adam, for many short and long scientific discussions on diffractive optics and especially in helping me to create a simple model for a complicated phenomenon. I would like to thank you Dr. Silvania Pereira and Dr. Sarathi Roy, whom I had a chance to collaborate with in one of their many projects. Thanks to Dr. Nandini Bhattacharya for her great contribution in Optica. Additionally, I would like to show my gratitude to Ms. Yvonne van Aalst for doing all the paper works and the arrangements. Yvonne, I know that from the bureaucratic point of view I never fell in the normal category of students/candidate and you always had to find a way to deal with my case. I would like to say that I really appreciate your effort and I am very thankful. Having a desktop in Optics research group and running heavy simulations on a remote server is not possible without the help from Mr. Roland Horsten and Mr. Thim Zuidwijk. Your hard effort in the background to keep everything functional and working is very much appreciated. Thank you very much for teaching me how to connect to a remote server and to spend hours to facilitate my large simulations. A special thanks to my Optica colleagues which are more friends to me for your hospitality and for accepting me in your group especially during the time that I, myself, had no idea whether I stay in Delft or I have to go back to Madrid. Dr. Nitish Kumar, you were always giving me the courage and hope to continue especially at the beginning when I was completely lost. Dr. Alessando Polo I really enjoyed any discussion with you, serious, funny, and scientific or even cooking. I am really glad that you are still my colleagues. Dr. Adonis Reyes Reyes, the gods of experiments, I really thank you Adonis for your helps for finding the right contact person to analyse my hornet, for patiently listening to my broken Spanish and for introducing me to the right people in the job market. Zhe Huo, my lovely officemate in Optica, I want to thank you for your friendship, for going through all our frustrations together and for always being a good company. knock, knock, knock, coffee?, that is Dr. Andreas Hänsel, trying to remind you that you need a coffee break. Andreas, of course, this is not the

only memory I have from you, but let us not to go through all of them. I really enjoyed your sense of humour, as much as our serious discussions and practicing Jujitsu. Dr. Matthias Strauch thanks for your Christmas cookies. Dr. Yifeng Shao, I really appreciate your frank, to the point and insisting attitude. Thanks for sharing the real tea with us and teaching us how to make it. Dr. Luca Chisotto, Dr. Ying Tang, Dr. Daniel Nascimento-Duplat and Dr. Priya Dwivedi we have managed to revitalize the SPIE student chapter in Optica. We have funded few students to attend SPIE conference, we arranged workshops and regular meetings. I really enjoyed working with all of you. In fact, I am very happy that we are still working in a same company.

The second phase of my PhD started when I moved to the group of Photovoltaic Material and Devices (PVMD) to start a joint collaboration between Optica and PVMD. I would like to start by thanking my first promotor Prof. dr. Miro Zeman for giving me the opportunity to work in the Photovoltaic Materials and Devices (PVMD) research group. Miro, I really liked the way you lead the group to keep it collaborative, nationally and internationally, and to make sure the group provides the necessary means to do the good work. I sincerely believe that the success of PVMD is greatly because of your good leadership. Furthermore, I would like to thank my second promotor Dr. Olindo Isabella. Olindo, it is very hard to show my gratitude in just few words. You are my promotor and supervisor, but at the same time you are a source of inspiration and a guru. I really appreciate all those late evenings that you stayed at work to teach me, all those weekends that you were available to read my manuscripts or talk to me to make sure I am in the right path. Without your help, support and great supervision I would not have been here. Thank you for every piece of advice and every criticism you have given to me. I sincerely like to thank you for all of your support and wish you all the best in your carrier (I am very sure you will be). I would also like to thank the rest of my committee, Prof. dr. J. Poortmans, prof.dr. A. Neto, Prof. dr. Janez Krč, Dr. Christian Seassal, and Dr. O. El Gawhary. I want to thank you for coming out to Delft for my defence. Moreover, I also want to thanks the secretaries of the PVMD and EKL for the perfect job in solving bureaucratic problems. Especially, I want to thank Ilona van der Wenden (get well soon), Sharmila Rattansingh, and Claudia de Kooter. I would like to thanks my officemates Robin Vismara and Dr. Hesan Ziar. Robin, thank you very much for all of those discussions on counting the number of resonances in thin-film structure. I always liked your critical mind and enjoyed our discussions. Thanks for helping me in my manuscripts either by correcting my mistakes or by asking right questions. Hesan, I should also thank you for answering my questions and doubts on discrete Fourier transform. I really enjoyed our coffee breaks and short chats. From other members of PVMD, I like to thanks Associate Professor, Dr. René van Swaaij; René, your discipline and your critical nature was an inspiration for me. Thanks for helping me to do one of my left-over exams in Madrid. Furthermore, I cannot miss Professor dr. Arno Smets with his warm cheerful personality. Arno, I am really inspired by your effort and motivation to create Solar Energy MOOC. Thanks for your positive and warm personality. I also would like to thanks the rest of PVMD group for being such warm and welcoming colleagues. Dr. ir. Rudi Santbergen, Dr. Paul A. Procel Moya, Dr. Guangtao Yang, Dr. Ravi Vasudevan, Johan Blanker, Gianluca Limodio, Nasim Rezaei, Yilei Tian , Dr. Dimitris Deligiannis and Fai Tong Si. I must also acknowledge my own family. Dad, you never gave up supporting us in our education. In fact, you always

pushed me to go forward and encouraged me to study harder. You never hesitate to work harder and longer to provide us with a better school and education. I would like to thank you with all of my heart. Without your courage my life would have been probably different. Mom, you also never stopped encouraging me to study harder. I really appreciate the way you did your study while working full time, rising us and handling the house. I am not as strong as you mom, but I am very happy to follow your advice and study hard. Mojde, my sweetheart, I think you were the only one who was involved with my PhD almost as I was. You always encouraged me to continue. Without your patience, sacrifice and company I definitely would not be able to finish this journey. I am very happy to have you and owe a lot of my success to your love and support. I am sure that we will have more cheerful time. Thank you very much.

بابای مهربونم:

همیشه درس خوندن ما برات اولین اولویت بود. این جمله که "فرش زیر پام رو میفروشم که شما درس بخونین" رو هیچ وقت یادم نمیره. ازت میپرسیدم چرا باید درس بخونم؟ میگفتی واسه اینکه کار خوب گیرت بیاد، واسه اینکه موقعیت اجتماعی خوب داشته باشی، همسر خوبی گیرت بیاد... امروز به همه اونها رسیدم بابا! امروز و هر روز بیشتر میفهمم که اون روزها کجا رو میدیدی و برام چه چیزی رو متصور بودی. امروز اگر دقیقا اونجا نباشم، بهش خیلی نزدیکم، خوشحالم و احساس خوبی دارم، و همه اینها رو مدیون زحمت ها، راهنمایی‌ها و فداکاری‌های شما هستم. بابا ازت خیلی خیلی ممنونم بخاطر همه چیزهای که یادمون دادی.

مامان عزیزم:

همه جور زحمتی رو به جون خریدی که ما راحت و بی دغدغه به درس هامون برسیم، توی تمام درسها و امتحان‌ها همراه ما درس خوندی، انگار که خودت امتحان داری. هیچ وقت یادم نمیره اون روزهای سخت و پر از نا امیدیِ بعد از رد شدن توی المپیاد فیزیک رو، زمانی که اینقدر نا امید بودم که حتا نمی‌خواستم کنکور بدم. اگر تشویقِ ها، امیدها و هم دردی‌های تو نبود، حس خوب امروز رو نداشتم. اگر خون دل خوردن‌ها و صبوری‌هات نبود، این پسر بازیگوش و شیطون امروز اینجا نبود. ازت ممنونم مامان، به خاطر همه فشارهایی که روی ما آوردی و بخاطر تمام چیزهایی که بهمون یاد دادی و بخاطر همه زحمت‌هایی که کشیدی. امروز اون زحمت‌ها نتیجه داده و "کلاغ پرِ" منم تموم شده.

همسر نازنینم:

عزیزم با اطمینان می‌تونم بگم که بعد از من هیچ کسی اندازه تو درگیر دکتری من نبود. اگر دلداری‌های تو توی تمام روزهای خستگی و ناامیدیم نبود، اگر صبوری تو توی تمام آخر هفته‌هایی که توی خونه موندیم که من کار کنم نبود، من امروز اینجا نبودم. ازت ممنونم که توی تمام سختی‌ها با من بودی و بهم امید دادی، ازت ممنونم که وقتی در اوج ناامیدی بودم، بهم انگیزه می‌دادی. مژده نازنینم، از بودن کنار تو احساس خوشبختی و بخاطر داشتنت از خدا ممنونم. امروز همه اون سختیها و شب زنده داری‌ها به ثمر میرسه. و من مطمئنم که روزهای خیلی خوش تری منتظر ماست.

CURRICULUM VITÆ

EDUCATION

2013-Now	**PhD candidate** at PVMD Group, DELFT UNIVERSITY OF TECHNOLOGY (TUDELFT)	Netherlands
Thesis	**Light trapping in Si thin film solar cells**	
2007-2009	**M.Sc** in PHOTONICS,	Sweden - Belgium
	Vrije Universiteit Brussel & Royal Institute of Technology	
Thesis	**"Design of laser illumination system for projection display"**	
2000-2004	**B.Sc** in APPLIED PHYSICS,	Iran
	Iran University of Science and Technology	
Thesis	**"Speed measurement by means of laser speckle"**	

WORK EXPERIENCE

Present Jun-2018	**Design Engineer** at ASML, *Beam Delivery and spatial quality*	Veldhoven
Jun-2018 May-2017	**Opto-mechanical Designer** at OCÉ TECHNOLOGIES, *Beam delivery and illumination system for extended UV-LED source*	Venlo
Nov-2014 Mar-2014	**Internship** at DUTCH METROLOGY INSTITUTE (VSL), *Optical properties of oriental hornets cuticle*	Delft
Aug-2013 Feb-2011	**Researcher** at RESEARCH CENTRE FOR SMART BUILDINGS AND ENERGY EFFICIENCY, *1-Light Diffraction in a Multichannel Lens system for Imaging application* *2-Sub-wavelength resolution with positive refraction index*	Madrid

Dec-2009 Nov-2009	**Lab Assistant** at VRIJE UNIVERSITEIT BRUSSEL, *Spectroscopy*	Brussels
Jul-2007 Nov-2006	**Manager** at KAVAK PARTO ARIA, *Opto-mechanics*	Tehran
Aug-2006 Jul-2004	**Technical engineer** at LASER AND PHOTONICS TECHNOLOGY TRANSFERRING(LAPHTEC), *Trading, Industrial Lasers, Opto-mechanics*	Tehran

SCHOLARSHIPS AND GRANTS

2013-2016 Merit Scholarship Programme for High Technology (MSP)
2011-2013 Technology Transfer Office (OTT), Technical University of Madrid
2007-2009 Erasmus Mundus scholarship

July 2019

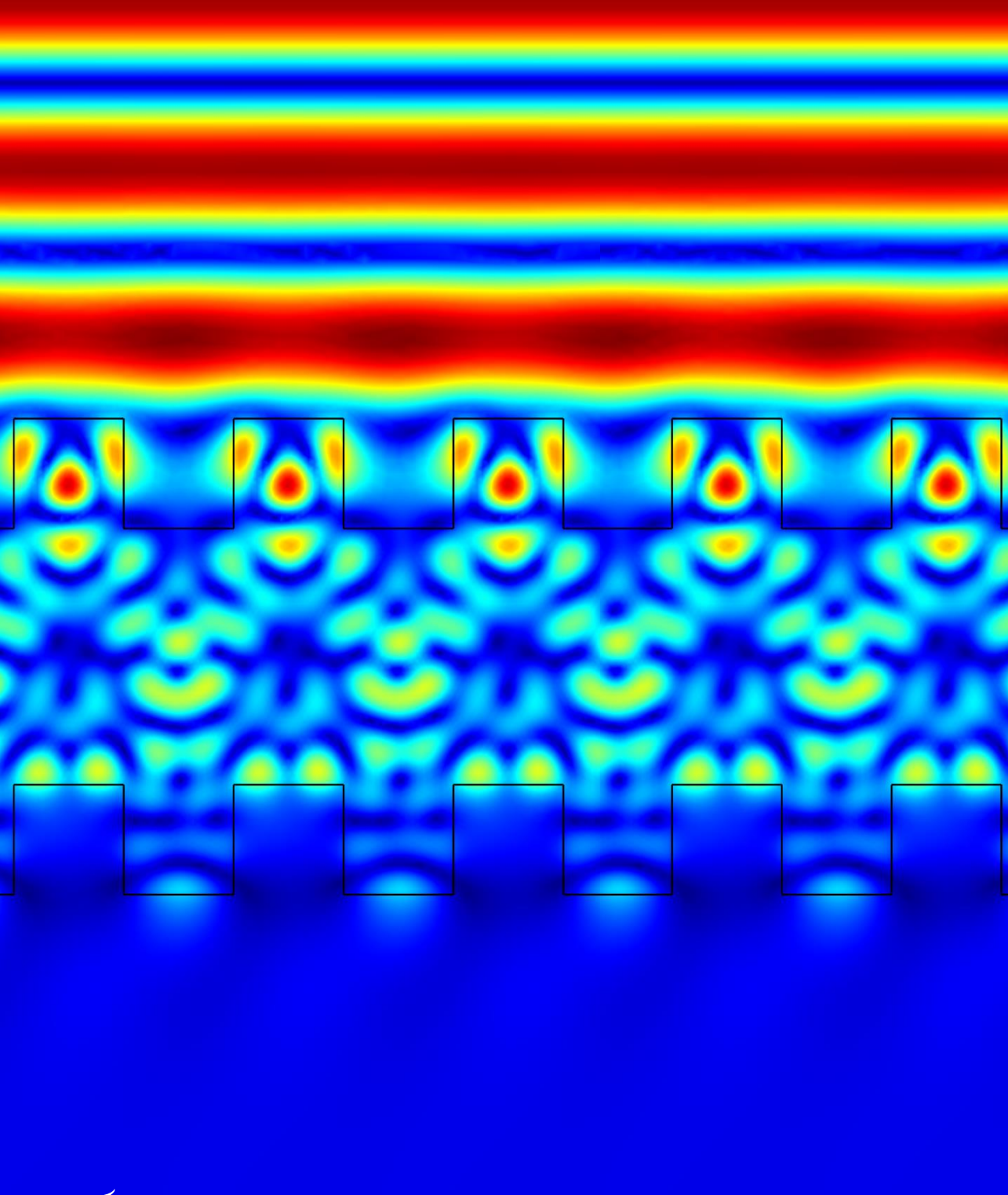

TU Delft